Newly identified climatically and environmentally significant high-latitude dust sources

Outi Meinander[1], Pavla Dagsson-Waldhauserová[2,3], Pavel Amosov[4], Elena Aseyeva[5], Cliff Atkins[6], Alexander Baklanov[7], Clarissa Baldo[8], Sarah Barr[9], Barbara Barzycka[10], Liane G. Benning[11,23], Bojan Cvetkovic[12], Polina Enchilik[5], Denis Frolov[5], Santiago Gassó[13], Konrad Kandler[14], Nikolay Kasimov[5], Jan Kavan[15], James King[16], Tatyana Koroleva[5], Viktoria Krupskaya[5,6], Markku Kulmala[18], Monika Kusiak[19], Hanna K Lappalainen[18], Michał Laska[11], Jerome Lasne[20], Marek Lewandowski[19], Bartłomiej Luks[19], James B McQuaid[10], Beatrice Moroni[21], Benjamin J Murray[10], Ottmar Möhler[22], Adam Nawrot[19], Slobodan Nickovic[13], Norman T. O'Neill[23], Goran Pejanovic[13], Olga B. Popovicheva[5], Keyvan Ranjbar[23,a], Manolis N. Romanias[20], Olga Samonova[5], Alberto Sanchez-Marroquin[10], Kerstin Schepanski[24], Ivan Semenkov[5], Anna Sharapova[11], Elena Shevnina[1], Zongbo Shi[9], Mikhail Sofiev[1], Frédéric Thevenet[20], Throstur Thorsteinsson[25], Mikhail A. Timofeev[5], Nsikanabasi Silas Umo[22], Andreas Uppstu[1], Darya Urupina[20], György Varga[26], Tomasz Werner[19], Olafur Arnalds[2], and Ana Vukovic Vimic[27]

[1]Finnish Meteorological Institute, Helsinki, 00101, Finland
[2]Agricultural University of Iceland, Reykjavik, 112, Iceland
[3]Czech University of Life Sciences Prague, Prague, 16521, Czech Republic
[4]INEP Kola Science Center RAS, Apatity, Russia
[5]Lomonosov Moscow State University, Moscow, 119991, Russia
[6]Institute of Geology of Ore Deposits, Petrography, Moscow, 119017, Russia
[7]Te Herenga Waka—Victoria University of Wellington, Wellington, 6012, New Zealand
[87]World Meteorological Organization, WMO, Geneva, 1211, Switzerland
[9]University of Birmingham, Birmingham, B15 2TT, United Kingdom
[10]University of Leeds, Leeds, LS2 9JT, United Kingdom
[11]University of Silesia in Katowice, Sosnowiec, 41-200, Poland
[12]German Research Centre for Geosciences, Helmholtz Centre Potsdam, 14473, Germany
[13]Republic Hydrometereological Service of Serbia, 11030, Belgrade, Serbia
[14]University of Maryland, College Park MD, 20742, United States of America
[15]Technical University of Darmstadt, Darmstadt, 64287, Germany
[16]Masaryk University, Brno, 61137, Czech Republic
[17]University of Montreal, Montreal, H3T 1J4, Canada
[18]Institute for Atmospheric and Earth System Research, University of Helsinki, Helsinki, 00101, Finland
[19]Institute of Geophysics, Polish Academy of Sciences, Warsaw, 01-452, Poland
[20]IMT Lille Douai, SAGE, Université de Lille, 59000 Lille, France
[21]University of Perugia, Perugia, 06123, Italy
[22] Institute of Meteorology and Climate Research, Karlsruhe Institute of Technology, Karlsruhe, 76227, Germany.
[23]Université de Sherbrooke, Sherbrooke, J1K, Canada
[24]Free University of Berlin, Berlin, 12165, Germany
[25]University of Iceland, Reykjavik, 102, Iceland

41 [26]Research Centre for Astronomy and Earth Sciences, Budapest, 1112, Hungary
42 [27]University of Belgrade, Faculty of Agriculture, Belgrade, 11080, Serbia
43 [a]now at: Flight Research Laboratory, National Research Council Canada, Ottawa, ON, Canada
44
45
46 *Correspondence to*: Outi Meinander (outi.meinander@fmi.fi)

47 **Abstract.** Dust particles from high latitudes have a potentially large local, regional, and global significance to climate and the
48 environment as short-lived climate forcers, air pollutants, and nutrient sources. Identifying the locations of local dust sources
49 and their emission, transport, and deposition processes is important for understanding the multiple impacts of High Latitude
50 Dust (HLD), ≥ 50°N and ≥ 40°S) on the Earth's systems. Here, we identify, describe, and quantify the Source Intensity (SI)
51 values, which show the potential of soil surfaces for dust emission scaled to values 0 to 1 concerning globally best productive
52 sources, using the Global Sand and Dust Storms Source Base Map (G-SDS-SBM). This includes sixty-four HLD sources in
53 our collection for the Northern (Alaska, Canada, Denmark, Greenland, Iceland, Svalbard, Sweden, and Russia) and Southern
54 (Antarctica and Patagonia) high latitudes. Activity from most of these HLD dust sources shows seasonal character. It is
55 estimated that high-latitude land areas with higher (SI≥0.5), very high (SI≥0.7), and the highest potential (SI≥0.9) for dust
56 emission cover >1 670 000 km^2, >560 000 km^2, and >240 000 km^2, respectively. In the Arctic HLD region (≥ 60°N), land area
57 with SI≥0.5 is 5.5% (1 035 059 km^2), area with SI≥0.7 is 2.3% (440 804 km^2), and with SI≥0.9 is 1.1% (208 701 km^2).
58 Minimum SI values in the north HLD region are about three orders of magnitude smaller, indicating that the dust sources of
59 this region greatly depend on weather conditions. Our spatial dust source distribution analysis modeling results showed
60 evidence supporting a northern High Latitude Dust (HLD) belt, defined as the area north of 50°N, with a 'transitional HLD-
61 source area' extending at latitudes 50–58°N in Eurasia and 50–55°N in Canada, and a 'cold HLD-source area' including areas
62 north of 60°N in Eurasia and north of 58°N in Canada, with currently 'no dust source' area between the HLD and LLD dust
63 belt, except for British Columbia. Using the global atmospheric transport model SILAM, we estimated that 1.0% of the global
64 dust emission originated from the high-latitude regions. About 57% of the dust deposition in snow- and ice-covered Arctic
65 regions was from HLD sources. In the south HLD region, soil surface conditions are favorable for dust emission during the
66 whole year. Climate change can decrease snow cover duration, retrieval of glaciers, and increase drought, heatwave intensity,
67 and frequency, leading to the increasing frequency of topsoil conditions favorable for dust emission, which increases the
68 probability of dust storms. Our study provides a step forward to improve the representation of HLD in models and to monitor,
69 quantify, and assess the environmental and climate significance of HLD going forward.

70 **1 Introduction**

71 Mineral dust is an essential and relevant climate and environmental variable with multiple socioeconomic effects on, e.g.,
72 weather and air quality, marine life, climate, and health (Creamean et al., 2013; Terradellas et al., 2015; Shepherd et al., 2016;
73 Querol et al., 2019; Nemuc et al., 2020). Mineral dust is transported from local sources of high-latitude dust (HLD, ≥50°N and

≥40°S, Bullard et al., 2016), low-latitude dust (LLD, mostly 0-35°N), and the so-called 'global dust belt' (GDB, Prospero et al., 2002), defined to extend into the Northern Hemisphere from the west coast of North Africa, over the Middle East (West Asia), Central and East Asia, and south-west North America (Ginoux et al., 2012), with only minor sources in Southern Hemisphere (Prospero et al., 2002; Ginoux et al., 2012; Bullard et al., 2016; Terradellas et al., 2017). Dust is often associated with hot, subtropical deserts, but the importance of dust sources in the cold, high latitudes has recently increased (Arnalds et al., 2016; Bullard et al., 2016; Groot Zwaafting et al., 2016, 2017; Kavan et al., 2018, 2020a,b; Boy et al., 2019; Gassó and Torres, 2019; IPCC, 2019; Tobo et al., 2019; Bachelder et al., 2020; Cosentino et al., 2020; Ranjbar et al., 2021; Sanchez-Marroqin et al., 2020). Dust produced in high latitudes and cold climates (Iceland, Greenland, Svalbard, Alaska, Canada, Antarctica, New Zealand, and Patagonia) can have regional and global significance (Bullard et al., 2016). Local HLD dust emissions are increasingly being recognized as driving the local climate, biological productivity, and air quality (Groot Zwaafting et al., 2016, 2017; Moroni et al., 2018; Crocchianti et al., 2021; Varga et al., 2021). HLD can induce significant direct (blocking sunlight) and indirect (clouds and cryosphere) radiative forcing (Kylling et al., 2018) on solar radiation fluxes and snow optical characteristics, strongly impacting Arctic amplification, including glacier melt (Boy et al., 2019).

HLD aerosols consist of a variety of different dust particle types with various particle sizes and shapes distributions, as well as physical, chemical, and optical properties that differ from the crustal dust of the Sahara or American deserts (Shepherd et al., 2016; Arnalds et al., 2016; Bachelder et al., 2020; Baldo et al., 2020; Crucius, 2021). Therefore, impacts on climate, environment, and human health can differ from those of LLD. For example, Icelandic dust is of volcanic desert origin, often dark, and has higher proportions of heavy metals than crustal dust (Arnalds et al., 2016). The IPCC special report (IPCC, 2019) recognizes dark dust aerosols as a short-lived climate forcer (SLCF) and light-absorbing aerosols connected to cryospheric changes. Light-absorbing HLD particles can induce direct effects on solar radiation fluxes as SLCF and snow optical characteristics impacting cryosphere melt via radiative feedback (Peltoniemi et al. 2015; Boy et al., 2019; Dagsson-Waldhauserová and Meinander, 2019, 2020; IPCC, 2019; Kylling et al., 2018). HLD significantly affects the formation and properties of clouds (Abbatt et al., 2019; Sanchez-Marroquin et al., 2020; Murray et al., 2021).

Dust is connected to climate change: Historical dust (paleo dust) is not only a contributor to climate change but a record of previous dust and climate conditions (Lamy et al., 2014; Lewandowski et al., 2020). Dust can significantly contribute to air pollution mortalities (Terradellas et al., 2015; Nemuc et al., 2020). Deposition at high latitudes can provide nutrients to the marine system; mineral and organic matter on glaciers, including natural and anthropogenic dust, can form cryoconite granules. Cryoconite, dust, and ice algae can reduce surface albedo and accelerate the melting of glaciers (Lutz et al., 2016; McCutcheon et al., 2021). Monitoring dust in remote, high-latitude areas has crucial value for climate change assessment and understanding the impacts of global warming on natural systems and socioeconomic sectors. Bullard et al. (2016) summarized natural HLD sources as covering over 500 000 km^2 and producing particulate matter of ca. 100 Mt dust per year.

108 Dust emissions respond to changes in wind speed, soil moisture, and other parameters affected by climate change; changes in
109 land cover and surface properties by human activities can affect dust emissions (Kylling et al., 2018). The fundamental
110 processes controlling aeolian dust emissions in high latitudes are essentially the same as in temperate regions. However, there
111 are other processes specific to or enhanced in cold regions. Low temperatures, humidity, strong winds, permafrost, and niveo-
112 aeolian processes, which can affect the efficiency of dust emission and distribution of sediments, were listed in Bullard et al.
113 (2016).

114

115 The modeling of emissions, transport, and deposition complemented with available observations, can provide essential
116 information related to dust's impact on the climate and environment in the high latitudes (IPCC, 2019). The locations and
117 characteristics of local dust sources are two of the major observations documented for inputting information into numerical
118 models to predict or simulate the HLD process from its emission to downwind deposition. In some cases, model results can
119 indicate possible but not yet identified dust sources in the HL regions. A general lack of observational and long-range transport
120 modeling studies results in poor HLD monitoring and predicting. Models have predictive capacity and, without the
121 observations, can constitute a source of information and indicate where more direct observations are needed. The first long-
122 range transport modeling studies show that main transport pathways from HLD sources clearly affect the High Arctic (>80°N)
123 and European mainland (Baddock et al., 2017; Beckett et al., 2017; Đorđević et al., 2019; Groot Zwaafting et al., 2016, 2017;
124 Moroni et al., 2018). The World Meteorological Organization Sand and Dust Storm Warning Advisory and Assessment System
125 (WMO SDS-WAS) monitors and predicts dust storms from the world's major deserts (https://www.wmo.int/sdswas), where
126 HLD sources have recently been included in the SDS-WAS dust forecasts. Europe's largest desert is at a high latitude in
127 Iceland (Arnalds et al., 2016), with dust transport observed over the North Atlantic to European countries (Ovadnevaite et al.,
128 2009; Prospero et al., 2012; Beckett et al., 2017; Đorđević et al., 2019).

129

130 HLD is a short-lived climate forcer, air pollutant, and nutrient source, showing the need to identify the geographical extent
131 and dust activity of the HLD sources (Arnalds et al., 2014, 2016; Dagsson-Waldhauserová et al., 2014, 2015; Terradellas et
132 al., 2015; Arnalds et al., 2014, 2016; USGCRP, 2018; IPCC, 2019). Bullard et al. (2016) designed the first HLD map based
133 on visibility and dust observations, combined with field and satellite observations of high-latitude dust storms, resulting in 129
134 locations described in 39 papers. Here, we compile and describe sixty-four HLD sources in the northern and southern high
135 latitudes. Since dust particles emitted from high latitudes can have a large local, regional, and global significance to climate
136 and the environment, identifying where local dust sources are is important. Climate change and land-use change can further
137 increase the number of dust sources and their emissions when, for example, snow, ice, or glaciers melt, exposing new open
138 soil areas and generating more glacial dust particles. This work's main aim is to:

139   (i)   identify new and previously unpublished HLD sources using direct observations and measurements, satellite
140   data, literature sources (including media and social media), and include HLD sources identified in recent

141 ~~literature from 2017- 2021, which have not been part of previously published collections of HLD sources, as~~
142 ~~well as update some of the previously documented sources~~
143   (ii)   estimate the high-latitude land area with potential dust activity and calculate the source intensity (SI) for the
144 identified sources
145   (iii)   provide model results on HLD emission, long-range transport and deposition at various scales of time and
146 space
147   (iv)   specify key climatic and environmental impacts of HLD and related research questions, which could improve
148   our understanding of HLD sources, with the help of literature surveys on clouds and climate feedback,
149   atmospheric chemistry, marine environment, cryosphere, and cryosphere-atmosphere feedbacks.
150
151
152 We focus on high latitudes with natural dust sources and include some anthropogenic dust sources, such as road dust, when
153 unpaved roads serve as a significant dust source. Direct emissions of volcanic eruptions and road dust formed via abrasion and
154 wear of pavement or traction control materials are excluded. Identifying dust sources is the first step to understand the HLD
155 life-cycle (dust emission, transport, and deposition). After that, impacts and feedback mechanisms can be identified and
156 quantified as physical, chemical, and optical properties of dust from these source areas. Their properties during emission,
157 transport, and deposition are needed to be characterized to allow a holistic understanding.

158 **2 Materials and methods**

159 **2.1 Identification and characteristics of dust sources**

160 Three topical workshops in Russia, Finland, and Iceland (Meinander et al., 2019a,b) on HLD were organized in 2019 to
161 identify, describe, and assess new high-latitude dust sources (~~at~~ ≥ 50°N and ≥ 40°S, according to Bullard et al. 2016, and
162 ~~(~~including the Arctic as a subregion at ≥ 60°N). The HLD source map and observations on dust properties provided here are
163 based on:
164   (i)   new field and satellite observations not described in published academic papers
165   (ii)   newly identified HLD source locations reported in recent literature but not included in previous collections
166   (iii)   updated observations on previously documented sources.
167 Each location was assessed to classify each source: Category 1 refers to an active dust source with high ecological significance,
168 category 2 to a semi-active source with moderate ecological significance, and category 3 to new sources with unknown activity
169 and importance. Moreover, SI values for each HLD location in the Northern and Southern (Antarctica and Patagonia) high
170 latitudes were quantified, and the potential land surface area for dust emissions in the north, Arctic, and south HLD regions
171 was calculated (Section 2.2).

2.2 High-latitude dust sources from UNCCD G-SDS-SBM

The Global Sand and Dust Storms Source Base Map (G-SDS-SBM), developed by the United Nations Convention to Combat Desertification (UNCCD) in collaboration with the United Nations Environment Programme (UNEP) and World Meteorological Organization (https://maps.unccd.int/sds/; Vukovic, 2019, 2021) represents gridded values of SDS source intensity (SI, values 0 to 1) on a resolution of 30 arcsec. The Source Base Map was developed by including the information on soil texture, bare land fraction, and NASA satellite Moderate-resolution Imaging Spectroradiometer Enhanced Vegetation Index, MODIS EVI, as well as the data on land cover, topsoil moisture, and temperature. Values of SI represent topsoil's potential to emit soil particles under windy conditions, assigning the highest values of source intensity to the most productive surfaces. SI values are derived under the assumption they are exposed to the same velocity of surface wind. Input data, which change depending on the weather (and possibly human activities) for bare land fraction, moisture, and temperature data, are defined for four months (January, April, July, October—each month representing one season) by using extreme values. This was observed from 2014 to 2018, providing favorable conditions for surfaces to act as sources. Thus, sources that may appear during heatwaves and drier conditions (or drought), when the surface in high latitudes is unfrozen, snow-free, and more susceptible to wind erosion, are included in this map. Such weather extremes under climate change are becoming more frequent and are projected to increase (IPCC, 2013), justifying the source mapping approach using the information on extreme topsoil conditions. Using the maps produced for the four seasons, maximum and minimum values are determined for each grid point to explore the potential of high-latitude land surfaces to act as dust sources, their seasonality, and to compare values of source intensity with marked locations of HLD sources.

2.3 Methods used to identify and study the dust sources

Various methods identified the HLD sources (Table 1), including direct observations and measurements; satellite data; emission, long-range transport and deposition modeling; media, social media, and literature sources (e.g., web pages, conference abstracts). More details and literature references can be found in each source section. Dust emission, long-range transport, and deposition modeling calculations were made to study if the HLD sources have local, regional, or global significance. Two well-established dust atmospheric models—SILAM and DREAM—were used to simulate the atmospheric dust process over high latitudes. Both models have been thoroughly evaluated for other deserts where the accuracy of their results has been verified.

Table 1. Methods used to identify and study the dust sources

Method	Sources

Direct observation: photographs and visual observations	Marambio, Antarctic Peninsula, Schirmacher Oasis, East Antarctica McMurdo Sound/Ross Sea
Satellite images: Meteosat-11 images	Denmark, Sweden, Iceland
Instrumentation: SEM	Svalbard
Instrumentation: LOAC	James Ross Island
Instrumentation: SL-501 surface and snow albedo	Marambio, Antarctic Peninsula
Instrumentation: Magnetic susceptibility upon heating, magnetic hysteresis parameters	Svalbard
Instrumentation: ICP-MS, AES-ICP, XRD, XRF	Russia (sources no. 2–5 of Fig.1)
Instrumentation: high performed liquid chromatography, potentiometry	Russia (sources no. 7–8 of Fig.1)
Passive deposition samplers	James Ross Island
Snow samples	Svalbard (Hornsund, Pyramiden), Antarctica
Social media: Twitter account (@SanGasso) and hashtag (#highlatitudedust)	South America (Patagonia), Alaska, Greenland, Iceland
Literature sources	Denmark, Sweden
SILAM model	Arctic
DREAM model	Arctic, Antarctic

200

201

202 Estimates of the emission and deposition of global and Arctic dust were computed separately to assess Arctic dust's global
203 impact using the SILAM model (Sofiev et al., 2015)—a global to meso-scale atmospheric dispersion and chemistry model—
204 applied for air quality and atmospheric composition modelling. The dust emission estimate is driven by the European Centre
205 for Medium Range Weather Forecast ECMWF IFS meteorological model at a resolution of 0.1 x 0.1 degrees. The computations
206 were performed using ECMWF ERA5 meteorological reanalysis data for 2017 at a resolution of 0.5 x 0.5 degrees. The dust
207 emission model was validated against AERONET (AErosol RObotic NETwork, www.aeronet.com) aerosol optical density
208 (AOD) data and provided unbiased results for the main dust emission areas. For Arctic areas, where dust is not contributing to
209 the AOD as much, the simulated AOD from all aerosols is unbiased concerning the measurements. While the simulation's

210 relatively coarse resolution cannot capture the smaller point-like dust sources, it is still expected to give a good approximation

211 of the overall patterns and magnitudes of dust emission and deposition. The SILAM results are presented in sections 3.3 (Fig.

212 4) and 3.4 (Fig. 12 and Fig. 15).

214 DREAM is a fully dynamic numerical prediction model for atmospheric dust dispersion originating from soil. The dust

215 component of this system (Pejanovic et al., 2011; Nickovic et al., 2016) is online and driven by the atmospheric model NMME

216 (Janjic et al., 2001). Dust concentration in the model is described with eight particle bins, with radii ranging from 0.18 to 9

217 μm. DREAM-ICELAND is the model version to predict dust transport emitted from Iceland's largest European dust sources

218 (Cvetkovic et al., 2021, submitted). The size distribution of particles in the model is specified according to in situ measurements

219 in the Icelandic hot spots. The model horizontal resolution of ~3.5 km is sufficiently fine to resolve the Icelandic dust sources'

220 rather heterogeneous and small-scale character. As the first operational numerical HLD model in the international community,

221 DREAM-ICELAND is used daily, having predicted Icelandic dust since April 2018. DREAM results are included in sections

222 3.4 (Fig. 8 and 11) and 3.6 (Fig. 16), and as a supplementary animation.

224 **3 Results and discussion**

226 **3.1 Locations of the HLD sources**

228 Sixty-four HLD sources at northern and southern high latitudes (Fig. 1) were identified. In the north HLD region are 49

229 locations (47 locations ≥50°N and two >47°N) in Alaska, Canada, Denmark, Greenland, Iceland, Svalbard, Sweden, and

230 Russia, of 35 are in the Arctic HLD subregion (≥60°N). In the south HLD region (≥40°S), 15 sources were identified in

231 Antarctica and Patagonia, South America. The sources included the Arctic and Antarctic, boreal, remote, rural, mountain,

232 marine and coastal, river sediments, mining, unpaved roads, soils (Podzols, Retisols, Gleysols, Phaeozems, and Stagnosols;

233 USS Working Group WRB, 2015), and glacial dust. The observational periods for these locations varied from days or weeks

234 to multiple years and included data from ground-based measurements, remote sensing data, and modeling results. Results on

235 the calculated source intensity and areas of high-latitude surface land with higher (SI≥0.5), very high (SI≥0.7), and the highest

236 potential (SI≥0.9) for dust emission are shown in Section 3.2. Observations and characteristics of the identified dust sources

237 in our collection (Fig. 1) are presented in Section 3.4 and the Supplement Tables S1-S7 (including the contemporary

238 classification for each source into categories 1–3, based on the currently available observations, in S1; satellite observations

239 on new HLD sources in Iceland in S2; observations on new HLD sources in Greenland and Canada in S3; SI values for each

240 source in S4 and S5, including latitude and longitude; and results from Russian HLD sources in S6-S7).

241
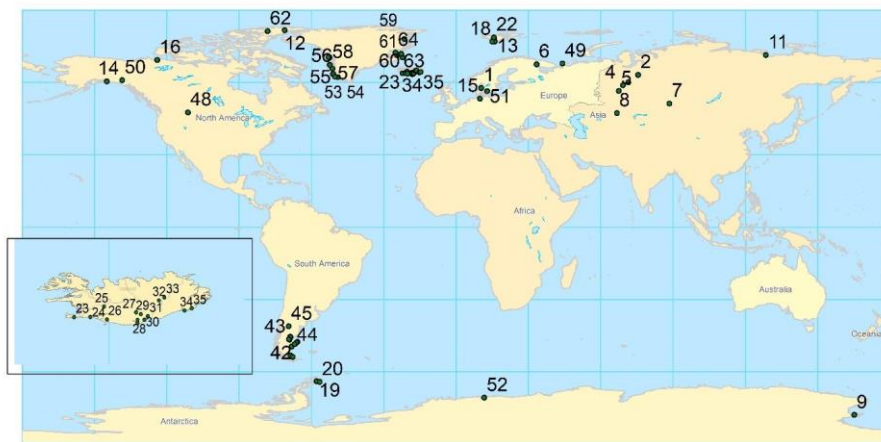
Figure 1. Map of the locations of the northern (north of 50°N) and southern (south of 40°S) high-latitude dust (HLD) sources identified and included in this study. The numbers are the identified 64 dust sources, as shown in Figure 1.

3.2 Source intensity from UNCCD G-SDS-SBM

Figure 2 presents the G-SDS-SBM source intensity values (maximum and minimum) for the north HLD region. The north HLD region ~~also~~ includes the area north of latitude 50°N and the Arctic region (as a subregion of the HLD region) north of 60°N. HLD dust sources show extreme seasonal characteristics, with some exceptions. The sources appear and disappear (or change SI values) seasonally or appear (or increase source intensity values) only during favorable extreme weather conditions. Figure 3 shows G-SDS-SBM source intensity values for the south HLD region (south of 40°S) without values for Antarctica since G-SDS-SBM does not include areas south of 60°S. Supplementary Tables S4 and S5 give the values of SI for specific locations marked in Figure 1. Further analysis consists of assessing the areal coverage of sources, with different thresholds for

253   SI values in absolute values (km²) and the percentage they occupy concerning the total land surface area in the defined HLD

254   regions.

255
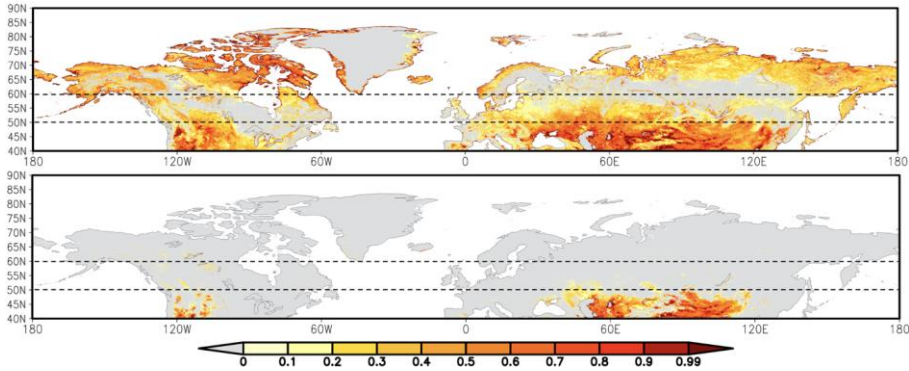
256
257
258
259   **Figure 2. UNCCD Global Sand and Dust Storms Source Base Map (G-SDS-SBM) for annual maximum (upper panel) and**
260   **minimum (lower panel) source intensity for the north HLD region and Arctic sub-region (north of 50°N and 60°N, respectively,**
261   **marked with dashed lines).**

262
263
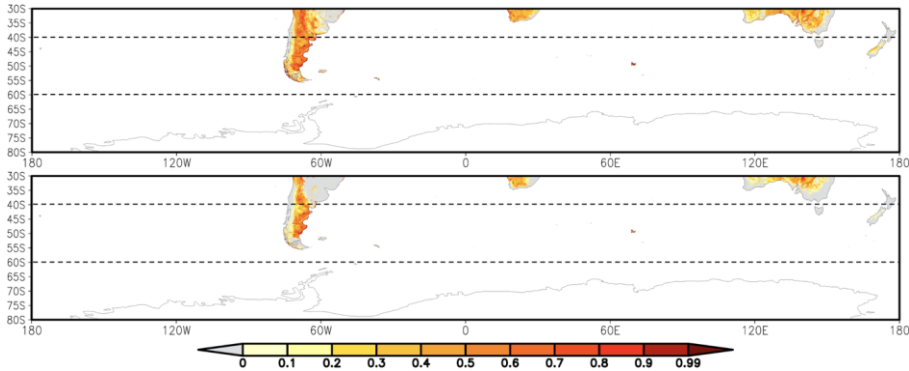
264
265
266   **Figure 3. UNCCD Global Sand and Dust Storms Source Base Map (G-SDS-SBM) for annual maximum (upper panel) and**
267   **minimum (lower panel) source intensity for the south HLD region (south of 40°S) without Antarctica (south of 60°S), marked with**
268   **dashed lines.**

269
270

The total surface area of dust sources with a higher potential for dust emission (SI$\geq$ 0.5) over the north HLD region (north of 50°N) is 3.9% of the total land surface (1 364 799 km^2). The area with a very high potential for dust emission (SI$\geq$0.7) is 1.5% (509 965 km^2). The area with the highest dust emission potential (SI$\geq$0.9) is 0.7% of the total land area (233 336 km^2) (Table 2). In the Arctic region (north of 60°N)—the subregion of the north HLD area—dust sources with a higher potential for dust emission (SI$\geq$0.5) are 5.5% of the total land surface (1 035 059 km^2). The area with a very high potential for dust emission (SI$\geq$0.7) is 2.3% (440 804 km^2). The area with the highest dust emission potential (SI$\geq$0.9) is 1.1% (208 701 km^2). The surface of dust-productive areas with minimum seasonal SI values in the north HLD region is about three orders of magnitude smaller than the maximum, meaning the north HLD dust sources highly depend on weather conditions. Maximum surfaces contain dust-productive regions that are defined under the most favorable weather conditions for soil exposure to wind erosion (including extreme weather). All sources defined here are not necessarily active every year nor in the same period, meaning these surfaces can seasonally or occasionally (under severe weather) appear as dust sources.

For the south HLD region (40°S–60°S, area without Antarctica), the land surface is only 2% of the total surface area (Table 3). The surface area of dust sources with SI$\geq$0.5 is 22.6% of the total land surface (309 520 km^2). The area with SI$\geq$0.7 is 4.5% (61 527 km^2). The area with the highest dust emission potential (SI$\geq$0.9) is 0.6% (8 630 km^2). The surface areas for minimum SI values above these thresholds are two to three times smaller than the surfaces for maximum SI values compared to the difference in the north HLD region. This means that soil surface conditions in the south HLD region are favorable for dust emission over the whole year. Especially in locations of HLD markers, SI maximum and minimum values do not change over most locations or decrease by 0.1 or 0.2, except for one location (no. 38), which has SI values changing from 0.9 to 0 at the location of an HLD marker.

Table 2. Relevant surfaces for the north HLD and Arctic regions: surface of total area of the region, surface of land area within the region (in km^2 and % of total surface), total surface (in km^2 and % of land surface) of areas with SI values above thresholds (0.5 for surfaces with at least "higher" dust emission potential, 0.7 for surfaces with at least "high" dust emission potential, and 0.9 for surfaces with "highest" dust emission potential) in maximum (max) and minimum (min) seasonal values; values are derived from UNCCD G-SDS-SBM.

NORTH HLD REGION (NORTH OF 50°N)				
total area (km^2)		**land area (km^2)**	**land area (%)**	
64392015		34695710	54	
	max		**min**	
	surface area (km^2)	**surface area (%)**	**surface area (km^2)**	**surface area (%)**
SI $\geq$ 0.5	1364799	3.9	1916	0.006
SI $\geq$ 0.6	803372	2.3	1053	0.003
SI $\geq$ 0.7	509965	1.5	718	0.002

	surface area (km²)	surface area (%)	surface area (km²)	surface area (%)
SI ≥ 0.8	342913	1.0	562	0.002
SI ≥ 0.9	233336	0.7	451	0.001

ARCTIC REGION (NORTH OF 60°N)

total area (km²)	land area (km²)	land area (%)
36876709	18853826	51

	max		min	
	surface area (km²)	surface area (%)	surface area (km²)	surface area (%)
SI ≥ 0.5	1035059	5.5	515	0.003
SI ≥ 0.6	665082	3.5	350	0.002
SI ≥ 0.7	440804	2.3	297	0.002
SI ≥ 0.8	303521	1.6	264	0.001
SI ≥ 0.9	208701	1.1	217	0.001

299
300
301
302
303 **Table 3. Relevant surfaces for the south HLD region: surface of total area of the region, surface of land area within the region (in**
304 **km² and % of total surface), total surface (in km² and % of land surface) of areas with SI values above thresholds (0.5 for surfaces**
305 **with at least "higher" dust emission potential, 0.7 for surfaces with at least "high" dust emission potential, and 0.9 for surfaces**
306 **with "highest" dust emission potential) in maximum (max) and minimum (min) seasonal values; values are derived from UNCCD**
307 **G-SDS-SBM.**
308

SOUTH HLD REGION (SOUTH OF 40°S)

total area (km²)	land area (km²)	land area (%)
61435208	1367987	2

	max		min	
	surface area (km²)	surface area (%)	surface area (km²)	surface area (%)
SI ≥ 0.5	309520	22.6	186266	13.616
SI ≥ 0.6	151480	11.1	81522	5.959
SI ≥ 0.7	61527	4.5	29256	2.139
SI ≥ 0.8	25416	1.9	10842	0.793
SI ≥ 0.9	8630	0.6	2747	0.201

309
310

311 **3.3 Emission and deposition of global and Arctic dust**

312   The SILAM model estimated the total emission of annual dust and its deposition (data for 2017) onto snow-covered land,

313   frozen sea, and total sea surfaces (frozen and non-frozen) (Fig. 4). The computations were also performed for Arctic dust and

314   total global dust, with results for overall dust (diameter less than 30 μm) and fine dust (diameter less than 2.5 μm) separately

315   (Fig. 15 of Section 3.5). Based on the model, the total emission of Arctic dust equals approximately 1.0% of the globe's total

316   dust emission. The deposition of Arctic dust onto snow- and ice-covered surfaces equals about 19% of the total dust deposition

317   onto these areas and around 57% of the deposition onto the areas explicitly located in the Arctic region. For fine dust, the

318   corresponding figures are 7% and 22%. Compared to the deposition of black carbon (anthropogenic sources and wildfires

319   combined; Fig. 15 of Section 3.5) onto snow and ice, the deposition of fine Arctic dust is about 70% higher globally and around

320   580% higher in the Arctic regions. While these figures provide a general quantification of the deposited amounts, detailed

321   calculations of the thermal and optical properties of dust and black carbon deposited on snow would be required to compare

322   the deposited substances' net impacts on the climate.

323

324
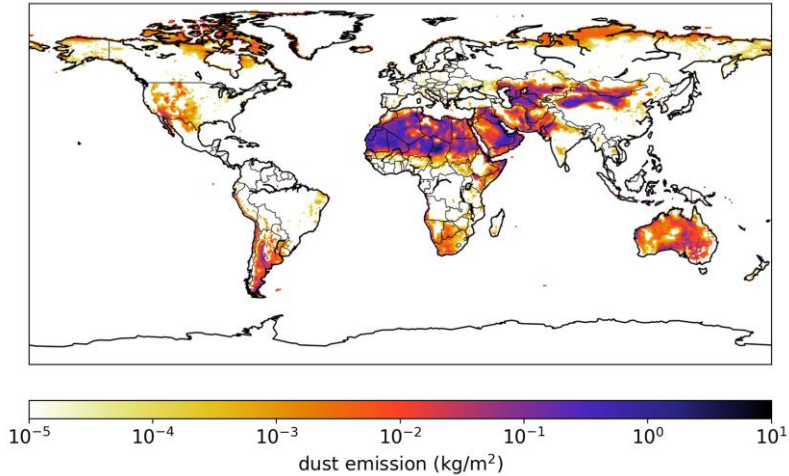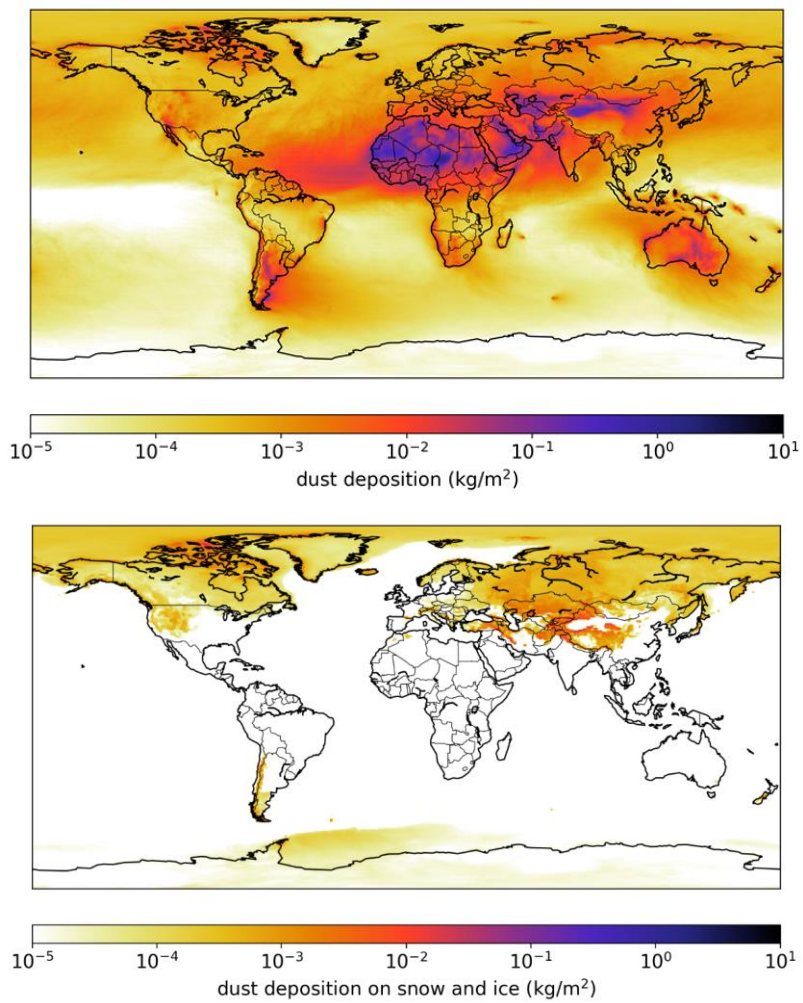
Figure 4. SILAM emission and deposition modeling results of dust emission (above), dust deposition (middle) and dust deposition on snow and ice (below), in [kg/m²].

327

3.4 The identified dust sources

Observations of the identified sixty-four dust sources in our collection (Fig. 1) are presented and discussed in alphabetical order as follows: 1. Alaska (sources no. 14 and 50 in Fig. 1); 2. Antarctica (no. 9, 19, 20, 52); 3. Canada (no. 2, 16, 48, 62); 4. Denmark and Sweden (no. 1, 15, 51); 5. Greenland (no. 53–61, 64); 6. Iceland (no. 23–45); 7. Russia (no. 2–11); 8. South America and Patagonia (no. 17, 21, 46, 47, 49, 52, 63); and 9. Svalbard (no. 13, 18, 22). Dust events originating simultaneously from Greenland, Iceland, and northern America are demonstrated in the Supplementary animation. The numbers are the identified 64 dust sources shown in Figure 1. Additional information, including latitude, longitude, and SI values, can be found in Supplement (Tables S1-S4).

3.4.1 Alaska, Copper River Valley, USA

Alaskan dust sources were identified over a century ago (Tarr and Martin, 1913). However, limited satellite detection due to abundant cloud cover and isolated location resulted in sparse information on this region (Crusius et al., 2011). The main identified sources are piedmont glaciers (Malaspina, Bering), resuspension of ash from past eruptions (Hadley et al., 2004), and major rivers carrying glacial sediment (Copper, Yukon, Tanana, and Alsek) (Gassó, 2020a,b; 2021a,b). Resuspension of glacial dust transported by these rivers can be abundant, often triggering air quality alerts by the Alaska Department of Environment (USGCRP, 2018). The largest and most active of such dust sources is the Copper River (Fig. 5), estimated to transport 69 million tons of suspended sediment annually (Brabets, 1997). Transported sediment is deposited on the Copper River Delta, an alluvial floodplain covering an area of 2800 km^2. When conditions allow, sediment is resuspended, resulting in dust plumes that can extend hundreds of kilometers over the Gulf of Alaska. Dust events, often lasting several days or weeks (Schroth et al., 2017), are most common in late summer and autumn when the river discharge and snow cover are at their minimum and high wind speeds are commonplace (Crusius, 2021). However, these occurrences have been observed year-round (Gassó, 2021a; January 2021). Dust reaches the open waters beyond the continental shelf and the influence of coastal sediments (Crusius et al., 2017). Thus, it has been proposed that dust from coastal sources such as the Copper River Delta can be an important source of bioavailable iron in the Gulf of Alaska (Crusius et al., 2011; Crusius, 2021; Schroth et al., 2017). Further work is also needed to investigate the relative importance of dust emissions from Alaska and East Asia (Bishop et al., 2002) in other areas. Also, dust from this region may initiate ice production in supercooled clouds, which is crucial for climate feedback (Murray et al., 2021). Regarding the magnitude and seasonal variability of emissions of sources in southern Alaska, a few dedicated studies have focused on dust from the Copper River Delta (Crusius, et al., 2017; Schroth et al., 2017; Crusius, 2021). However, to our knowledge, no dust activity and source characterization has been carried out along the coast of the Gulf of Alaska. Moreover, resuspended road dust is a major air quality issue throughout Alaska.

Figure 5. Satellite image (left) of the Copper River region and photo (right) taken at the Copper River Delta on the same day (14th October 2019). The common occurrence of clouds prevents directly viewing the dust in suspension, illustrating the difficulty of observing dust activity from space. (Satellite image from NASA Worldview; photo by Sarah Barr).

3.4.2 Antarctica

3.4.2.1 James Ross Island, Ulu Peninsula

The northern part of James Ross Island—Ulu Peninsula—represents one of Antarctica's largest ice-free areas (312 km^2). Its bare surface, consisting mainly of weathered sedimentary rocks, is an active HLD source (Kavan et al., 2018). Suspended sediments originate from outside the local fluvial systems based on the elemental ratios of Sr/Ca and Rb/Sr (Kavan et al., 2017). The wind speed threshold of 10 ms^{-1} is needed for activating local dust sources, with most of the particles captured (by mass) in size bins between 2.5–10 µm. Mean (median) mass concentrations of the PM10 were 6.4 ± 1.4 (3.9 ± 1) µg m^{-3}, while the PM2.5 was 3.1 ± 1 (2.3 ± 0.9) µg m^{-3} for the whole measurement period from January to March 2018. Mean PM10 values are comparable to background stations in Northern Europe. The highest daily aerosol concentration was 57 µg m^{-3} for PM10, with hourly PM10 with > 100 µg m^{-3}. Higher aerosol concentration occurs in late austral summer when the soil water content in the upper soil layer is significantly lower than in early summer. Long-range transport of dust originating in Patagonia was observed during aerosol measurements (Kavan et al., 2018). A higher proportion of long-range transported dust was found in snow pits on higher elevated glaciers compared to a higher proportion of locally transported dust in lower elevated glaciers (Kavan et al., 2020b). Kňažková et al. (2020) identified a redistribution of mineral material within the HLD source area in Abernethy Flats, impacting the local microtopography.

3.4.2.2 Marambio, Antarctic Peninsula

The Marambio Base (64°14'S, 56°37'W, 198 m a.s.l.) on Marambio Island, Graham Land, Antarctic Peninsula, is a member of the Global Atmosphere Watch (GAW) programme of the WMO, with personnel available year-round. This region has ice-free areas and cold desert soils (Cryosols) that can be seasonally susceptible to wind erosion and weathering. The removal of fine materials occurs mainly by wind action. The Finnish-Argentinian co-operative research in Marambio includes measurements of ozone, solar irradiance, aerosols, and ultraviolet (UV) albedo (Aun et al., 2020). The UV Biometer Model 501 from Solar Light Co. (SL501) UV albedo data of 2013–2017 in Marambio were used to analyze the effects of local HLD on measured snow UV albedo and solar UV irradiance and differences in simulated UV irradiances (Meinander et al., 2018; data not presented here). For validating the UV albedo data, surface photos were taken regularly. The surface photos and UV albedo measurements show that local dust can be detected on the snow and ice. Also, the optical dome of the SL-501 sensor was found to be sandblasted by the windblown dust when returning to Finland for maintenance. These findings suggest that in Marambio, local dust can decrease surface snow/ice albedo, possibly enhance the cryosphere melt, and contribute to warming in the Antarctic Peninsula due to the ice-albedo feedback mechanism.

3.4.2.3 McMurdo Sound, Antarctica

The McMurdo Sound area of the Ross Sea region is widely recognized as the dustiest place in Antarctica, where locally sourced aeolian accumulation is up to two to three orders of magnitude above global background and dust fallout rates for the continent (Chewings et al., 2014; Winton et al., 2014). The area includes the McMurdo Dry Valleys (MDV), the largest ice-free area (4 800 km^2) in Antarctica. The MDV has high but extremely variable fluxes of locally derived aeolian sand (e.g., Speirs et al., 2008; Lancaster et al., 2010; Gillies et al., 2013; Diaz et al., 2020) and common aeolian landforms. Such has led to the assumption that the MDV is a significant regional dust source (e.g., Bullard, 2016). Some modeling studies suggest the MDV could supply large volumes of dust to a wide area of the Southern Ocean (e.g., Bhattachan et al., 2015). However, field-based observations show that very little sediment is transported out of the MDV (Ayling and McGowan, 2006; Atkins and Dunbar, 2009; Chewings et al., 2014; Murray et al., 2013) because the valleys have already been extensively winnowed into a well-developed deflation surface and large coastal piedmont glaciers form a topographic barrier, preventing aeolian sediment from escaping. The dominant source of aeolian sediment in the McMurdo Sound area is the debris-covered surface of the McMurdo Ice Shelf (1500 km^2), with minor contributions from local ice-free headlands. This ice shelf is unusual because it has high surface ablation and a continuously replenishing supply of fine-grained sediment advected from the seafloor. The sediment is blown off the ice shelf by frequent intense southerly wind events, forming a visible sediment plume onto coastal sea ice. Within a few km of the ice shelf, accumulation rates on sea ice are up to 55g m^{-2}yr^{-1}, reducing rapidly downwind to an average of 1.14 g m^{-2} yr^{-1}, equating to 0.6 kt yr^{-1} of aeolian sediment entering McMurdo Sound annually (Atkins and Dunbar, 2009; Chewings et al., 2014). Some sediment is transported at least 120 km from the source and could travel much farther, contributing iron-rich dust to the Ross Sea (Winton et al., 2014). Coastal areas and lowland parts of the MDV are on the

413 threshold of climatically driven change with observed increases in ablation and seasonal meltwater flow incising into

414 permafrost (Fountain et al., 2014), suggesting the dust potential of McMurdo Sound and MDV could rapidly change. The

415 McMurdo Dry Valleys (4800 km^2) is estimated to best fit Category 3 (source with unknown activity, Table S1). The McMurdo

416 Ice Shelf 'debris bands' are estimated to best fit Category 2 (moderately active source).

3.4.2.4 Schirmacher Oasis, East Antarctica

418 The Schirmacher Oasis (70° 45′ 30″ S, 11° 38′ 40″ E) is approximately 80 km from the coast of Lazarev Sea, Queen Maud

419 Land, East Antarctica. The oasis is an ice-free area of over 35 km^2 with typically hillocky relief. The oasis and surrounding

420 area have been explored since the early 1960s. However, no systematic studies of dust on local ice and snow have been done.

421 Most of this region's dust is assumed to be formed with the soils blown in the air because of strong winds. Human activity

422 produces some of the dust in this region: The oasis shelters four bases, which use diesel oil and petrol to supply heat and

423 transport operations. Two airports are nearby, which operate during the summer—lasting from late November to late February.

424 In December 2019, we collected the snow samples on eleven sites near the local ice roads, bases, and airports. These data will

425 contribute to our future study.

3.4.3 Canada

3.4.3.1 Lake Hazen, Ellesmere Island

428 Evidence of dust activity in Canada has been reported, e.g., in the prairie, crater lake, and river valley environments (e.g.,

429 Wheaton et al., 1990; Neuman, 1990; Wheaton, 1992; Hugenholtz and Wolfe, 2010; Fox et al., 2012). Satellite observations

430 of high-latitude dust events over water are relatively common (see, for example, Bullard et al., 2016). Whether directly

431 concerning explicit plume remote sensing or indirectly regarding plume deposition, the detection of such events has remained

432 largely unreported. Ranjbar et al. (2021) recently reported detecting a drainage-flow induced dust plume over (frozen) Lake

433 Hazen, Nunavut, Canada, using a variety of remote sensing techniques (Lake Hazen is the Arctic's largest lake, by volume, at

434 81.8°N latitude in the northernmost portion of Ellesmere Island). Figure 6 shows a true-color georeferenced RGB MODIS-

435 Terra image acquired on 19 May 2014 at 19:50 UT (15:50 EDT) over Lake Hazen. The authors employed MISR stereoscopy,

436 CALIOP, and CloudSat vertical profiling, as well as MODIS thermal IR techniques, to identify and characterize the plume as

437 it crossed over a complex springtime terrain of snow, ice, and embedded dust. While limited by the lack of dedicated dust

438 remote sensing algorithms over snow and ice terrain, the plume characterization boded well for developing systematic,

439 satellite-based, high-latitude dust detection approaches using current and future generations of aerosol and cloud remote

440 sensing platforms.

441

442
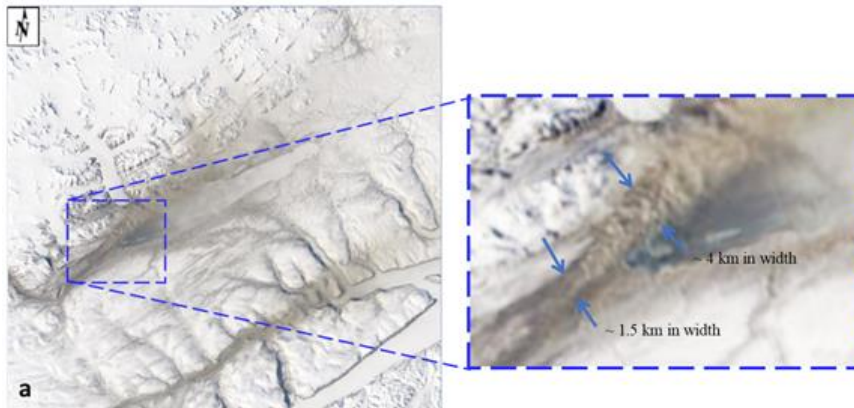
Figure 6. MODIS-Terra satellite image on 19 May 2014 at 19:50 UTC (a) True-color image: MODIS channels 1 (620–670nm), 3 (459–479 nm), and 4 (545–565 nm) were loaded into the RGB channels of the display. The sub-image is a zoom of the most discernible part of the plume (outlined by the blue broken-line square).

3.4.3.2 Kluane Lake, Yukon

Within the St. Elias Mountain range at the north end of the Pacific Coast Range on the continental side of the Yukon Territory lies the Kluane Lake region (KLR), which contains Łhù'ààn Mân' (Kluane Lake) (no. 50 in Fig. 1). The lake is fed primarily from the meltwater of the Kaskawulsh glacier down the A'äy Chù (formally the Slims River) and snowmelt from the surrounding regions in the springtime. This seasonal discharge has, in recent history, been known to be highly variable as the glacier terminates at the fork of two distinct watersheds—one draining into the Bering Strait through the Yukon River and the other into the Gulf of Alaska—supplying the two watersheds' inconstant ratios. In 2016, most of the glacier's discharge was diverted to the Gulf of Alaska in an intense discharge event, dramatically decreasing the Łhù'ààn Mân's water levels and increasing the dust emission potential from the A'äy Chù (Shugar et al., 2017). This drastic change makes the KLR an excellent natural laboratory for investigating the impact of pro-glacial hydrology on dust emission potential under past and future climates. Research was conducted in the early 1970s in this same valley as a comprehensive set of dust flux measurements as part of several publications (Nickling, 1978; Nickling and Brazel, 1985). Nickling (1978) concluded that there is a dynamic relationship between soil moisture (driven by precipitation and nighttime radiation insolation) and wind, resulting in periodicity of dust emissions from the valley in all but the mornings throughout the snow-free seasons. Within a more recent study by Bachelder et al. (2020), soil and aerosol samples were collected within the Ä'äy Chù delta, where air quality thresholds were exceeded, indicating a negative impact on local air quality throughout May. Notably, daily particle size distributions of PM10

463 were very fine (mode of 3.25 µm) compared to those measured at more well-characterized, low-latitude dust sources.

464 Moreover, mineralogy and elemental composition of ambient PM10 were found to be enriched in trace elements (e.g., As and

465 Pb) compared to dust deposition, bulk soil samples, and fine soil fractions (d < 53 µm). Finally, through a comparison of the

466 elemental composition of PM10, dust deposition, and fine and bulk soil fractions, as well as meteorological factors measured,

467 Bachelder et al. (2020) propose that the primary mechanisms for dust emissions from the Ä'äy Chù are the rupture of clay

468 coatings on particles and the release of resident fine particulate matter.

3.4.4 Denmark and Sweden

470 In Denmark, large areas with severe wind erosion have been documented (Kuhlman, 1960). Published literature on the activity

471 of dust sources in Denmark is rare; some documentation is only in Danish. On 23 April 2019, a dust plume from Denmark's

472 west coast, with dust plumes from Sweden 12 km long Mellbystrand around the mouth of the Lagan River (no. 51 in Fig. 1);

473 Poland could be observed in Meteosat-11 Dust RGB and Natural Colour images, 23 April 12:30 UTC. These dust plumes were

474 observed to travel to the North Sea (Meteosat, 2019). The source in Denmark appears to be from Holmsland Dunes (no. 15 in

475 Fig. 1). Other potential dust sources in Denmark include, e.g., the Råbjerg mile (no. 1 in Fig. 1), the largest moving dune in

476 Northern Europe with an area of around 2 km^2 (Doody et al., 2014), located between Skagen and Frederikshavn. Råbjerg Mile

477 moves at approximately 15 meters per year due to wind and has moved around 1.5 km further east in the last 110 years. The

478 drifting sand is not considered to be transported very far. In general, dust storms in Denmark are considered small, and locally

479 based dust storms can be expected when farmers prepare the arable soils in spring, creating dust in case of a very dry April

480 month. In Tilviden, flying sand took over (after King Frederik II cut the oak trees for building ships in 1600). Also, a regional

481 soil and sand event in Denmark, reportedly common in April, was recently documented between Mejrup and Holtebro on 6

482 April 2021 (Television Midtvest, 2021; not identified in Fig. 1; coordinates are estimated as 56º23'N, 8º41'E). This location

483 between Mejrup and Holtebro remains to be marked as a potential dust source for future observations. The event was observed

484 over roadways in several parts of the region, reducing visibility due to a long period without rain and with strong winds for >

485 24 hours, causing the soil to blow off the harrowed fields.

3.4.5 Greenland

487 Greenland's ice-free areas have long been identified as locally important dust sources (Hobbs, 1942), with dust storms

488 described as reaching >100 m high (Dijkmans and Törnqvist, 1991). These storms can cause the darkening of the Greenland

489 Ice Sheet by deposition, which may affect albedo and rates of ice melt (Wientjes et al., 2011; McCutcheon et al., 2021).

490 Potential dust source areas in Greenland are mapped in the recently issued global dust atlas by A. Vukovic (UNCCD, 2021).

491 Dust input to soils and lakes may also have substantial ecological impacts (Anderson et al., 2017). Bullard and Mockford

492 (2018) investigated the seasonal and decadal variability of dust emissions in southwest Greenland and presented the first long-

493 term assessment of dust emissions. Dust emissions occur all year but peak in spring and early autumn. The evidence linking

494 increased dust emissions to preceding jökulhlaup (a type of glacial outburst flood) events is inconclusive, requiring further

495 exploration. The decadal record confirmed that dust-storm magnitude may have increased from 1985 to the 1990s (Bullard
496 and Mockford, 2018). Amino et al. (2020) also showed that dust deposition on the southeastern dome in Greenland has
497 increased in recent decades. They link this increase to dust emissions in coastal Greenland, where snow cover is decreasing.
498 However, further work is needed to characterize the magnitude of dust events at the source and how their emissions are
499 changing. Bullard and Mockford (2018) also presented preferential dust-event pathways from Kangerlussuaq, indicating that
500 most events travel toward the Davis Strait and the Labrador Sea, where the dust might impact boundary layer of mixed-phase
501 clouds (Murray et al., 2021).

502 Modern satellite remote sensing methods can detect dust storm events in Greenland's different valleys and coastal areas. The
503 new HLD sources identified in this study based on satellite observations are in Supplementary Table S3. Figure 7 illustrates
504 one such dust storm episode on the Nuussuaq Peninsula, Greenland, on 1 October 2020 (Markuse, 2020). One example of
505 DREAM regional-scale modeling of atmospheric transport of dust from Greenland potential dust sources is demonstrated in
506 Figure 8 (animation available in Supplementary), where the DREAM circumpolar prediction experiment example shows the
507 predicted surface dust concentration for 4 November 2013 and Icelandic volcanic desert dust to reach Greenland, as discussed,
508 e.g., in Meinander et al. (2016).

509

511 **Figure 7. High-latitude dust storm on the Nuussuaq Peninsula, Greenland – 1 October 2020 (Markuse, 2020; cc-by-2.0.2020)**

512
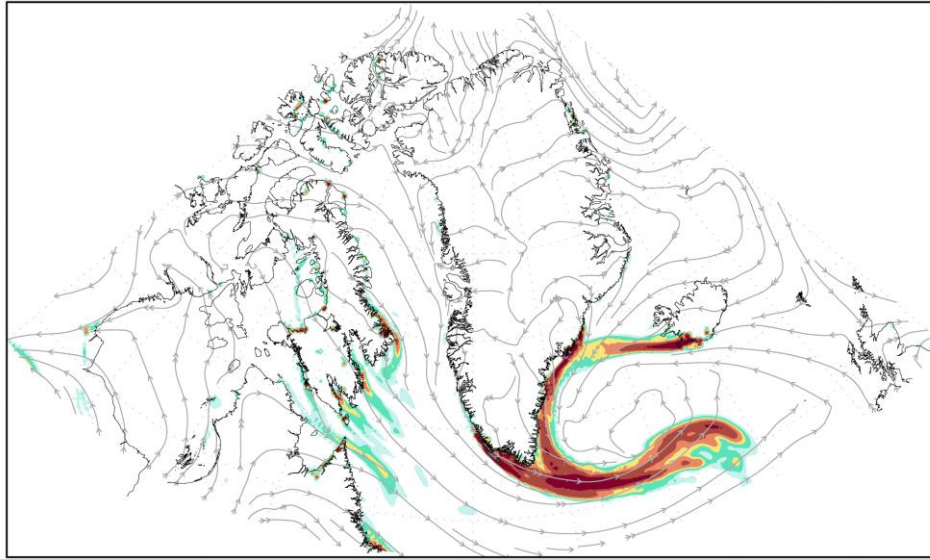
Figure 8. DREAM model predicted dust load for 4 November 2013 (animation available in Supplementary).

3.4.6 Iceland

Iceland has been recognized for a while as a potentially important dust source. In our collection, 13 new sources in Iceland were included (Table S2), compared to previous sources, in which eight Icelandic dust hot spots were identified (Arnalds et al., 2016). Sandkluftavatn, Kleifarvatn, Skafta jökulhlaup deposits and other areas have also been found to produce large amounts of dust (Dagsson-Waldhauserová et al., 2019). In recent years, increased dust activity has been reported in Flosaskard and Vonaskard (Gunnarsson et al., 2020). These dust hotspots cover almost 500 km^2, while deserts are over 45 000 km^2 (Arnalds et al., 2016). Most of the dust hotspots are near glaciers: glacial floodplains, old lakes, jökulhlaup (a type of glacial outburst flood) deposit areas, or sandy beaches. Glacio-fluvial plains receive a massive amount of unconsolidated silty material during the melting of nearby glacial regions.

524   New dust sources with the number of events are identified here and presented based on satellite image observations from 2002
525   to 2011 (Supplementary Table S2), suggesting that Iceland's entire southern coast could be considered one source. However,
526   previous results on Icelandic dust suggest that nearby locations may have different particle characteristics (Fig. 9). Therefore,
527   each source must be studied independently. For example, the grain size distribution curves of the samples from Dyngjusandur,
528   Hagavatn, Landeyjarsandur, Maelifellsandur, Myrdahlsandur, and Sandkluftavatn showed generally unimodal distributions
529   with a rather diverse character (average diameters ranging from 19.8 to 97.7 µm, Fig. 9). Richards-Thomas et al. (2021)
530   identified a range in particle diameter between 0.4 µm and 89 µm, with the medians (d50) of the distributions from 12 to 25
531   µm). Some hotspot particles are bimodal with peaks at 2 µm and 30 µm and a more significant proportion of the sample within
532   the silt-size range.
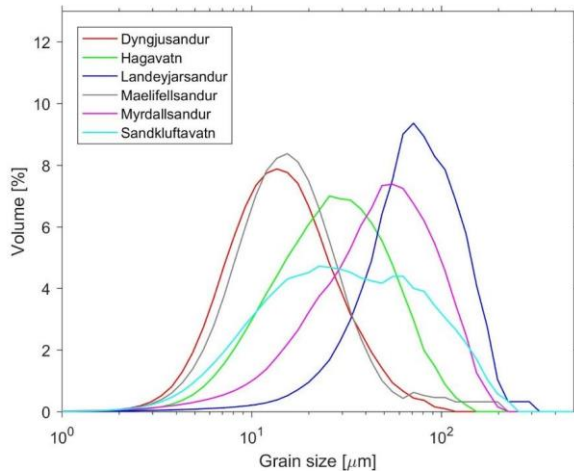
533

534   **Figure 9. Grain size distributions of samples from Icelandic source areas (redrawn from Varga et al., 2021)**

535   Icelandic dust particles have different shapes, lower densities, higher porosity, increased roughness, and darker colors than
536   other desert dust (Butwin et al., 2020; Richards-Thomas et al., 2021). Those greater than 20 µm retain the volcanic
537   morphological properties of fresh volcanic ash. Dust and fresh volcanic ash particles less than 20 µm are crystalline and blocky.
538   Icelandic dust particles contain amorphous glass, large internal voids, and copious dustcoats comprised of nano-scale flakes.
539   The amorphous basaltic material is mostly aluminosilicate glass ranging from 8 wt% (Hagavatn hotspot) to 60–90 wt%, with
540   relatively high total Fe with higher Fe solubility and magnetite fraction than low-latitude dust (10–13 wt%, Baldo et al., 2020).
541   PM10 concentrations measured during severe Icelandic dust storms well exceeded 7000 µgm^{-3} (Dagsson-Waldhauserová et

542 al., 2014, 2015; Mockford et al., 2018). Submicron particles contribute with high proportions (> 50%) to PM10 mass
543 concentrations and number concentrations (Dagsson-Waldhauserová et al., 2014, 2016, 2019). Aeolian transport of 11 t of
544 dust over one meter transect was measured during the severe dust/ash storm in 2010, when grains > 2 mm were uplifted
545 (Arnalds et al., 2013).

546 As well as differences in Icelandic dust sources, the chemical composition of the aircraft-collected Icelandic dust particles has
547 a different chemical signature than, e.g., airborne Saharan dust particles transported to Barbados (Sanchez-Marroquin et al.,
548 2020). This difference can be observed in Figs. 10a and 10b, where the chemical composition of most Icelandic dust particles
549 falls in a different area of the chemical composition ternary diagram than the Saharan dust particles from Barbados. One of the
550 most prominent differences between these types of dust is Ti's presence in ~ 30% of the Icelandic dust particles, while this
551 element is almost absent in the Saharan dust particles and dust collected elsewhere, shown in Fig. 10c. Furthermore, the
552 chemical composition of the aircraft-collected Icelandic dust is consistent with surface scooped samples of dust or volcanic
553 ash from Iceland. Moreover, a droplet freezing-based assay confirmed that the sampled Icelandic dust has a high ice-nucleation
554 ability and can influence the radiative and lifetime properties of clouds containing water and ice.

555
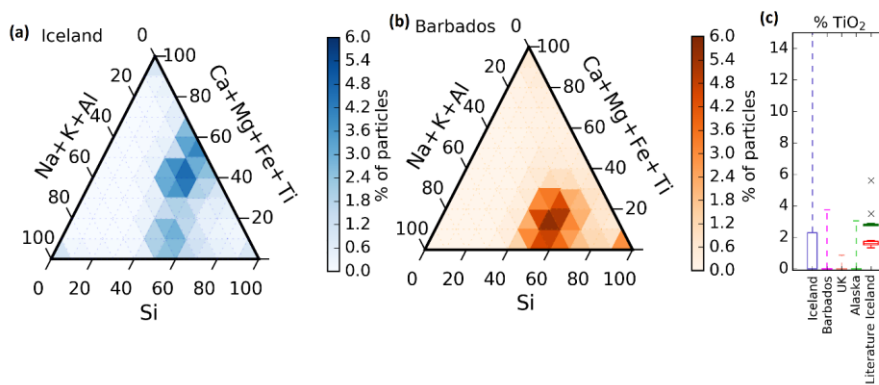
556

557 **Figure 10. Ternary graphs of the chemical composition of Icelandic dust particles (a) and Saharan dust particles collected in**
558 **Barbados (b). Each graph contains a heat map with the percentage of dust particles in each sample compositional bin. The chemical**
559 **composition of each aerosol has been recalculated from the weight percentages given by the SEM software, excluding elements that**
560 **are not Si, Al, Fe, Mg, Ca, Na, K, Ti, Mn, and P. (c) The box represents particles in the Q3 percentile of the percentage of the**
561 **composition of Ti in all the dust particles in each sample (Icelandic dust, Saharan dust collected in Barbados, dust collected in the**
562 **UK, and dust collected in Alaska). The whiskers represent the composition of all particles between the median plus and minus two**

563 **standard deviations. The data has been compared with the Ti weight percentage of different Icelandic dust and ash samples from**
564 **the literature. (Figure extracted from the Supplementary Material of Sanchez-Marroquin, 2020).**

565 No direct observations or measurements of the new sources were available. Instead, two model computations are presented for
566 Iceland because of the lack of observations and complexity of the AOD interpretation in polar and subpolar regions. Without
567 high uncertainty of direct measurements, the importance of the HLD modeling rises; models validated over better-observed
568 regions may become an important or primary source of information. Results using the DREAM model, with a horizontal
569 resolution of ~3.5 km, were used here to resolve the heterogeneous and small-scale character of the Icelandic dust sources
570 (Fig. 11). As the first operational numerical HLD model, DREAM-ICELAND predicted the Icelandic dust for the example
571 case of 18 September 2020 (Fig. 11).

572
573
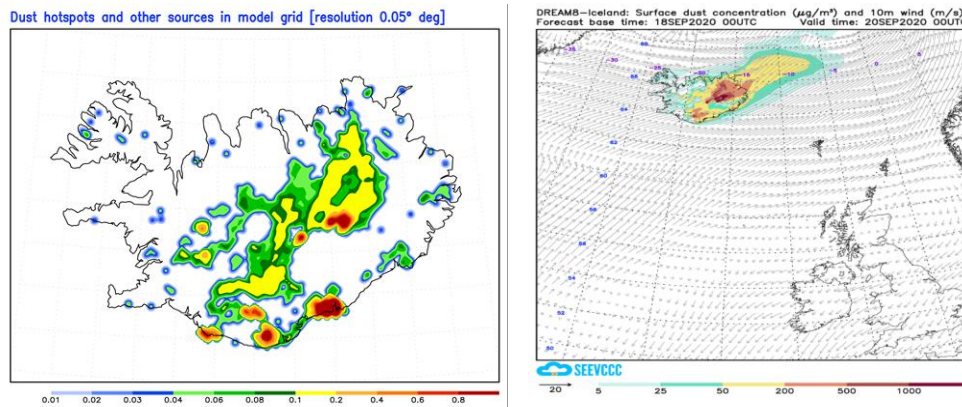
574

575 **Figure 11. Left panel: dust sources in DREAM-ICELAND model grid with areas vulnerable to erosion and containing hot spots**
576 **(Arnalds et al., 2016). Right panel: An example of the operational Icelandic dust surface concentration forecast for 18 September**
577 **2020 (available at the Republic Hydrometeorological Service of Serbia site, http://www.seevccc.rs/?p=8).**

578

579 In Figure 12, dust emissions in Iceland are presented in three-months periods for March 2020–August 2021. The modeled
580 results clearly show the seasonal nature of the dust sources. The summer season (June–August) appears to be the strongest
581 dust season. However, there are also dust emissions in wintertime with snow-covered land surfaces, according to observations
582 of dust events during snowfall (e.g., Dagsson-Waldhauserová et al., 2015). The 2021 summer season in these modeled emission

583 results appears in the same locations as summer 2020 but with more severe emissions in the highlands in 2021, agreeing with
584 the field observations in Vatnajökull national park during the HiLDA measurement campaign in the 2021 season
585 (https://gomera.geo.tu-darmstadt.de/wordpress/), where the most severe dust events were measured.
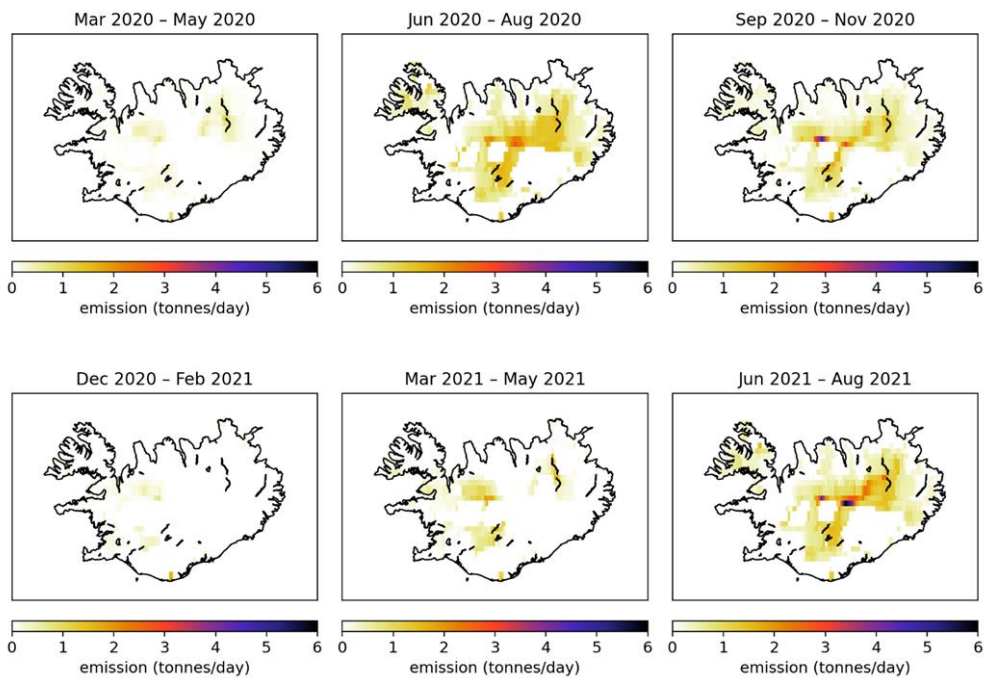
586
587 **Figure 12. SILAM modeled dust emissions (tonnes/day) in Iceland for three months periods in March 2020 – August**
588 **2021.**
589

590 **3.4.7 Russia**

591 The Russian Arctic and subarctic are the most relevant regions connected to the HLD sources. In these territories, atmospheric
592 dust is produced due to burning gas (Novy Urengoy is named the gas capital of Russia) and forest fires (especially in Siberia;
593 see MODIS or Sentinel images for Novy Urengoy on 3-8 August 2021), dusting of abandoned and non-reclaimed heaps).
594 Wind erosion is followed by vegetation destruction from gas and oil extraction, especially in Western Siberia. Some Russian

sources included in our collection (e.g., no. 7 and 8 of Fig. 1) could be identified as dust sources on the periphery of HLD and low-latitude source regions. Source no. 7 of Fig. 1 is the Altai Mountains. Some parts of these territories are covered by permafrost, where winter lasts for 5–6 months. From October, in lower mountains (less than 1000 m a.s.l.), and from September, in higher mountains (more than 1500 m a.s.l.), a stable snow cover persists. The mean daily air temperature during winter within the lower, middle, and higher mountains is –21°C, –29°C, and below –30°C, respectively. Source no. 8 is in Central Kazakhstan. From late December to early March, a stable snow cover from 5 cm to 30 cm occurs within plains and up to 50 cm within hollows. Periods of snow cover and thaw correspond to transitions of the mean daily temperature of air through 0°C, which, on average, are the 7 November and 23 March plus/minus 10–12 days. From early January to late February, the air's mean daily temperature can be as low as –20°C. Soil Atlas of the Northern Circumpolar Region (https://esdac.jrc.ec.europa.eu/content/soilatlas-northern-circumpolar-region) covers all land surfaces in Eurasia and North America above the latitude of 50°N. Thus, these territories are considered high-latitude.

3.4.7.1 Western Siberia, Altai Mountains, and Central Kazakhstan

In the most widespread undisturbed soils (Gleysols, Phaeozems, Podzols, Retisols, and Stagnosols) in Western Siberia (Semenkov et al., 2015a, 2015b)—the vastest plain in the world—mineralogical and elemental composition (Supplementary Table S6) were studied using X-ray diffractometry, X-ray fluorescence spectrometry, ICP-MS, ICP-AES, and content of total organic carbon (TOC), as reported in detail in (Semenkov et al., 2019; Semenkov and Koroleva, 2019; Semenkov and Yakushev, 2019). At locations no.7 and no. 8 of Fig. 1 (Table 4), the concentration of N-containing substances, pH values, dust content and dust deposition rate were measured in snow in winter from 2009 to 2019 (Koroleva et al., 2016, 2017; Semenkov et al., 2021; Sharapova et al., 2020).

Table 4. Major ions (mg/L), pH value, dust content (mg/m^2 in snow), and deposition rate (mg/m^2/d) during winter at HLD sources no. 7 and no. 8 in Fig. 1.

HLD no	M	SD	Me	Min	Max	N
No. 7						
Dust content mg/m^2	316	439	112	0	1542	30
NH$_4^+$ mg/L	0.75	0.98	0.30	0	3.60	43
NO$_2^-$ mg/L	0.015	0.019	0.008	0	0.08	107
NO$_3^-$ mg/L	2.3	3.4	1.4	0	20.4	118
pH	6.6	0.8	6.7	4.1	8.4	129

No. 8						
Dust deposition rate mg/m²/d	1.67	1.67	1.08	0.05	6.6	38
NH_4^+ mg/L	0.20	0.009	0.10	0	1.34	682
NO_2^- mg/L	0.027	0.007	0	0	0.61	127
NO_3^- mg/L	0.47	0.02	0.19	0	3.93	697
pH	6.1	0.02	6.1	4.6	8.0	585

M – mean, max – maximum, Me – median, min – minimum, N – number of observations, SD – standard deviation

3.4.7.2 Murmansk region: Apatity, Kirovsk, Kovdor

Large amounts of displaced rock have been breaking the balance of geological emissions of gas and dust from mining, dumps, and tailing pits (e.g., Csavina, et al. 2012). Over 150 Mt of industrial wastes are disposed of in the Murmansk region annually, achieving about 8 Gt (Supplementary Table S7). The dusting of processing tailing is one of the main sources of air pollution resulting from suspended matters near the mining enterprises. About 30% of all suspended matter is released from the mining enterprises into the atmosphere due to wind-induced dusting of beaches and slopes of tailings dumps. Elevated concentrations of suspended matter are registered every summer in Apatity's atmosphere. Dust storms from technogenic dust sources of the mining industry on the Kola Peninsula are presented, e.g., in Baklanov and Rigina (1998), Baklanov et al., (2012), and Amosov and Baklanov (2015).

3.4.7.3 Tiksi

Aerosol characterization was performed at the Hydrometeorological Observatory (HMO) Tiksi (71.36N; 128.53E) on the coast of the Laptev Sea in Northern Siberia from 2014 to 2016 (Popovicheva et al., 2019). FTIR analyses of functionalities and ionic and elemental components provided insight into the dust source-influenced and season-dependent composition of East Siberian Arctic aerosols. Analysis of wind and aerosol pollutants roses, with long-range transport analysis, helped identify the dust sources at Tiksi, demonstrating impacts from lower latitudes or local emissions from the adjacent urban Tiksi area. In warm periods, Na^+, Cl^-, K^+, and Mg^{2+} are found to be the major ions in the sea-salt aerosols, which are ubiquitous in the marine boundary layer, significantly impacting the dust concentrations in the coastal region. However, Cl^- and K^+ could also originate from biomass burning during the warm period. Ammonium is mainly produced by the soil and emission from biota and the ocean, commonly found in the form of $(NH_4)_2SO_4$ and NH_4Cl. Like sulfates, ammonium is influenced by regional sources of

637 secondary aerosol formation and transport. Bands of carbonates CO_3^{2-} (at 871 cm^{-1}) and ammonium NH_4^+ (3247 cm^{-1}) indicate

638 the dominance of dust carbonates in the natural inorganic aerosol. Also, S, Fe, Na, Al, Si, Ca, Cl, K, Ti, Mn, Co, Cu, Zn, Ga,

639 Sr, Ba, Hg, and Pb were detected in the background dust, with sulfur displaying the highest concentration, followed by Fe, Na,

640 and Al.

641 According to individual particle analyses by SEM-EDX, during the summer and autumn, when the wind comes from the

642 southwest and air masses arrive from the ocean, aerosol particles demonstrate a large variability in shapes, sizes, and

643 composition (Fig. 13.1). Elemental composition is characterized by a dominant weight percentage of C, K, Na, Cl, O, and Fe.

644 The distribution of elements over particles is heterogeneous, with greater amounts of Cl, K, and Na than C and O in around

645 50% of particles, indicating that background aerosols contain soil, salts, minerals, and carbonaceous compounds. Group Na-

646 rich with dominant Na and Cl is the most abundant at 32.5%, originating from sea spray near the ocean (Fig. 13.2). The other

647 particles contain small amounts of K, Ca, and Mg from seawater impurities, as well as S, gained through acid displacement.

648 The second most abundant group of individual particles is Group K-rich at 28.8%, dominated by K and Cl, which are not of

649 marine origin because the concentration of NSS K$^+$ ions significantly exceeds K's possible concentration in SSA. Instead,

650 Group K-rich particles are of natural mineral sylvite (KCl), transformed from genuine ones because the average weight ratio

651 of K/Cl was found to be equal to 3.3—significantly higher than 1.1—in sylvite (Fig. 13.3). KCl is water-soluble and may react

652 in a polluted atmosphere. The variation of wt% of K vs. Cl shows the lack of Cl compared to genuine sylvite and the formation

653 of complex chemical compounds K_xCl_y with various K and Cl atoms. A representative micrograph of particles in Group K-

654 rich demonstrates the reacted sylvite in Fig. 13.3, with slight damage by an electronic beam that can prove the presence of

655 nitrates that were easily evaporated during EDX analyses. A part of Group Na-rich and K-rich, 20% and 5%, respectively,

656 contains Na, Cl, and K and is assumed to be particles comprised of natural sylvite from alternative layers of halite and sylvite

657 (nNaCl + mKCl) (Fig. 13.4). They have distinctive mineral shapes and are stable regarding evaporation by an electron beam.

658 About 14.8% of individual particles composed of Group Organic made almost exclusively from C and O. These particles are

659 roughly spherical or liquid-like shaped (Fig. 13.5): Around half contain only C and O, being probably secondary organic

660 aerosol from the biogenic source; the other half come from the seawater of the Arctic Ocean, as demonstrated by trace amounts

661 of Na, Cl, and Mg. The oxidation of volatile organic compounds, humic-like substances (HULIS) in the marine environment,

662 perhaps contributes to observed organic matter.

663 Finally, a few biogenic particles such as pollen, spore, algae, bacteria, and plant or insect remnants are found in natural aerosols,

664 indicated by the specific shape and presence of K, S, Si, and Cl with C. The remaining groups—Fe-rich (14.4%), Ca-rich

665 (6.4%), and Al, Si-rich (3%)—are representative of atmospheric dust derived from the Earth's crustal surface. Dust particles

666 have solid irregular shapes of round and euhedral morphology. Analyses of the soil sample taken near the CAF showed stony

667 material with minimal fertile ground cover. EDX analyses demonstrated 27.7 and 9.8 wt% of Si and Al, 46 and 10.6 wt% of

668 O and Fe, respectively, and 3.5 w% of K in various Fe,K—aluminosilicates containing small additives (less than 1.7 wt%) of

669 Na and Mg. Since the tiny dust of stony soil may be easily dispersed into the atmosphere by wind, we assume that Group Al,

670 which is Si-rich, and around half of Group Fe-rich, is composed of Fe,K—aluminosilicates (Fig. 13.6). Group Fe-rich

671 containing Fe, Ni, Ca, and Si is composed of soil particles of iron-nickel ore (Fig. 13.7). Finally, Ca carbonates and sulfates

672 with Ca, C, S, and O are found in Group Ca-rich (Fig. 138.8), according to the observation of Ca^{2+}, CO_3^{2-}, and SO_4^{2-} ions

673 described above. With aluminosilicates, they are most likely windblown dust.
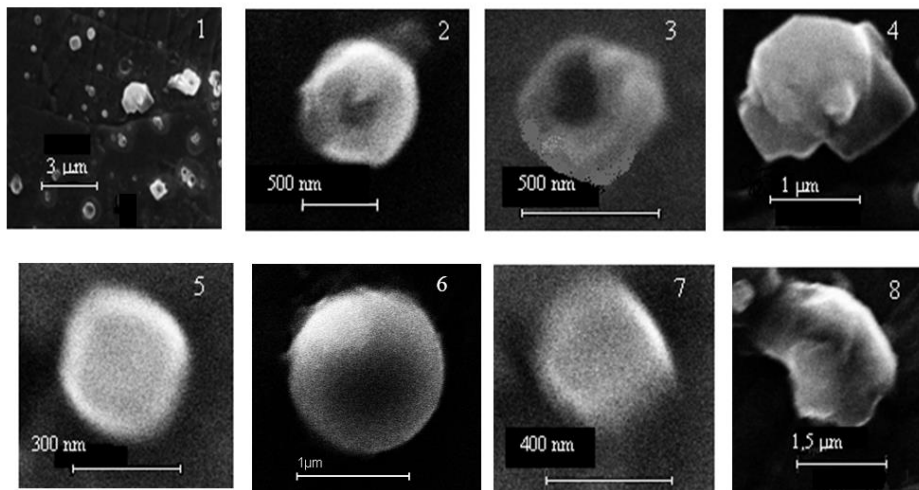
Figure 13. 1. Panorama and representative micrographs of natural background aerosols at HMO Tiksi; 2. reacted sea salt NaCl in Group Na-rich; 3. reacted sylvite KCl and 4. sylvinite (nNaCl + mKCl) in Group K-rich; 5. an organic particle in Group Organic; 6. Fe, Ca- aluminosilicate in Group Al, Si-rich; 7. Fe/Ni particle in Group Fe-rich and 8. CaCO₃ in Group Ca-rich of natural aerosols on 27.09.2014. New unpublished results of Popovicheva et al. (2019) investigation.

3.4.8 South America and Patagonia

683 Extending from 39°S to 54°S, with an area of 600 000 km², dust activity (Fig. 14) from this large desert remains largely

684 unknown. Some basic facts must be formally assessed, such as the location of sources and geomorphological features

685 associated with dust, as well as the seasonality and frequency of the dust's activity. To date, limited surveys of dust activity

686 (Crespi-Abril et al., 2017; Gaiero et al., 2003; Gassó and Torres, 2019) and case studies of individual sources exist (Gassó et
687 al., 2010; Gassó and Stein, 2007; Johnson et al., 2011). Recently, a list of dust activities and sources in Tierra del Fuego
688 (Cosentino et al., 2020) has been published. Generally, dust sources in Patagonia are at topographic lows, and the river valleys
689 (e.g., the Deseado and Santa Cruz rivers) (Coronato et al., 2017; Hernández et al., 2008) are associated with the late Holocene
690 para-glacial environments. The most active modern source of dust is the drying of Colhué Huapi Lake (CHL) in Central
691 Patagonia (45.5°S and 68°W) (Montes et al., 2017)—a shallow lake with variable water levels exposed to intense
692 evapotranspiration. An anthropogenic component appears to be linked to intense farming, oil prospection, and supplying water
693 to urban centers (Gaitán et al., 2009; Hernández et al., 2008; Mazzonia and Vazquez, 2009; Valle et al., 1998). CHL has been
694 steadily shrinking (Llanos et al., 2016) and was dried up by the summer of 2020. Consequently, dust activity originating in
695 CHL has increased with frequent blowouts large enough to be easily detected from space (Gassó and Torres, 2019).
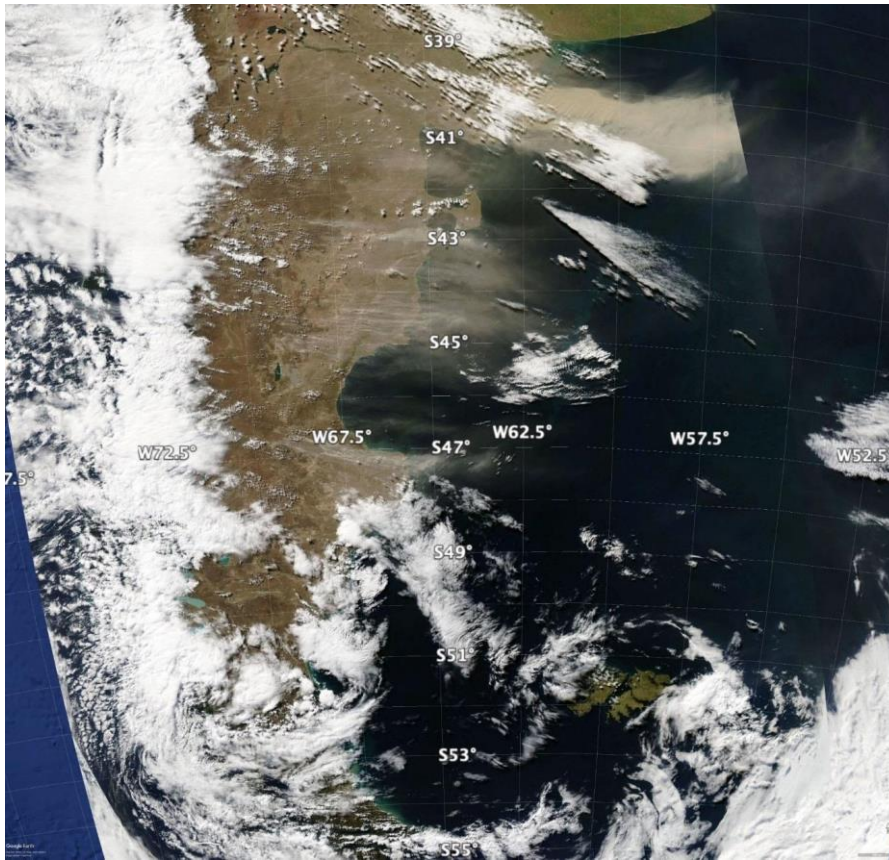
696

697 **Figure 14. A dust event spanning the north and central sections of the Patagonian Desert (+1000 km) on March 28, 2009. Events this**
698 **large occur about once every one to three years. This event is typical in that it was triggered by the passage of a powerful low-**
699 **pressure center commonly found in these high latitudes. Also, this event is singular in that a large portion of it is cloudless, enabling**
700 **a direct view from space (most dust activity in Patagonia occurs under cloudy conditions). The thick dust cloud in the upper right**
701 **corner is from an area used for cattle farming, which was undergoing a drought, whereas the active sources further south can be**
702 **considered more naturally occurring with less anthropogenic interference. Source: NASA's Worldview interface image processed**
703 **with Google Earth.**

704

705 Overall, satellite detection in the Patagonia region remains challenging. There are several difficulties in surveying dust activity

706 in the area: obstructed views from space because of cloudiness, nighttime dust activity, and sparse population. Also, except

707 for a few sources, the lack of recurrence in dust emission is a general feature of the desert: Sources that were active during one

708 season do not reactivate until two or three seasons later. A comprehensive and dedicated survey combining surface and space-

709 based detection networks is needed for a better understanding.

710 **3.4.9 Svalbard**

711 Evidence of the presence and activity of dust sources in Svalbard is only recent and quite rare. Yet, for example, dust storms

712 in Longyearbyen are reported as a regular feature in autumn. Dörnbrack et al. (2010) documented and characterized a strong

713 dust storm in the Adventdalen valley—the center of Spitsbergen Island—in May 2004, using airborne lidar observations and

714 mesoscale numerical modeling. In the same area, near Longyearbyen, dust emissions from an active coal mine were

715 documented by Khan et al. (2017). Kandler et al. (2020) also reported Svalbard measurements in Longyearbyen in September

716 2017, with high iron and chlorite-like contributions in dust.

717 The accelerated ablation of Svalbard's glaciers (Schuler et al., 2020) and the increasing melt rate of permafrost are causing

718 accelerated growth in periglacial and proglacial areas. The significance of the morphogenetic processes of deflation,

719 denudation, and sediment transport on slopes and in river channels in glaciers' marginal zones is increasing (Zwolinski et al.,

720 2013). Thus, these areas have become potential sources of dust and, as such, have been investigated for the physical and

721 chemical properties of their sediments, regardless of the documented occurrences of the dust events these areas have

722 experienced.

723 Fluvial, glaciofluvial, and weathering deposits at five different sites on the coastal plains near the Ny-Ålesund Research Station

724 (78.92481°N, 11.92474°E), NW Spitsbergen were investigated (Moroni et al., 2018). The mineralogical assemblage is

725 characterized by dolomite, calcite, quartz, albite, and sheet silicates (vermiculite, muscovite, clinochlore) in variable amounts,

726 along with monazite, zircon, apatite, baryte, iron sulfate, Fe, Ti, Cu, and Zn ores as accessory minerals. With a weight fraction

727 of 4 to 53% of particles smaller than 100 μm, these deposits should be considered a valid dust source. However, the contribution

728 is influenced by the modest extension of bare soils (less than 4 km^2) and the brief duration of the area's driest summer. The

729 composition of the aerosols collected at the Gruvebadet lab near Ny-Ålesund during the summer-fall period reveals the

730 presence of such a local dust component (Moroni et al., 2016; Moroni et al., 2018). Further evidence of local dust sources in

731 the Ny-Ålesund area and Brøgger Peninsula also results from the annual snowpack's chemical composition (Gallet et al., 2018,

732 Jacobi et al., 2019). The contribution of local dust sources on this site is of secondary importance compared to that of long-

733 range transport (Moroni et al., 2015; Moroni et al., 2016; Moroni et al., 2018, Conca et al., 2019).

734 A similar study was conducted on the loose sediment deposits in the neighborhood of the Polish Polar Station Hornsund
735 (77.00180°N, 15.54057°E), SW Spitsbergen, where a belt of nearshore plains consisting of marine terraces and nival moraine
736 bars, with bare surfaces available for mineral dust uplift from late spring, widely outcrop (Zwolinski et al., 2013). The
737 mineralogical assemblage consists of quartz, alkali feldspar, plagioclase, dark mica, and chlorite, with zircon, apatite,
738 monazite, iron sulfide, and Fe ore as accessory minerals. The same assemblage was found in the aerosols and snow cover
739 collected at the base station and the surrounding glaciers in the same period. This fact, along with the significant proportion of
740 particles smaller than 50 µm in the loose sediment deposits, supports the prevalence of the local dust source in the melting
741 season. Further evaluation of the impact of local dust sources was obtained from analyzing shallow and deep cores from
742 different glaciers in the Hornsund area (Lewandowski et al., 2020; Spolaor et al., 2020). The results suggest that for Spitsbergen
743 glaciers with the summit close (Ny-Ålesund) or below (Hornsund) the equilibrium line, the summer dust deposition from the
744 local sources is predominant, affecting the glacier ice's chemical composition. However, the dating of monazite grains and
745 presence of magnetite and iron sulfide (magnetic susceptibility and SEM data, Lewandowski et al., 2020) also suggest the
746 existence of regional wind transport from Nordaustlandet and Edgeøya, respectively. Further, a long-range component from
747 Northern Europe, Siberia, and, to a limited extent, Greenland, Iceland, and Alaska, was also evidenced (Moroni et al., 2018;
748 Crocchianti et al., 2021).

749 Recent estimations of dust load in Central and Southern Svalbard from different sources range from 4 g up to $4 - 5$ kg m^{-2}
750 (Rymer, 2018; Rymer et al. 2022), with the highest values in the Ebba Valley due to frequent dust storms in this area (Strzelecki
751 and Long, 2020). Kavan et al. (2020a) found a negative correlation between deposition rate and altitude at Pyramiden
752 (78.71060°N, 16.46059°E), the west coast of Petuniabukta, and Ariekammen (77.00035°N, 15.53674°E), and Hornsund area.
753 The pattern was clear up to the altitude of approximately 300 m a.s.l., suggesting the influence of local sources in the lower
754 levels of the atmosphere and long-range transport at higher altitudes. The lower values of the deposition rates found at
755 Ariekammen were ascribed due to the more frankly maritime climate of the Hornsund region.

756 **3.5 Climatic and environmental impacts of HLD**

757 Climatic and environmental impacts of HLD on clouds and climate feedback, atmospheric chemistry, marine environment and
758 cryosphere-atmosphere feedback (Fig. 15) were investigated with the help of topical literature surveys (Sections 3.5.1 - 3.5.4).
759 Direct radiative forcing of HLD dust (blocking sunlight) and comparison of dust and black carbon as SLCF in the cryosphere
760 are included in the cryosphere-atmosphere feedback section.
761
762 The amounts of dust emission and deposition (megatonnes) of annual global and Arctic dust (data for 2017), as compared to
763 anthropogenic and wildfire black carbon (Fig. 15), were studied using the SILAM model (Sofiev et al., 2015). The results of
764 black carbon emissions presented in Figure 15 were based on the Copernicus Atmosphere Monitoring Service (CAMS) global

765 emission inventory version 4.2 and black carbon originating from wildfires from the SILAM IS4FIRES fire emission model,

766 equaling 5 % of the total primary fire PM emissions of the model. The IS4FIRES model is based on fires observed by the

767 MODIS instrument onboard the Terra and Aqua satellites.

768

769

EMISSION (MEGATONNES)	GLOBAL DUST < 30 μm	GLOBAL DUST < 2.5 μm	ARCTIC DUST < 30 μm	ARCTIC DUST < 2.5 μm	ANTHROPOGENIC BLACK CARBON (CAMS global emissions v4.2)	WILDFIRE BLACK CARBON (5% of fire PM emissions)
Total emission	3000	160	30	1,6	4,6	1,9
Deposition on snow	32	5,2	4	0,21	0,18	0,029
Deposition on sea ice	5,5	0,59	3	0,17	0,009	0,008
Deposition on Arctic snow	7,6	1,1	4	0,19	0,027	0,013
Deposition on Arctic Sea ice	4,7	0,52	3	0,17	0,0055	0,0074
Deposition on sea surface	500	86	15	1,0	1,7	0,9
Deposition on Arctic Sea surface	21	2,4	12	0,68	0,035	0,063

770

FLUX (MEGATONNES)	GLOBAL DUST < 30 μm	GLOBAL DUST < 2.5 μm	ARCTIC DUST < 30 μm	ARCTIC DUST < 2.5 μm	ANTHROPOGENIC BLACK CARBON (CAMS global emissions v4.2)	WILDFIRE BLACK CARBON (5% of fire PM emissions)
Total emission	3000	160	30	1,6	4,6	1,9
Deposition on snow	32	5,2	4	0,21	0,18	0,029
Deposition on sea ice	5,5	0,59	3	0,17	0,009	0,008
Deposition on Arctic snow	7,6	1,1	4	0,19	0,027	0,013
Deposition on Arctic Sea ice	4,7	0,52	3	0,17	0,0055	0,0074
Deposition on sea surface	500	86	15	1,0	1,7	0,9
Deposition on Arctic Sea surface	21	2,4	12	0,68	0,035	0,063

Figure 15. Climatic and environmental impacts of high latitude dust include direct radiative forcing (blocking sunlight), indirect radiative forcing (clouds and cryosphere) as well as effects on atmospheric chemistry and marine environment. The amounts of dust emission and deposition (megatonnes) of global and Arctic dust, as compared to black carbon, were estimated using the SILAM

775 **model (Sofiev et al., 2015). The black carbon emissions are based on the CAMS global anthropogenic emission dataset v4.2 and the**
776 **wildfire black carbon emissions are based on the IS4FIRES fire emission model, equaling 5 % of the total primary fire PM emissions**
777 **of the model.**

3.5.1 Impacts of HLD on atmospheric chemistry

779 Icelandic dust, a specific HLD of volcanic origin, is constantly resuspended from the deserts. Regarding atmospheric
780 chemistry, the most substantial impact comes from the particles in the 0.002 to 10 µm range, as they can be carried over more
781 considerable distances (Finlayson-Pitts, 1999). The Icelandic dust in the troposphere is not as addressed as the impact of desert
782 dust. This HLD is very likely a long-range transporting carrier for many species adsorbed on its surface, which can act as a
783 sink of trace gases and a subsequent platform for transferring taken-up species. Along with transport, adsorbed species may
784 undergo different heterogeneous reactions that can lead to secondary compound formation. Such processes can influence the
785 reactivity and balance of atmospheric species. Optical, hygroscopic, and, more generally, physicochemical properties of the
786 HLD can change due to surface processes, implying atmospheric trace gases due to heterogeneous interactions (Usher et al.,
787 2003). The consequences can be starkly different depending on the nature of atmospheric trace gases interacting with HLD.
788 This section aims to illustrate the diversity of interactions between HLD and atmospheric trace gases to emphasize the various
789 impacts of these aerosols on atmospheric physics and chemistry. In the case of ozone, if the direct heterogeneous interaction
790 with dust does not play a major role in the atmospheric concentration decrease of the primary compound, surface processes
791 are triggered, affecting the atmospheric budget of ozone. In the case of NO_2, heterogeneous processes on dust can significantly
792 lead to HONO species forming, with direct impacts on gas-phase atmospheric reactivity. In the case of SO_2, beyond a complex
793 reaction pathway, the heterogeneous process dually affects the budget of the taken-up species and the chemical and physical
794 properties of the dust surface.

795 If the heterogeneous reaction of NO_2 on various types of atmospheric particles, e.g., salts, soot, mineral dust, and proxies, was
796 addressed in the literature (George et al., 2015), the interaction of NO_2 with volcanic particles, typical HLD desert dust, under
797 atmospheric conditions, has only been studied by Romanias et al. (2020). They explore the possible formation of a short
798 lifetime key atmospheric species, considered a trigger of numerous atmospheric processes: HONO, a precursor of OH radicals
799 in the atmosphere. To that end, NO_2 uptake on Icelandic HLD is explored under various and contrasting atmospheric
800 conditions. Despite the relatively close volcanic regions where the selected samples originate, uptake coefficients of NO_2
801 contrasted significantly with the dust location due to magmatic and morphological differences among samples. This point
802 confirms that concerning heterogeneous atmospheric chemistry, sample behavior can dramatically deviate from one class of
803 dust to another, with physical and chemical characterizations of the samples remaining key intrinsic descriptors. Nonetheless,
804 volcanic dust appears as effective NO_2 scavengers from the atmosphere. The interaction of NO_2 with HLD is evidenced as a
805 source of NO and, more interestingly, HONO, with kinetics and formation yields highly dependent on relative humidity.
806 Higher HONO formation yields on volcanic samples are observed for RH values exceeding 30% RH. Heterogeneous

807 construction of HONO from NO_2 interaction with Icelandic dust is estimated as atmospherically significant under volcanic

808 eruptions or, more frequently in Iceland, during typical volcanic dust storms. Such leads to HONO formation rates up to 10

809 pptV/hr, which can significantly influence the regional atmosphere's oxidative capacity. The experimental determination of

810 NO_2 uptake coefficient γ allows including such processes in atmospheric modeling, improving their representativeness.

811 A transient uptake of SO_2 – an initially important uptake of SO_2 that is progressively reduced – leads to low steady-state uptake

812 coefficients of SO_2 after several hours of exposure in the range of 10–9 to 10–8. The surface coverages were in the range of

813 1014 molecule cm-2 or 1016 molecule cm-2 using the total surface area or the geometric surface area of aerosols, respectively

814 (Urupina et al., 2019). Zhu et al. (2020) estimated that around 43% more volcanic sulfur is removed from the stratosphere

815 within months due to SO_2 heterogeneous chemistry on volcanic particles than without. Concomitantly with SO_2 uptake, sulfites

816 and sulfates are monitored on the surface of volcanic dust, with sulfates being the final oxidation product, attesting to SO_2

817 surface reaction. Through surface hydroxyl groups, the dust surface's chemical composition plays a crucial role in converting

818 SO_2 to sulfites, as evidenced experimentally using lab scale but atmospheric relevant experimental setups (Urupina et al, 2019).

819 This provides original insights into the kinetics and mechanism of SO_2 uptake and the transformation on volcanic material

820 under simulated atmospheric conditions, bringing an accurate perspective on SO_2 heterogeneous sinks in the atmosphere on

821 the HLD surface. The model simulations of Zhu et al. (2020) suggested that the transformation of SO_2 on such particles plays

822 a key role in the stratosphere's sulfate content. Interestingly, this transformation and accumulation of sulfates on the surface

823 of particles could turn the unreactive ozone material into reactive, especially in the stratosphere, where volcanic particles have

824 longevity.

825 The case of SO_2 uptake points to the aging of the HLD surface with subsequent impacts on its chemical (e.g., hygroscopicity)

826 and physical (e.g., optical) properties. Changes in hygroscopic properties can correlate with HLD's erratic behavior to act as

827 cloud-or ice-nucleating particles, depending on their interactions with atmospheric gases. Similarly, sulfate and sulfuric acid's

828 high surface coverage for volcanic dust, as reported by Urupina et al. (2019), questions the variability of the HLD refractive

829 index and the impact on remote sensing of fresh vs. aged dust.

830 **3.5.2 Impacts of HLD on clouds and climate feedback**

831 Clouds across the mid- and high latitudes are of first-order importance. Climate and HLDs may play a first-order but highly

832 uncertain role in defining their properties through the initiation of ice formation. Clouds frequently persist in a supercooled

833 state. However, even a few droplets converting to ice crystals through heterogeneous freezing can lead to microphysical

834 processes that dramatically reduce a cloud's liquid water content, reducing its albedo and exposing the surface underneath

835 (Murray et al., 2021; Tan and Storelvmo, 2019). Only a small subset of atmospheric aerosol can nucleate ice; concentrations

836 of around only 1 INP per liter of air active at the cloud temperature can dramatically alter cloud albedo. In contrast, the

837 concentration of aerosol particles capable of serving as cloud condensation nuclei (CCN) are orders of magnitude larger.

838 Hence, dust particles in the high latitudes will rarely exist in high enough concentrations to dramatically impact cloud droplet
839 numbers by providing additional CCN. However, high-latitude dust has been shown to serve as an effective INP in sufficient
840 concentrations to potentially impact mixed-phase clouds (Sanchez-Marroquin, 2020). Ice formation's role in climate
841 projections depends on the clouds' location. In the following paragraphs, we discuss two distinct classes of clouds that may be
842 influenced by HLD particles serving as INPs.

843 For boundary layer clouds over oceans between approximately 45–70°, the amount of ice versus supercooled water, as well as
844 albedo, is critical for global climate (Vergara-Temprado et al., 2018; Bodas-Salcedo et al., 2014). These clouds are where
845 substantial solar insolation exists, and the contrast between a high albedo cloud and a dark ocean surface is significant. Hence,
846 these clouds are implicated in the cloud-phase feedback, where water replaces ice, increasing their albedo as the world warms
847 with increased carbon dioxide (Storelvmo et al., 2015). This feedback's uncertainty is very high, with the temperature rise
848 associated with a doubling of carbon dioxide, rising from around 4 K to well above 5 K, simply by increasing the amount of
849 supercooled water in clouds in the current climate (Frey and Kay, 2018). Hence, understanding the sources of ice-nucleating
850 particles in the high latitudes, including HLDs, is critical to understanding these climate-relevant issues (Murray et al., 2021).

851 The second group of clouds is those occurring at high latitudes. For example, in the central Arctic, mixed-phase clouds play a
852 critical role in the local Arctic climate and the phenomenon of Arctic amplification. In a corollary to the cloud-phase feedback,
853 water replacing ice leads to more downward longwave radiation, resulting in positive feedback (i.e., amplification) (Tan et al.,
854 2019). Hence, the phase of clouds and, therefore, the INP population in clouds in the present Arctic atmosphere are key for
855 defining this feedback's strength. Moreover, any changes in the INP population with a changing climate may also provide
856 feedback on cloud properties (Murray et al., 2021).

857 Given the apparent importance of INPs in defining cloud properties and climate feedback, surprisingly little is known about
858 the ice-nucleating properties of HLDs. Mineral dust is one of the most important types of atmospheric INPs in clouds below
859 approximately -15°C around the globe because of its relatively high ice-nucleating activity and abundance in the atmosphere
860 (Murray et al., 2012). A handful of papers have also identified HLDs as significant contributors to the Arctic's INP population
861 (Irish et al., 2019; Sanchez-Marroquin, 2020; Tobo et al., 2019; Šantl-Temkiv et al., 2019). HLDs may differ in their ice-
862 nucleating ability from LLDs for several reasons: Firstly, the HLDs from glacial valleys, for example, are often richer in
863 primary minerals (olivenes, pyroxenes, feldspars, and amphiboles) and less rich in clays compared to LLDs. This is crucial
864 because K-rich feldspars are known for their exceptional ice-nucleating ability, whereas clays are much less active (Harrison
865 et al., 2019; Atkinson et al., 2013). Secondly, the most prominent LLD sources, like those in Africa, are abiotic (Price et al.,
866 2018), whereas it has been found that HLDs can be associated with highly effective biogenic ice-nucleating material (Tobo et
867 al., 2019; Šantl-Temkiv et al., 2019). The inclusion of biological ice-nucleating material, which can be ice-active at
868 temperatures much higher than -15 °C, may mean that these dust sources have a disproportionately greater impact on cloud

869 glaciation and climate than their low-latitude counterparts. Much more research is needed to define and understand the ice-
870 nucleating ability of these HLD sources.

871 **3.5.3 Impacts of HLD on the marine environment**

872 Mineral dust particles are a source of essential nutrients such as phosphorus (P) and iron (Fe) to the ocean ecosystems (e.g.,
873 Jickells et al., 2005; Mahowald et al., 2005; Stockdale et al., 2016). Dust deposition onto the ocean's surface can stimulate
874 primary productivity and enhance carbon uptake, indirectly affecting the climate (e.g., Jickells and Moore, 2015; Mahowald,
875 2011). The extent of these impacts primarily depends on the dust deposition fluxes, its chemical properties, and the nutrients
876 of (co)limitations patterns in the ocean waters (e.g., Boyd et al., 2007; Boyd et al., 2010; Kanakidou et al., 2018; Mahowald et
877 al., 2010; Mills et al., 2004; Moore et al., 2013; Shi et al., 2012; Stockdale et al., 2016). Arctic Ocean is often nitrogen-limited
878 (von Friesen and Riemann, 2020).

879 The aerosol fractional Fe solubility (%) is defined as the ratio of dissolved Fe (in the filtrate, which has passed through 0.2 or
880 0.45 µm pore size filters) to the total Fe in the bulk aerosol (e.g., Meskhidze et al., 2019; Shi et al., 2012). This is typically
881 used to indicate the fraction of Fe, which is likely to be bio-accessible for marine ecosystems (Meskhidze et al., 2019).

882 Sub-Arctic oceans are Fe-limited or seasonally Fe-limited. Fe limits primary productivity in the Sub-Arctic Pacific Ocean
883 (Martin and Fitzwater, 1988). The atmospheric Fe deposition in the Gulf of Alaska is dominated by dust transported from
884 glacial sediments from the Gulf of Alaska coastline (Crusius et al., 2011), with relatively high fractional Fe solubility—around
885 1.4% (Schroth et al., 2017). Although the upwelling of deep water is the major source of dissolved Fe, the atmospheric flux of
886 dissolved Fe to the Gulf of Alaska's surface water is comparable to the Fe flux from eddies of coastal origin (Crusius et al.,
887 2011). The magnitude of glacial dust's deposition to the Gulf of Alaska varies significantly depending on the regional weather
888 conditions. However, the extent of its impacts is still unclear (Schroth et al., 2017). Currently, the spatial resolution of global
889 dust models is too low to accurately reproduce Alaskan dust flux, generated by anomalous offshore winds and channeled
890 through mountains (Crusius, 2021). Recently, Crusius (2021) determined dissolved Fe inventories based on time series of
891 dissolved Fe and particulate Fe concentrations from the Ocean Station Papa in the central Gulf of Alaska, including
892 measurements from September 1997 to February 1999. The analysis showed 33%–70% increases in dissolved Fe inventories
893 between September and February of successive years. These increases were possibly linked to dust fluxes from the Alaskan
894 coastline—known to occur mostly in autumn (Crusius et al., 2011; Schroth et al., 2017). These new results support the
895 importance of atmospheric Fe's contribution, although more work is needed to confirm the sources of dissolved Fe in the Gulf
896 of Alaska.

897 The Sub-Arctic North Atlantic Ocean is seasonally Fe-limited (Nielsdottir et al., 2009; Ryan-Keogh et al., 2013). Natural dust
898 from Iceland largely contributes to the atmospheric dust deposition in the North Atlantic Ocean (Bullard, 2016). Icelandic dust

899 originates from volcanic sediments and has a relatively high total Fe content—about 10% (e.g., Arnalds et al., 2014, Baldo et
900 al., 2020). The estimated total Fe deposition from Icelandic dust to the ocean's surface is 0.56–1.38 Mt yr-1 (Arnalds et al.,
901 2014). The initial Fe solubility observed in dust samples from Icelandic dust hotspots is from 0.08 % to 0.6%—comparable to
902 that of mineral dust from low-latitude regions such as Northern Africa, while the fractional Fe solubility at low pH (i.e., 2) is
903 significantly higher than typical low-latitude dust (up to 30%) (Baldo et al., 2020). Achterberg et al. (2018) argued that deep-
904 water mixing is the dominant source of Fe in the Sub-Arctic North Atlantic Ocean's surface water, which is up to ten times
905 higher than the Fe supply by atmospheric Fe deposition. However, during the 2010 eruption of the Icelandic volcano
906 Eyjafjallajökull, Achterberg et al. (2013) observed elevated dissolved Fe concentration and nitrate depletion in the Iceland
907 Basin, followed by an early spring bloom. They measured an initial fractional Fe solubility of 0.04 %–0.14 % for Icelandic
908 ash, which is below or towards the lower end of the range of values estimated for Icelandic dust (0.08%–0.6%) (Baldo et al.,
909 2020). High deposition flux (Arnalds et al., 2016) and higher Fe solubility of Icelandic dust (Baldo et al., 2020) suggest that
910 they may impact Fe biogeochemistry and primary productivity in the surface ocean. However, more research is needed to
911 confirm this.

912 The Southern Ocean is known to be Fe-limited (Moore et al., 2013). Major atmospheric dust sources include, for example,
913 Australia, southern South America, and Southern Africa (e.g., Ito and Kok, 2017). Contribution from local sources in
914 Antarctica is also observed (e.g., Chewings et al., 2014; Winton et al., 2014; Winton et al., 2016). Winton et al. (2016) reported
915 a background fractional Fe solubility from Antarctic dust sources of 0.7%—similar to the upper limit of Fe solubilities observed
916 in Icelandic dust (Baldo et al., 2020). However, mineral dust originating from glacial sediments from the Gulf of Alaska
917 coastline showed higher Fe solubilities (1.4%) (Schroth et al., 2017)—likely due to the different mineralogy and Fe speciation
918 in the samples. The various methods used to determine the fractional Fe solubility in these studies may also contribute to this
919 difference (Perron et al., 2020).

920 Although the upwelling of deep water is a major source of dissolved Fe, the atmospheric deposition of dissolved Fe can locally
921 contribute to the phytoplankton bloom (Winton et al., 2014). However, evidence exists that increased dust flux enhanced
922 primary production in the Southern Ocean in the last glacial age (Martínez-García et al., 2014). The Ross Sea is a continental
923 shelf region around Antarctica and a highly biologically productive area in the Southern Ocean, which has important
924 implications for global carbon sequestration (e.g., Arrigo et al., 2008; Arrigo and Van Dijken, 2007). In the Ross Sea, an
925 additional Fe supply is required to sustain the intense phytoplankton bloom during the austral summer (Tagliabue and Arrigo,
926 2005). Measurements conducted on snow pits and surface snow samples showed that local Antarctic dust contributes to Fe
927 deposition. However, this contribution is only a minor component of the total Fe supply to the Ross Sea, with most being
928 supplied by the upwelling of deep water (Winton et al., 2014; Winton et al., 2016a,b).

929 In the Polar regions, atmospheric dust is mostly delivered to the sea ice, where melting and freezing cycles (ice processing)
930 can enhance the formation of relatively more soluble phases of Fe oxide-hydroxide minerals such as ferrihydrite. This
931 formation can increase the flux of atmospheric dissolved Fe to the ocean (Raiswell et al., 2016).

932 **3.5.4 HLD impacts on cryosphere and cryosphere-atmosphere feedback**

933 The cryosphere is the frozen water part of the Earth system, including sea, lake, and river ice; snow cover, glaciers, ice caps,
934 and ice sheets; permafrost and frozen ground. These components play a crucial role in the Earth's climate (IPCC, 2019).
935 Temperatures in fragile areas, such as the pristine polar regions, have been increasing at twice the global average; the highest
936 increase in the temperature on the coldest days—up to three times the rate of global warming—is projected for the Arctic
937 (IPCC, 2021). Warming in vulnerable cold climate land areas causes glacier retreat, permafrost thaw, and a decrease in snow
938 cover extent (IPCC, 2019). Consequently, potential HLD sources, such as glacial sediments, can increase (e.g., Nagatsuka et
939 al., 2021). When dust is long-range transported and wet- or dry-deposited or windblown from local dust sources, the ice and
940 snow albedo decrease and influences glacier melt (e.g., Boy et al., 2019) via the positive ice-albedo feedback mechanism
941 (AMAP, 2015; Flanner et al., 2007; Gardner and Sharp, 2010; IPCC, 2019). Cryospheric melt processes are controlled by
942 many environmental factors (IPCC, 2019), such as solar irradiance, ambient temperature, and precipitation (e.g., Meinander
943 et al., 2013, 2014; Mori et al., 2019). Kylling et al. (2018) used dust load estimates from Groot Zwaaftink et al. (2016) (using
944 low-latitude dust complex refractive index for high-latitude dust) to quantify the mineral dust instantaneous radiative forcing
945 (IRF) in the Arctic for 2012. They found that the annual-mean top of the atmosphere IRF (0.225 W/m^2) had the largest
946 contributions from dust transported from Asia south of 60°N and Africa; high-latitude (>60°N) dust sources contributed about
947 39% to the top of the atmosphere IRF. However, HLD had a larger impact (1 to 2 orders of magnitude) on IRF per emitted
948 kilogram of dust than low-latitude sources. They also reported that mineral dust deposited on snow accounted for nearly all
949 the bottom of the atmosphere IRF (0.135 W/m^2), with over half caused by dust from high-latitude sources north of 60°N.

950 For snow and ice (glacier) surface radiation balance, the net energy flux E_N is due to differences between downward (↓) and
951 upward (↑) non-thermal shortwave (SW) and thermal longwave (LW) radiative fluxes. Such is most critically influenced by
952 the surface characteristics of the bi-hemispherical reflectance (BHR), i.e., albedo (Manninen et al., 2021). Therefore, melt is
953 also controlled by dark impurities in snow and ice (IPCC, 2019). Black carbon (BC) is, climatically, the most significant and
954 best-studied dark light-absorbing aerosol particle in snow (e.g., Bond et al., 2013; Dang et al., 2017; Evangeliou et al., 2018;
955 Flanner et al., 2007; Forsström et al., 2013; Mori et al., 2019; Meinander et al., 2020a,b). Radiation-transfer (RT) calculations
956 indicate that seemingly small amounts of black carbon (BC) in snow, in the order of 10–100 parts per billion by mass (ppb),
957 decrease its albedo by 1–5% (Hadley and Kirchtetter, 2012). BC has been shown to enhance snowmelt (AMAP, 2015; Bond
958 et al., 2013; IPCC, 2019). Other light-absorbing particles include organic carbon (OC, including brown carbon BrC) and dust.
959 Also, blooms of pigmented glacier ice algae can lower ice albedo and accelerate surface melting (McCutcheon et al., 2021),

960 showing a direct link between mineral phosphorus in surface ice and glacier ice algae biomass. They say nutrients from mineral

961 dust likely drive glacier ice algal growth, identifying mineral dust as a secondary control on ice sheet melting. Some Icelandic

962 dust sources have particles almost as black as black carbon by the reflectivity properties when measured as bulk material or

963 on snow and ice surfaces (Peltoniemi et al., 2015). Unlike black carbon, Icelandic dust has been shown to melt snow quicker

964 in small amounts and insulate and prevent melt in larger amounts (e.g., Dragosics et al., 2015; Möller et al., 2016; Boy et al.,

965 2019). Changes related to permafrost thaw and snow and ice melt, including disappearing glaciers, rising sea levels, and

966 drinking water shortages, are among the most serious global threats (IPCC, 2019). Water availability is vital in regions where

967 crops depend most on snowmelt water resources (Qin et al., 2020). Snow is also essential in the catchment areas (i.e., areas

968 supplying watercourses) and for many snow-dependent organisms, including plants, animals, and microbes (Zhu et al., 2019).

969 Melt can also run hydroelectric power plants that supply electricity (e.g., Lappalainen et al., 2022). This all highlights the

970 importance of investigations and continuous assessment of the temporal and spatial significance and contribution of different

971 light-absorbing impurities in enhancing or initiating cryospheric melt in the changing climate.

972 **3.6 Understanding the HLD sources**

973 The HLD results are further discussed from the perspective of HLD source intensity values; comparison with available HLD

974 information on the various regions; geological perspective on sources, focusing on a gap identified in HLD observations for

975 the Central part of the East European Plain and dust particle properties; and local HLD sources and long-range transport of

976 dust with the focus on results from the observations in Svalbard and Antarctica.

977 **3.6.1 Source intensity values**

978 Most of the HLD study sites agree with UNCCD G-SDS-SBM source intensity (SI) values of the highest dust productive areas,

979 identifying an environment from a given location within a distance $\leq 0.1°$. Surfaces with higher maximum SI include a

980 significant portion of the land surface in HLD regions. In the south HLD region, an annual change of SI exists. However,

981 approximately half the dust productive surface stays exposed to wind erosion during the year. In the north HLD region, SI

982 intensity varies significantly with the weather. High values of SI may not always coincide with high surface winds, meaning

983 high values may exist but not necessarily result in a dust storm. In case emissions occur, dust may remain undetected because

984 of the absence of ground observations over most of the HLD region and frequent cloud cover over airborne dust, obscuring

985 remotely sensed imagery.

986 Based on the SI values, the East Greenland sources in this study (no. 58–64 in Fig. 1) are seasonal, meaning their SI minimum

987 value is zero. Conversely, the West Greenland sources are not necessarily seasonal since their SI minimum values are

988 somewhat reduced (but not to zero). However, the term "seasonal" regarding the SI values means the soil surface conditions

989 are suitable for dust emissions, although that doesn't mean emissions will happen. Similarly, the seasonality of all sources in
990 this collection can be further studied.

991 When the newly identified sources are close together, such might indicate they are part of the larger dust source area, like
992 South Iceland, West Greenland, or East Greenland. The discovered sources could be considered to represent the hot spot
993 locations, i.e., the most emissive or active locations, of those dust-productive areas. Simultaneously, however, the land surface
994 and soil composition can be very complex and spatially variable, and the identification of single sources justified until the
995 source characteristics and particle properties have been characterized in more detail. For example, Icelandic sources have
996 shown that each source, even proximate ones, may have different particle size distributions and optical properties. The results
997 (Fig. 2) suggest two northern high-latitude dust belts. The first HLD belt would extend at 50–58°N in Eurasia and 50–55°N in
998 Canada, and the second dust belt at >60°N in Eurasia and >58°N in Canada, with a "no dust" belt between the HLD and LLD
999 dust belts (except for British Columbia).

1000 Uncertainties about the detected locations of the HLD sources and G-SDS-SBM source intensity values arise from the
1001 methodology for determining HLD source locations. These locations are ad-hoc location sources from satellite images of dust
1002 plumes; other kinds of airborne dust observations may introduce some errors in location estimation compared to on-site land
1003 surface monitoring and the precision of available data locations. The resolution of G-SDS-SBM may be too coarse for small-
1004 scale source areas (in this case, the representative grid point value shows reduced source intensity value since it represents the
1005 whole grid box). However, the in-point (at location) values are also given maximum values in the area around the given
1006 location (one point distance: 30 arcsec, 0.1°, 0.5°, and 1° distance). Values of source intensity above 0.9 have topsoil potential
1007 for SDS production in the top 10% of grid boxes with some emission potential in G-SDS-SBM (or in the top 10% of most
1008 dust-productive surfaces globally in case of favorable weather conditions), above 0.8 in the top 20%, above 0.7 in the top 30%,
1009 and so forth. Factors reducing source function value or topsoil dust productivity are sparse vegetation, coarser soil texture,
1010 higher moisture, and temperatures near the freezing point. Uncertainties in methodology for deriving G-SDS-SBM arise from
1011 the quality and resolution of available global datasets and the determination of thresholds for EVI in defining bare land fraction
1012 (primarily for brown grassland, which may appear as potential dust sources but with lower productivity). Surfaces with low SI
1013 values in favorable conditions for dust emission, in case of high winds, may produce some blowing dust events; sources with
1014 higher values of SI may generate dust storms. Real dust production from sources depends on high winds occurring while SI is
1015 high.

1016 Forty-nine locations were in the north HLD region (47 according to HLD definition by Bullard et al. (2016), (except for two:
1017 no. 8 and no. 48, with latitudes 4͟3͟7.7°N and 47͟3.6°N, respectively), while 15 were in the south HLD region, including four
1018 south of 60°S, where the values of SI are not provided. In the north HLD region, higher dust productive potential (SI 0.5) has
1019 17 of 49 marked locations at the HLD source marks exact location. Also, 38 sites are where a distance from a mark point (D)
1020 is equal to or less than 0.1° (Supplementary Table S4). Very high dust productivity, with SI 0.7, has 33 locations within D

1021 0.1°, and 42 and 46 within 0.5° and 1°, respectively. The highest dust productive potential, with SI 0.9°, has 27 locations within

1022 D 0.1°, and 39 and 44 within 0.5° and 1°, respectively. One point has the highest SI value, with less than 0.5° and five less

1023 than 0.9° away, when considering the largest environment of the HLD source mark. Three HLD source region marks are in

1024 the sea, so their source values are marked as -99 (undefined). In the south HLD region, 11 locations are considered (situated

1025 between 40°S and 60°S). Seven sources have very high dust productivity with SI 0.7 where the HLD source marker is; three

1026 more have SI 0.7° in the area of the source marker with D 0.1°. The highest dust productive potential, with SI 0.9°, has seven

1027 sources in the area with the source marker with D 0.1°, and three more in the area with D 0.5°. The source maximum and

1028 minimum intensities in these south HLD regions differ much less than in the north HLD region.

1029 As a summary, our modeling results on the spatial distribution of the dust sources (Fig. 2) showed evidence supporting a

1030 northern High Latitude Dust (HLD) belt, defined as the area north of 50°N, where we distinguish the following HLD-source

1031 areas: (a) "transitional HLD-source area," which extends at latitudes 50–58°N in Eurasia and 50–55°N in Canada, and (b)

1032 "cold HLD-source area," which includes areas north of 60°N in Eurasia and north of 58°N in Canada, with currently "no dust

1033 source" area between the HLD and LLD dust belts (except for British Columbia).

1034 **3.6.2 Comparison of various regions**

1035 For the HLD sources identified and included in our collection, the available information varied from detailed characterizations

1036 to the first satellite observations, waiting to be complemented with measurement data. Model output of dust transport can

1037 provide valuable additional information. The sources are in the northern and southern high latitudes and include a variety of

1038 environments. Particle properties, such as particle size distributions, have been determined for only some of the identified

1039 HLD sources. For example, our study's many Iceland south coast sources have not had any characterization done. Previous

1040 results on the known sources in Iceland's south coast region show that the particle size distributions vary substantially from

1041 location to location. No assumptions can be made based on characterization in one place.

1042 For Iceland seasonality, the correlation of SILAM modeled and measured PM10 and PM2.5 total aerosol concentration in

1043 Iceland is low, especially in 2018, which can mainly be explained by the measurement locations being far from the source

1044 locations and showing the effects of road dust rather than long-range transported dust. Also, the Reykjavik and Akureyri dust

1045 inventories are unrepresentative due to the challenge of fitting the modeled long-range transported dust emissions 695 to the

1046 measurement data within the 0.1 degrees model resolution. Near Reykjavik, dust emissions, e.g., from Landeyjasandur, may

1047 contribute to the measured dust concentrations. However, the 0.1 degrees resolution of the model is too scarce to simulate

1048 them.

1049 The end of summer and autumn (October) are the seasons for dust activity in Greenland. For example, on 19 October 2021,

1050 there was significant dust activity in western Greenland; several glacial valleys emitted dust along the 700-km coast. During

that dust event was a good Sentinel overpass showing a long narrow valley with a great deal of haze(dust) suspended (appearing as fuzziness in the image) (Gassó, 2021b). As far as we know, no previous observations for this source exist. Greenland's HLD sources (no. 53–58 of Fig. 1) from its west coast are considered new and identified here using satellite observations. Currently, further knowledge on the recurrency and area of the emission source is lacking. It is probable that these Greenland HLD sources from the west coast have been unidentified due to frequent cloudy conditions. The representation of dust sources in modeling approaches requires information on the location, soil characteristics, and temporal changes. A detailed specification of the geographic distribution of potential dust sources and their physical (e.g., particle size distribution, optics) and mineralogical/chemical (mineral fractions, chemical composition, etc.) properties is critical to accurately parameterize dust emission's potential in numerical dust models. Various methods exist to detect new sources; remote sensing is one of the most powerful tools, as demonstrated in Iceland's southern coast and Greenland's west and east coasts.

The central part of the East European Plain, with the wide occurrence of silty soils derived from loess-like sediments and reduced natural vegetation, is a potential aeolian dust source (Bullard et al., 2011; Sweeney and Manson, 2013). However, this region currently lacks observations on dust lifting and transport. Therefore, this region was not included in our collection of HLD sources. The gap for observations in the central part of the East European Plain for potential HLD source updates is filled here with new data in the Supplement Figures S1–S4 on the partitioning of elements among the five particle-size fractions separated from the natural soils of a rural area 100 km southwest of Moscow (Fig. S1). The study area (55°12–13'N, 36°21–22'E) belongs to the southeastern part of the Smolensk-Moscow Upland (314 m a.s.l.), representing a marginal area of the Middle Pleistocene (MIS 6) glaciation with moraine topography modified by post-glacial erosional and fluvial processes. The major soil reference group is Retisol (IUSS Working Group WRB, 2015), developed on the loess-like loam. About 50% of the soils in the interfluve area were subjected to arable farming. A new and unpublished independent dataset on 33 elements in topsoil horizons was obtained with a higher accuracy ICP-MS/AES analysis (compared to the DC-ARC-AES data set of Samonova and Aseyeva, 2020).

Additional dust sources with massive dust storms causing severe traffic disruption have been documented outside the dust belt in higher latitudes. These sources were mainly arable fields, such as those in Germany and Poland, as well as Montana and Washington state (in the US) (Hojan et al., 2019).

3.6.3 A geological perspective on HLD sources and particle properties

Dust sources involve very different formations and geological environments, each leaving its own imprint on the sediments. Thus, the geomorphological, sedimentological, petrological, and geochemical study of the loose sedimentary formations in the source areas provides information on the origin and provenance of dust when it is transported out or far away. These types of studies—quite typical for Saharan dust—are not so well-established in the case of HLD sources. These territories are not all

1081 easily accessible. Even when they are, the time may not coincide with the dust production and/or dust emission period, which
1082 may be one reason for this missing source area characterization.

1083 Geomorphological studies cover a wide range of subjects and topics, from characterizing specific dust sources (e.g., Arnalds
1084 et al., 2016; Bullard and Mockford, 2018; Bertran et al., 2021) to analyzing processes (e.g., Bullard and Austin, 2011; Hedding
1085 et al., 2015; Wolfe, 2020) to landform evolution (Heindel et al., 2017). Sedimentological studies on dust sources focus on the
1086 particles' morphological characteristics and textural details of the loose sediment formations. The size, shape, and surface
1087 characteristics of the particles result from morphogenetic processes. As such, these particles say a great deal about the source
1088 areas. Furthermore, the particles' size and shape influence their lifting and transport capacity and, finally, the distance they
1089 can reach from their site of origin. Such applies to the studies of the properties of volcaniclastic dust sources in Iceland (e.g.,
1090 Butwin et al., 2020; Richard-Thomas et al., 2021). From the petrological and geochemical perspective, the panorama is even
1091 wider and more varied. Save a few (e.g., Baratoux et al., 2011; Moroni et al., 2018), most studies are not aimed at studying
1092 dust sources but comprise different targets involving the parental soils (e.g., Antcibor et al., 2014; Brédoire et al., 2015).
1093 Although providing information on the (possible) source areas for dust, these latter studies are not explicitly aimed at studying
1094 dust sources, so they are not functional for that purpose. Specific survey and sampling activities by a team of experts would
1095 be required to address all aspects of dust sources and properties adequately. Thus, obtaining a database as rich and articulated
1096 as possible on the particles' physico-chemical properties within dust would be feasible, providing the ability to predict dust
1097 behavior within the aerosols and understand medium and long-range transport phenomena is present. A further aspect
1098 regarding dust sources and properties is the evolution of the particles' physico-chemical properties due to the lifting and
1099 transport mechanisms. The aerosols must be sampled in different places at different distances from the source. However, this
1100 approach is complicated by the air masses mixing during transport, requiring a deep investigation of air mass back trajectories.
1101 Conversely, treating the soils in the lab by re-suspending and sampling them using impactors at well-defined cut-off size ranges
1102 can be very advantageous. Such work has been carried out on Australian soils and southern African soils (Gili et al, 2021) to
1103 study the dust sources in Antarctica, which is now underway in Iceland (Moroni, 2021, personal communication).

3.6.4 Local HLD sources versus long-range transported dust: discussing Svalbard and Antarctica

1105 The same areas of dust lifting can also be deposition sites when particles leaving their respective source regions are deposited
1106 there after prolonged transport pathways. The extent of the contribution of local and long-range sources may vary during the
1107 year depending on the type of atmospheric circulation and state of the exposed surfaces, particularly the presence of bare
1108 deglaciated soils. Such is the case of Svalbard, where the local dust sources prevail over the long-range ones, especially in
1109 summer; the contrary occurs the rest of the year (Moroni et al., 2016; Spolaor et al., 2021). Conversely, and always in
1110 Spitsbergen, the type of contributions—local and long-range—may also depend on the altitude due to the stratified structure
1111 of the lower atmosphere frequently found at high latitudes (e.g., Moroni et al., 2015; Kavan et al., 2020a).

1112 Investigating the physico-chemical properties, and possibly estimating their contributions at different times of the year, is key
1113 to identifying the source regions of dust. For example, in Spitsbergen's case, the potential Source Contribution Function
1114 (PSCF) analysis of aerosol samples taken in Ny-Alesund clearly identified four different HLD sources in Eurasia, Greenland,
1115 Arctic-Alaska, and Iceland (Crocchianti et al., 2021). Conversely, chemical-mineralogical investigation and single-particle
1116 analysis recognized and estimated Icelandic dust's contribution to Ny-Alesund (Moroni et al., 2018).

1117 Kandler et al. (2020) collected dry dust deposition near sources in Northwestern Africa, Central Asia, on Svalbard, and at three
1118 locations of the African outflow region, and studied particle sizes and composition. Their results showed low temporal variation
1119 in estimated optical properties for each site but considerable differences among the African, Central Asian, and Arctic regions.
1120 An insignificant difference was found between the K-feldspar relative abundances, indicating comparable ice-nucleation
1121 abilities. The mixing state between calcium and iron compounds differed for near-source and transport regimes, potentially
1122 and partially due to size-sorting effects. Thus, in certain situations (high acid availability, limited time), atmospheric processing
1123 of the dust is expected to lead to less iron solubility for near-source dust (for Central Asian ones) than for transported ones
1124 (particularly those of Sahelian origin).

1125 In the southern part, under certain meteorological conditions, dust from lower latitudes can be transported far toward polar
1126 regions. Such was the case when a massive dust storm formed over Australia on 22 January 2020. Two days later, dust moved
1127 southward, covering a large part of Antarctica's eastern coast. The RHMSS global version of the DREAM model with
1128 incorporated ice nucleation parameterization due to dust (Nickovic et al., 2016) predicted the formation of cold clouds over
1129 the Antarctic. This ice cloud phase was also documented by NASA satellite observations (Fig. 16). The simulation was part of
1130 a WMO SDS-WAS initiative to include dust impacts on high latitudes in its agenda to better understand the role of mineral
1131 dust as a climate factor at high latitudes.

1132

1133
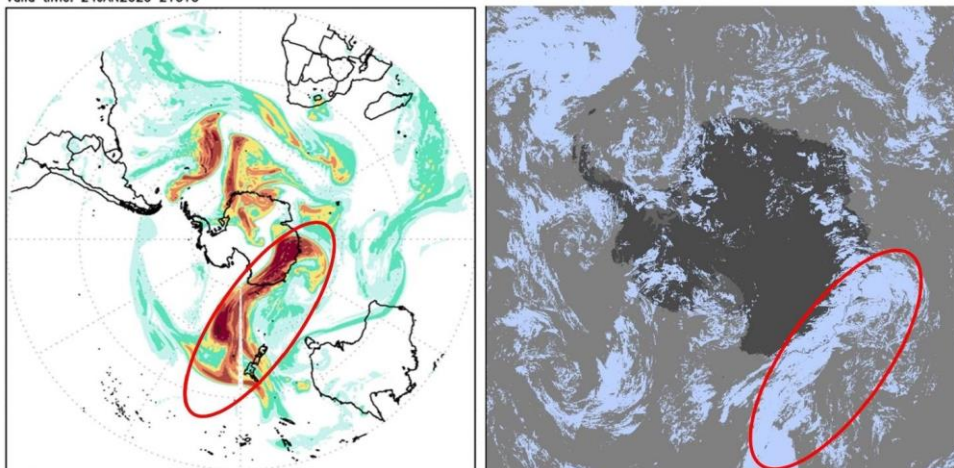
Figure 16. Global NMMB DREAM model experiments over Australia and the South Pole. Model dust load 22 January 2020; B) Model log$_{10}$ (vertical load of ice nuclei number) (left). NASA MODIS ice cloud phase for 24 January 2020 (right).

The McMurdo Dry Valleys (MDV) were previously assumed to be a significant regional source of dust (e.g., Bullard, 2016). New observations show otherwise. Instead, the McMurdo Ice Shelf's (sometimes called the McMurdo debris bands) debris-covered surface is the major dust source. In this study, more details are provided to underline the importance and estimates of the size of the areas. The MDV (4 800 km^2) was estimated to fit Category 3 best. Despite active local aeolian sediment transport with many annual occurrences, they are an insignificant source or exporter of dust regionally, thus having only a small but poorly known climatic or environmental significance. The MDV are changing quickly with increased ablation, meltwater, and permafrost incision, so their importance regarding dust generation may change in the near future. The McMurdo Ice shelf "debris bands" fit Category 2 best. Although it is only about 1500 km^2, the McMurdo Ice shelf is clearly the region's largest and most important dust source—active with a continuous supply of new sediment for export and exposed to frequent strong winds (with many events during the year), although few have been documented. The aeolian sediment impacts sea ice albedo (not directly measured) and marine sedimentation, contributing enough dissolved Fe to potentially support up to 15% of primary productivity in the SW Ross Sea (Winton et al., 2014).

1149 Ice core studies from Antarctica ice sheets show that Antarctica receives long-range dust transport from Australia, South
1150 America, South Africa, and New Zealand (e.g., Bullard, 2016). However, several studies around coastal areas have shown that
1151 locally, Antarctic sourced dust accumulation rates are at least two orders of magnitude higher than that recorded from the polar
1152 plateau or global dust models (Chewings et al., 2014; Winton et al., 2014).

1153 **4 Conclusions and outlook**

1154 This study aimed to identify new HLD sources with the focus on their potential climatic and environmental impacts. A
1155 literature survey on impacts and model calculations on emission, transport and deposition were made to investigate the local,
1156 regional, and global significance of the HLD sources. We identified 64 new HLD sources. We estimated that in the high
1157 latitudes, the land area with higher (SI≥0.5), very high (SI≥0.7), and the highest potential (SI≥0.9) for dust emission cover >1
1158 670 000 km^2, >560 000 km^2, and >240 000 km^2, respectively. These estimations agree with the first HLD sources' estimate of
1159 an area >500 000 km^2 by Bullard et al. (2016), which mainly included the sources with a very high potential for dust emission,
1160 as classified in this study. Our study shows that active sources cover a significantly larger area, confirmed by over 60 new
1161 HLD sources with evidence of their dust activity, which is not limited to dry areas. The potential HLD emission areas need
1162 proof of observed and identified HLD emission sources.

1163 Our modeling results on spatial distribution of the dust sources showed evidence supporting a northern High Latitude Dust
1164 (HLD) belt, defined as the area north of 50°N, with a "transitional HLD-source area," extending at latitudes 50–58 °N in
1165 Eurasia, 50–55°N in Canada, and a "cold HLD-source area," including areas north of 60°N in Eurasia and north of 58°N in
1166 Canada, with currently "no dust source" area between the HLD and LLD dust belt, except for British Columbia. Using the
1167 global atmospheric transport model SILAM, we estimated that 1.0% of the global dust emission originated from the high-
1168 latitude regions. About 57% of the dust deposition on snow and the ice-covered Arctic regions came from HLD sources.

1169 Our update provides crucial information on the extent of active HLD sources and their locations. Active HLD sources as
1170 essential sources of aerosols that directly and indirectly affect climate and the environment in remote regions are often poorly
1171 understood and predicted. HLD is likely a significant source of atmospheric iron deposition in the Southern Ocean encircling
1172 Antarctica. More research is needed to quantify the deposition flux of HLD and nutrient (Fe, P, and trace metals such as Co)
1173 content and solubility, which can then be fed to ocean biogeochemical models to quantify their impact on ocean
1174 biogeochemistry. HLD is also an active ice-nucleating particle changing cloud properties, which has severe consequences
1175 when deposited within the cryosphere. However, more studies are needed for HLD from different regions. For example,
1176 Northern Asia HLD sources are assumed to be numerous but are difficult to access and gain information from. Such points to
1177 the following main action items for monitoring dust in high latitudes:

1178 · Firstly, the work on HLD sources needs a multidisciplinary combination of field, laboratory, and experimental work; remote sensing; and emission, transport and deposition modeling. An increase in observational and modeling studies improves HLD monitoring and predicting.

1181 · Secondly, the activity of the currently identified active sources should be followed and reevaluated in the coming years and decades.

1183 · Thirdly, research gaps and future research directions essentially include finding, identifying, and characterizing new dust sources. As soon as there is evidence of finding a new HLD source, it should be included in the list of dust sources and subject to further study.

1186 · Fourthly, the role of different types of road dust in the Arctic could be separately assessed using a standard methodology.

1188 Namely, in Arctic communities, road dust as a signature of non-exhaust traffic dust formed via the abrasion and wearing down of pavement, traction control materials, vehicle brakes, and tires is a common concern (e.g., Kupiainen et al., 2016; Nordic Council of Ministers, 2017). This paper excluded this type of road dust and only included significant anthropogenic road dust sources where unpaved roads are a substantial dust source. Unpaved areas of parking lots, storage areas, road shoulders, roadside lawn dust, and winter's effects could be considered, too. During winter's cold and wet conditions, dust accumulates in snow and ice and the humid road surface texture. As snow and ice melt and street surfaces dry up in spring, high amounts of dust become available for suspension. For example, in Finland, north of 60°N, a major anthropogenic dust source comes from sand and gravel uptake for building purposes from ridges formed during the Ice Age. These nonrenewable ridges cover 1.5 million ha. Since 1960, it has been estimated that approximately 40 million tons per year have been utilized (Fig. 211 of Wahlström et al., 1996). These open-sand areas are visible in aircraft photos and satellite images. In Finland, long-range transported low latitude dust contributes to the dust amounts, too (e.g., Meinander et al., 2021). Another health-significant anthropogenic springtime dust source is wintertime pavement traction sanding (Kuhns et al., 2010; Kupiainen, 2007; Stojiljkovic et al., 2019). These springtime dust events are annual but local throughout the country. In comparison, the Moscow metropolitan area (55°45'N, 37°37'E) is one of the most significant sources of dust at latitudes above 50° N, where dust's impact can extend over several hundred kilometers (Adzhiev et al., 2017). Moscow's road dust is mainly generated on paved roads, but roadside soils also contribute (Kasimov et al., 2020). Most often, unsealed soils are covered with lawns and are widespread in parks and recreational and industrial zones, characterized by heavy pollution, mixed upper horizon, and a high degree of soil cover heterogeneity.

1206 This paper aimed to contribute beyond the state-of-the-art of HLD sources by focusing on collecting and providing information on the geographical distribution of dust-productive soils and potential dust sources. This is some of the most important

1208 information that is currently lacking but is necessary to perform successful long-range transport and deposition modeling. The
1209 information on the geographical distribution of dust-productive soils needs evidence and verification on detected dust events
1210 and is insufficient alone. Therefore, the paper focused on identifying new dust sources, clarifying their climatic and
1211 environmental importance, and using emission, long-range transport and deposition modeling to study where the potential
1212 impact areas of the HLD sources are. Our results suggest that future HLD studies should include and update sources within
1213 the here defined high latitude dust belt, i.e, at 50–58°N in Eurasia and 50–55°N in Canada, and at >60°N in Eurasia and >58°N
1214 in Canada, as well as sources in the periphery of these regions, especially if sources are highly elevated (Wang et al. 2016).

1215 Icelandic sources have shown that each source, even if nearby, may have different particle size distributions and optical
1216 properties. A detailed specification of the geographic distribution of potential dust productive soils, verified dust sources, and
1217 their physical (e.g., particle size distribution, optics, etc.) and mineralogical/chemical (e.g., mineral fractions, chemical
1218 composition, etc.) properties can contribute to the various topics: predicting dust forecasts (e.g., health protection warnings
1219 during extreme events); long-range emission, transport and deposition modeling; dust monitoring control; understanding
1220 extreme and rare events; Arctic protection; aviation control; health; tourist boards; assessing climate, environment, and air
1221 quality (e.g., Arctic Council Arctic Monitoring and Assessment Program AMAP, and Intergovernmental Panel on Climate
1222 Change IPCC reports); and implementing HLD in calculations on direct and indirect radiative forcing, including cloud
1223 formation, cryospheric effects, and modeling the impacts. The new observations in this study improved the representation of
1224 HLD sources for various approaches and applications related to the observed current, previous, and future environmental
1225 changes at high latitudes.

1226 In summary, establishing continuous monitoring of HLD sources and their future changes is key to understanding the climatic
1227 and environmental effects at high latitudes, especially in the Arctic. Climate change causes permafrost thaw, decreases snow
1228 cover duration, and increases drought, glacial melt, and heatwave intensity and frequency – all leading to increasing the
1229 frequency of topsoil conditions favorable for dust emission (increasing soil's exposure to wind erosion) and the probability of
1230 dust storms. Although dust originates from natural soils, dust sources are also influenced by human activities, e.g., when
1231 deforestation and land management in cold regions leads to ecosystem collapse and desertification (Prospero et al., 2012;
1232 Arnalds, 2015). Dust storms from agricultural fields (as reported, e.g., in Poland) can reach distances over 300 km, drastically
1233 reducing visibility and resulting in hundreds of car accidents and fatalities (Hojan et al., 2019). Whether natural or
1234 anthropogenic, wildfires can result from new dust sources also (Miller et al., 2012). Hence, human actions can positively and
1235 negatively influence HLD and its effects. To understand and assess the temporal activity changes in HLD sources and the
1236 multiple impacts of high-latitude dust on the Earth systems over time, continuous monitoring and regular updates on location,
1237 particle properties, and activities of current and new HLD sources are needed.

1238

1239

1240

1241 **Competing interests.** The authors declare they have no conflict of interest.

1242 **Special issue statement**. This article is part of the special issue "Arctic climate, air quality, and health impacts from short-
1243 lived climate forcers (SLCFs): contributions from the AMAP Expert Group (ACP/BG inter-journal SI)". It is not associated
1244 with a conference.

1245 **Acknowledgements**

1246 This paper was developed as part of the Arctic Monitoring and Assessment Programme (AMAP), AMAP 2021 assessment:
1247 Arctic climate, air quality, and health impacts from short-lived climate forcers (SLCFs). We are grateful to the anonymous
1248 referees whose comments have been most valuable and have greatly improved our manuscript. Kaarle Kupiainen, Johanna
1249 Ikävalko, and Terhikki Manninen are gratefully acknowledged. The staff's help regarding the stations is highly appreciated.

1250 **Financial support**
1251 This research has been supported by the Ministry for Foreign Affairs of Finland (IBA-project No. PC0TQ4BT-25). The study
1252 of dust composition in Moscow and Tiksi was supported by the Russian Science Foundation (No. 19-77-30004). Firn cores
1253 collection on southern Spitsbergen, Svalbard, has been co-funded by the Research Council of Norway, Arctic Field Grant 2018
1254 (No. 282538), funds of the Leading National Research Centre (KNOW) received by the Centre for Polar Studies of the
1255 University of Silesia, and statutory activities No. 3841/E-41/S/2018 of the Ministry of Science and Higher Education of Poland.
1256 The Czech Science Foundation projects 20-06168Y, GA20-20240S, and the Ministry of Education, Youth and Sports of the
1257 Czech Republic projects No. LM2015078 and CZ.02.1.01/0.0/0.0/16_013/0001708 are acknowledged. The support of the
1258 EPOS-PL project (No. POIR.04.02.00-14-A003/16), co-financed by the European Union from the funds of the European
1259 Regional Development Fund (ERDF) to the laboratory facilities at IG PAS used in the study, is also acknowledged. European
1260 Union COST Action InDust is acknowledged. The preparation of this paper was partially funded by the Icelandic Research
1261 Fund (Rannis) Grant No. 207057-051. O. Meinander acknowledges funding from the Academy of Finland (ACCC Flagship
1262 funding grant No. 337552 and BBrCAC No. 341271), H2020 EU-Interact (No. 730938), International Arctic Science
1263 Committee (IASC Cross-Cutting grant), and the Ministry for Foreign Affairs of Finland (IBA-project No. PC0TQ4BT-20). D.
1264 Frolov is thankful to Lomonosov Moscow State University (state topic "Danger and risk of natural processes and phenomena"
1265 No. 121051300175-4). K. Kandler was funded by the Deutsche Forschungsgemeinschaft (DFG, German Research Foundation
1266 No. 264912134, 416816480, 417012665N). J. King acknowledges NSERC Discovery 2016-05417, CFI 36564, and the CMN
1267 RES00044975. B. Murray, A. Sanchez-Marroquin, and S. Barr thank the European Research Council (648661 MarineIce) and
1268 the Natural Environment Research Council (NE/T00648X/1; NE/R006687/1). O. Möhler and N.S. Umo acknowledge the

1269 funding support from Helmholtz Association of German Research Centres through its 'Changing Earth — Sustaining our
1270 Future' Programme. M. Kulmala, N.S. Kasimov, and O. Popovicheva acknowledge funding from the Russian Ministry of
1271 Education and Science (075-15-2021-574). K. Ranjbar and N.T. O'Neill acknowledge the PAHA project (NSERC-CCAR
1272 program; RGPCC-433842-2012), the SACIA project (CSA-ESSDA program; 16UASACIA), and the NSERC DG grants of
1273 O'Neill (RGPIN-05002-2014). I. Semenkov, O. Popovicheva, and N. Kasimov acknowledge funding from the M.V.
1274 Lomonosov Moscow State University (the Interdisciplinary Scientific and Educational School «Future Planet and Global
1275 Environmental Change» and project No. 121051400083-1). Z. Shi and C. Baldo are funded by the UK Natural Environment
1276 Research Council (NE/L002493/1; NE/S00579X.

1277

Supplement

The supplement related to this article is available online at:

Data availability

Data are mostly included in this article or available on request via personal communication.

Author contribution

The paper was initiated and lead by O. Meinander. P. Dagsson-Waldhauserová co-coordinated and edited. HLD SI and area calculations were by A. Vukovic and B. Cvetkovic. New HLD sources were identified as follows: Alaska, Canada: S. Barr, P. Dagsson-Waldhauserová, P., S. Gassó, J. King, B.J. Murray, J.B. McQuaid, N.T. O'Neill, K. Ranjbar. Antarctica: P. Dagsson-Waldhauserová, J. Kavan, K. Láska, O. Meinander, E. Shevnina. Denmark and Sweden: O. Meinander. Greenland: A. Baklanov, L.G. Benning, P. Dagsson-Waldhauserová, S. Gassó. Iceland: T. Thorsteinsson. Russia: P. Amosov, A. Baklanov, P. Enchilik, T. Koroleva, V. Krupskaya, O. Popovicheva, A. Sharapova, I. Semenkov, M. Timofeev. Svalbard: B. Barzycka, M. Kusiak, M. Laska, M. Lewandowski, B. Luks, A. Nawrot, T. Werner, K. Kandler, N. S. Umo, B.J. Murray, J.B. McQuaid, A. Sánchez-Marroquín, O. Möhler. South America, Argentina, and Patagonia: S. Gassó. DREAM model: B. Cvetkovic, S. Nickovic. SILAM model: A. Uppstu and M. Sofiev. N. Kasimov, E. Aseyeva, and O. Samonova contributed supplementary material on the central part of European Russia (potential dust source). Dust and clouds: B.J. Murray and A. Sánchez-Marroquín. Dust and ocean biogeochemistry: Z. Shi and C. Baldo. Dust and atmospheric chemistry: F. Thevenet, M.N. Romanias, J.Lasne, D. Urupina. Dust and cryosphere: O. Meinander. All authors contributed significantly to preparing the manuscript.

References

1300 Abbatt, J. P. D., Leaitch, W. R., Aliabadi, A. A., Bertram, A. K., Blanchet, J.-P., Boivin-Rioux, A., Bozem, H., Burkart, J.,
1301 Chang, R. Y. W., Charette, J., Chaubey, J. P., Christensen, R. J., Cirisan, A., Collins, D. B., Croft, B., Dionne, J., Evans, G. J.,
1302 Fletcher, C. G., Galí, M., Ghahremaninezhad, R., Girard, E., Gong, W., Gosselin, M., Gourdal, M., Hanna, S. J., Hayashida,
1303 H., Herber, A. B., Hesaraki, S., Hoor, P., Huang, L., Hussherr, R., Irish, V. E., Keita, S. A., Kodros, J. K., Köllner, F., Kolonjari,
1304 F., Kunkel, D., Ladino, L. A., Law, K., Levasseur, M., Libois, Q., Liggio, J., Lizotte, M., Macdonald, K. M., Mahmood, R.,
1305 Martin, R. V., Mason, R. H., Miller, L. A., Moravek, A., Mortenson, E., Mungall, E. L., Murphy, J. G., Namazi, M., Norman,
1306 A.-L., O'Neill, N. T., Pierce, J. R., Russell, L. M., Schneider, J., Schulz, H., Sharma, S., Si, M., Staebler, R. M., Steiner, N. S.,
1307 Thomas, J. L., von Salzen, K., Wentzell, J. J. B., Willis, M. D., Wentworth, G. R., Xu, J.-W., and Yakobi-Hancock, J. D.:
1308 Overview paper: New insights into aerosol and climate in the Arctic, Atmos. Chem. Phys., 19, 2527–2560, doi:10.5194/acp-
1309 19-2527-2019, 2019.

1310 Achterberg, E. P., Moore, C. M., Henson, S. A., Steigenberger, S., Stohl, A., Eckhardt, S., Avendano, L. C., Cassidy, M.,
1311 Hembury, D., Klar, J. K., Lucas, M. I., Macey, A. I., Marsay, C. M., and Ryan-Keogh, T. J.: Natural iron fertilization by the
1312 Eyjafjallajokull volcanic eruption, Geophysical Research Letters, 40, 921-926, doi: 10.1002/grl.50221, 2013.

1313 Achterberg, E. P., Steigenberger, S., Marsay, C. M., LeMoigne, F. A. C., Painter, S. C., Baker, A. R., Connelly, D. P., Moore,
1314 C. M., Tagliabue, A., and Tanhua, T.: Iron Biogeochemistry in the High Latitude North Atlantic Ocean, Scientific Reports, 8,
1315 doi: 10.1038/s41598-018-19472-1, 2018.

1316 Adzhiev, A. H., Bartalyov, S. A., Bekkiev, M. Y., Biryukov, M. V., Biryukova, O. N., Bityukova, V. R., Bobylev, S. N.,
1317 Bogdanova, M. D., Bozhilina, E. A., Bronnikova, V. K., et al.: Ecological atlas of Russia, Feoria, Moscow, 510 p., 2017.

1318 AMAP: Black Carbon and Ozone as Arctic Climate Forcers. Arctic Monitoring and Assessment Programme (AMAP), Oslo,
1319 116, 2015.

1320 Amino, T., Y. Iizuka, S. Matoba, R. Shimada, N. Oshima, T. Suzuki, T. Ando, T. Aoki, and K. Fujita: Increasing dust emission
1321 from ice free terrain in southeastern Greenland since 2000, Polar Science, 100599, doi:10.1016/j.polar.2020.100599, 2020.

1322 Amosov P.V. and Baklanov A.A.: Assessment of dusting intensity on ANOF-2 tailing by using a Westphal D.L. dependency
1323 // Proceedings of the X International Symposium on Recycling Technologies and Sustainable Development, 4-7 November
1324 2015, Bor, Serbia. – Bor: University of Belgrade, Technical Faculty, 39-43, 2015.

1325 Anderson, N. J., J. E. Saros, J. E. Bullard, S. M. P. Cahoon, S. McGowan, E. A. Bagshaw, C. D. Barry, R. Bindler, B. T.
1326 Burpee, J. L. Carrivick, et al.: The Arctic in the twenty-first century: Changing biogeochemical linkages across a paraglacial
1327 landscape of Greenland. BioScience, 67, 118–133, doi:10.1093/biosci/biw158, 2017.

1328 Antcibor, I., Eschenbach, A., Zubrzycki, S., Kutzbach, L. et al: Trace metal distribution in pristine permafrost-affected soils
1329 of the Lena River delta and its hinterland, northern Siberia, Russia. Biogeosciences 11:1–15, 2014.

1330 Arnalds O.: The Soils of Iceland. World Soils Book Series, Springer, Dordrecht, The Netherlands, 2015.

1331 Arnalds, O., Thorarinsdottir, E.F., Thorsson, J., Dagsson-Waldhauserová, P., Agustsdottir, A.M.: An extreme wind erosion
1332 event of the fresh Eyjafjallajokull 2010 volcanic ash. Nature Scientific Reports 3, 1257, 2013.

1333 Arnalds, O., Olafsson, H., and Dagsson-Waldhauserová, P.: Quantification of iron-rich volcanogenic dust emissions and
1334 deposition over the ocean from Icelandic dust sources, Biogeosciences, 11, 6623-6632, doi: 10.5194/bg-11-6623-2014, 2014.

1335 Arnalds, O., Dagsson-Waldhauserová, P., and Olafsson, H.: The Icelandic volcanic aeolian environment: Processes and
1336 impacts — A review, Aeolian Res., 20, 176-195, doi: 10.1016/j.aeolia.2016.01.004, 2016.

1337 Arrigo, K. R., and Van Dijken, G. L.: Interannual variation in air-sea CO2 flux in the Ross Sea, Antarctica: A model analysis,
1338 Journal of Geophysical Research-Oceans, 112, doi: 10.1029/2006jc003492, 2007.

1339 Arrigo, K. R., van Dijken, G., and Long, M.: Coastal Southern Ocean: A strong anthropogenic CO_2 sink, Geophysical Research
1340 Letters, 35, doi: 10.1029/2008gl035624, 2008.

1341 Atkins, C.B., and Dunbar, G. B. Aeolian sediment flux from sea ice into Southern McMurdo Sound, Antarctica, Global and
1342 Planetary Change, 69, 133-141, 2009.

1343 Atkinson, J. D., B. J. Murray, M. T. Woodhouse, T. F. Whale, K. J. Baustian, K. S. Carslaw, S. Dobbie, D. O'Sullivan, and T.
1344 L. Malkin, The importance of feldspar for ice nucleation by mineral dust in mixed-phase clouds, Nature, 498, 7454, 355-358,
1345 doi:10.1038/nature12278, 2013.

1346 Aun, M., Lakkala, K., Sanchez,R., Asmi, E., Nollas, F., Meinander, O., Sogacheva, L., De Bock, V., Arola, A., de Leeuw, G.,
1347 Aaltonen, V., Bolsée, D., Cizkova, K, Mangold, A., Metelka,L., Jakobson, E., Svendby,T., Gillotay, D., and Van Opstal, B.:
1348 Solar UV radiation measurements in Marambio, Antarctica, during years 2017–2019, Atmos. Chem. Phys., 20, 6037–6054,
1349 doi:10.5194/acp-20-6037-2020, 2020.

1350 Ayling, B. F. and McGowan, H.A.: Niveo-eolian sediment deposits in coastal South Victoria Land, Antarctica: Indicators of
1351 regional variability in weather and climate, Arc. Antarct. Alp. Res., 38, 3, 313–324, 2006.

1352 Bachelder, J., Cadieux, M., Liu-Kang, C., Lambert, P., Filoche, A., Aparecida Galhardi, J., Hadioui, M., Chaput, A., Bastien-
1353 Thibault, M.-P., Wilkinson, K.J., King, J., and Hayes, P.J.: Chemical and microphysical properties of wind-blown dust near

1354 an actively retreating glacier in Yukon, Canada. Aerosol Science and Technology 54:1, 2-20, doi:
1355 10.1080/02786826.2019.1676394, 2020.

1356 Baddock, M., Mockford, T., Bullard, J.E., and Thorsteinsson, Th.: Pathways of high-latitude dust in the North Atlantic. Earth
1357 and Planetary Science Letters, 459: 170 – 182. doi: 10.1016/j.epsl.2016.11.034, 2017.

1358 Baklanov A. and Rigina O. Environmental modeling of dusting from the mining and concentration sites in the Kola Peninsula,
1359 Northwest Russia. The XI World Clear Air and Environment Congress, 14-18 September 1998, Durban, South Africa,
1360 IUAPPA-NACA. Durban, v. 1, 4F-3, 1-18, 1998.

1361 Baklanov, A., A. Mahura, L. Nazarenko, N. Tausnev, A Kuchin, and O. Rigina: Modelling of atmospheric Pollution and
1362 Climate Change in Northern Latitudes. Russian Academy of Sciences, Apatity, Russia, 106 p. Book in Russian,
1363 https://search.rsl.ru/ru/record/01006534167, 2012.

1364 Baldo, C., Formenti, P., Nowak, S., Chevaillier, S., Cazaunau, M., Pangui, E., Di Biagio, C., Doussin, J.-F., Ignatyev, K.,
1365 Dagsson-Waldhauserová, P., Arnalds, O., MacKenzie, A. R., and Shi, Z.: Distinct chemical and mineralogical composition of
1366 Icelandic dust compared to northern African and Asian dust, Atmos. Chem. Phys., 20, 13521–13539, doi:10.5194/acp-20-
1367 13521-2020, 2020.

1368 Baratoux, D., Mangold, N., Arnalds, O., Bardintzeff, J.-M., Platevoët, B., Grégoire, M. and Pinet, P.: Volcanic sands of Iceland
1369 - Diverse origins of aeolian sand deposits revealed at Dyngjusandur and Lambahraun. EARTH SURFACE PROCESSES AND
1370 LANDFORMS Earth Surf. Process. Landforms, doi: 10.1002/esp.2201, 2011.

1371 Beckett, F., Kylling, A., Sigurðardóttir, G., von Löwis, S., and Witham, C.: Quantifying the mass loading of particles in an ash
1372 cloud remobilized from tephra deposits on Iceland, Atmos. Chem. Phys., 17, 4401-4418, 2017.

1373 Bertran P, Bosq, M., Quentin Borderie, Coussot, C., Coutard, S., Deschodt, L., Franc, O., Gardère, P., Liard, M., and Wuscher,
1374 P.: Revised map of European aeolian deposits derived from soil texture data, Quaternary Science Reviews, 266, 107085,
1375 doi:10.1016/j.quascirev.2021.107085, 2021.

1376 Bhattachan, A., L. Wang, M. F. Miller, K. J. Licht, and P. D'Odorico: Antarctica's Dry Valleys: A potential source of soluble
1377 iron to the Southern Ocean?, Geophys. Res. Lett., 42, 1912–1918, doi:10.1002/2015GL063419, 2015.

1378 Bishop, J. K. B., Davis, R. E., and Sherman, J. T.: Robotic observations of dust storm enhancement of carbon biomass in the
1379 North Pacific. Science, doi:10.1126/science.1074961, 2002.

1380 Bodas-Salcedo, A., K. D. Williams, M. A. Ringer, I. Beau, J. N. S. Cole, J. L. Dufresne, T. Koshiro, B. Stevens, Z. Wang, and
1381 T. Yokohata: Origins of the Solar Radiation Biases over the Southern Ocean in CFMIP2 Models, J. Clim., 27, 1, 41-56,
1382 doi:10.1175/jcli-d-13-00169.1, 2014.

1383 Bond, T. C., Doherty, S. J., Fahey, D. W., Forster, P. M., Berntsen, T., DeAngelo, B. J., et al.: Bounding the role of black
1384 carbon in the climate system: a scientific assessment. J. Geophys. Res. Atmos. 188, 5380–5552, doi: 10.1002/jgrd.50171,
1385 2013.

1386 Boy, M., Thomson, E. S., Acosta Navarro, J.-C., Arnalds, O., Batchvarova, E., Bäck, J., Berninger, F., Bilde, M., Brasseur,
1387 Z., Dagsson-Waldhauserová, P., Castarède, D., Dalirian, M., de Leeuw, G., Dragosics, M., Duplissy, E.-M., Duplissy, J.,
1388 Ekman, A. M. L., Fang, K., Gallet, J.-C., Glasius, M., Gryning, S.-E., Grythe, H., Hansson, H.-C., Hansson, M., Isaksson, E.,
1389 Iversen, T., Jonsdottir, I., Kasurinen, V., Kirkevåg, A., Korhola, A., Krejci, R., Kristjansson, J. E., Lappalainen, H. K., Lauri,
1390 A., Leppäranta, M., Lihavainen, H., Makkonen, R., Massling, A., Meinander, O., Nilsson, E. D., Olafsson, H., Pettersson, J.
1391 B. C., Prisle, N. L., Riipinen, I., Roldin, P., Ruppel, M., Salter, M., Sand, M., Seland, Ø., Seppä, H., Skov, H., Soares, J., Stohl,
1392 A., Ström, J., Svensson, J., Swietlicki, E., Tabakova, K., Thorsteinsson, T., Virkkula, A., Weyhenmeyer, G. A., Wu, Y., Zieger,
1393 P., and Kulmala, M.: Interactions between the atmosphere, cryosphere, and ecosystems at northern high latitudes, Atmos.
1394 Chem. Phys., 19, 2015–2061, https://doi.org/10.5194/acp-19-2015-2019, 2019.

1395 Boyd, P. W., Jickells, T., Law, C. S., Blain, S., Boyle, E. A., Buesseler, K. O., Coale, K. H., Cullen, J. J., de Baar, H. J. W.,
1396 Follows, M., Harvey, M., Lancelot, C., Levasseur, M., Owens, N. P. J., Pollard, R., Rivkin, R. B., Sarmiento, J., Schoemann,
1397 V., Smetacek, V., Takeda, S., Tsuda, A., Turner, S., and Watson, A. J.: Mesoscale Iron Enrichment Experiments 1993-2005:
1398 Synthesis and Future Directions, Science, 315, 612-617, doi: 10.1126/science.1131669, 2007.

1399 Boyd, P. W., Mackie, D. S., and Hunter, K. A.: Aerosol iron deposition to the surface ocean - Modes of iron supply and
1400 biological responses, Mar. Chem., 120, 128-143, doi: 10.1016/j.marchem.2009.01.008, 2010.

1401 Brabets, T P.: Geomorphology of the lower Copper River, Alaska I by Timothy P. Brabets, U.S. Geological Survey
1402 professional paper, 1581, https://pubs.usgs.gov/pp/1581/report.pdf, 1997.

1403 Brédoire, F., Bakker, M.R., Augusto, L., Barsukov, P.A., Derrien, D., Nikitich, P., Rusalimova, O., Zeller, B., Acha, D.L.:
1404 What is the P value of Siberian soils? Biogeosci Discuss 12:19819–19859, 2015.

1405 Bullard, J. E.: The distribution and biogeochemical importance of high-latitude dust in the Arctic and Southern Ocean-
1406 Antarctic regions, Journal of Geophysical Research-Atmospheres, 122, 3098-3103, doi: 10.1002/2016jd026363, 2016.

1407 Bullard J. and Austin, M.J.: Dust generation on a proglacial floodplain, West Greenland Article in Aeolian Research · June
1408 2011, doi: 10.1016/j.aeolia.2011.01.002, 2011.

1409 Bullard, J.E. and Mockford, T.: Seasonal and decadal variability of dust observations in the Kangerlussuaq area, west
1410 Greenland, Arctic, Antarctic, and Alpine Research, 50:1, S100011, doi: 10.1080/15230430.2017.1415854, 2018.

1411 Bullard, J.E., Harrison, S.P., Baddock, M.C., Drake, N., Gill, T.E., McTainsh, G. and Sun, Y.: Preferential dust sources: A
1412 geomorphological classification designed for use in global dust-cycle models. Journal of Geophysical Research 116, doi:
1413 10.1029/2011JF002061, issn: 0148-0227, 2011.

1414 Bullard, J. E., Baddock, M., Bradwell, T., Crusius, J., Darlington, E., Gaiero, D., … McCulloch, R.: High-latitude dust in the
1415 Earth system. Reviews of Geophysics, 54, 2, 447–485, 2016.

1416 Butwin, M.K., Pfeffer, M.A., von Löwis, S., Støren, E.,W.N., Bali, E. and Thorsteinsson, T.: Properties of dust source material
1417 and volcanic ash in Iceland, Sedimentology, 67, 6, 3067-3087, doi:10.1111/sed.12734, 2020.

1418 Chewings, J., Atkins, C, Dunbar, G., and Golledge, N.: Aeolian sediment transport and deposition in a modern high latitude
1419 glacial marine environment. Sedimentology, v. 61, 6, 1485–1882, doi: 10.1111/sed.12108, 2014.

1420 Conca, E., Abollino, O., Giacomino, A., Buoso, S., Traversi, R., Becagli, S., Grotti, M., and Malandrino, M.: Source
1421 identification and temporal evolution of trace elements in PM10 collected near to Ny-Ålesund (Norwegian Arctic), Atmos.
1422 Environ., 203, 153–165, doi:10.1016/j.atmosenv.2019.02.001, 2019.

1423 Coronato, A., Mazzoni, E., Vázquez, M., and Coronato, F.: PATAGONIA Una síntesis de su Geografía Física (Ediciones).
1424 Río Gallegos, Argentina: Universidad Nacional de la Patagonia Austral. Retrieved from
1425 http://www.unpa.edu.ar/sites/default/files/publicaciones_adjuntos/PATAGONIA_una sintesis de su geografia fisica
1426 web_0.pdf, 2017.

1427 Cosentino, N. J., Ruiz-Etcheverry, L. A., Bia, G. L., Simonella, L. E., Coppo, R., Torre, G., et al. Does Satellite Chlorophyll-
1428 a Respond to Southernmost Patagonian Dust? A Multi-year, Event-Based Approach. Journal of Geophysical Research:
1429 Biogeosciences, 125, 12, doi:10.1029/2020JG006073, 2020.

1430 Creamean, J.M., Suski, K.J., Rosenfeld, D., Cazorla, A., DeMott, P.J., Sullivan, R.C., White, A.B., Ralph, F.M., Minnis, P.,
1431 Comstock, J.M., Tomlinson, J.M., Prather, K.A.: Dust and biological aerosols from the Sahara and Asia influence precipitation
1432 in the Western U.S., Science, 339, 6127, 1572-1578, doi:10.1126/science.1227279, 2013.

1433 Crespi-Abril, A. C., Soria, G., De Cian, A., and López-Moreno, C.: Roaring forties: An analysis of a decadal series of data of
1434 dust in Northern Patagonia. Atmospheric Environment, doi:10.1016/j.atmosenv.2017.11.019, 2017.

1435 Crocchianti,S.; Moroni,B.; Waldhauserová, P.D.; Becagli, S.; Severi, M.; Traversi, R.; Cappelletti, D. Potential Source
1436 Contribution Function Analysis of High Latitude Dust Sources over the Arctic: Preliminary Results and Prospects. Atmosphere
1437 2021, 12, 347, doi:10.3390/ atmos12030347, 2021.

1438 Crusius, J.: Dissolved Fe Supply to the Central Gulf of Alaska Is Inferred to Be Derived From Alaskan Glacial Dust That Is
1439 Not Resolved by Dust Transport Models. Journal of Geophysical Research: Biogeosciences, 126, 6, e2021JG006323,
1440 doi:10.1029/2021JG006323, 2021.

1441 Crusius, J., Schroth, A. W., Gassó, S., Moy, C. M., Levy, R. C., and Gatica, M.: Glacial flour dust storms in the Gulf of Alaska:
1442 Hydrologic and meteorological controls and their importance as a source of bioavailable iron, Geophysical Research Letters,
1443 38, doi: 10.1029/2010gl046573, 2011.

1444 Crusius, J., Schroth, A. W., Resing, J. A., Cullen, J., and Campbell, R. W. Seasonal and spatial variabilities in northern Gulf
1445 of Alaska surface water iron concentrations driven by shelf sediment resuspension, glacial meltwater, a Yakutat eddy, and
1446 dust. Global Biogeochemical Cycles, 31, 6, 942–960, doi:10.1002/2016GB005493, 2017.

1447 Csavina, J., Field, J., Taylor, M.P., Gao, S., Landázuri, A., Betterton, E.A., Sáez, A.E.: A review on the importance of metals
1448 and metalloids in atmospheric dust and aerosol from mining operations, Science of The Total Environment, 433, 58-73,
1449 doi:10.1016/j.scitotenv.2012.06.013, 2012.

1450 Cvetkovic, et al., 2021: Fully dynamic numerical prediction model for dispersion of Icelandic mineral dust (submitted), 2021.

1451 Dagsson-Waldhauserová P. and Meinander O.: Editorial: Atmosphere - cryosphere interaction in the Arctic, at high latitudes
1452 and mountains with focus on transport, deposition and effects of dust, black carbon, and other aerosols. Front. Earth Sci., 18
1453 December 2019, https://doi.org/10.3389/feart.2019.00337, 2019.

1454 Dagsson-Waldhauserová, P. and Meinander, O. (eds.): Atmosphere – Cryosphere Interaction in the Arctic, at High Latitudes
1455 and Mountains With Focus on Transport, Deposition and Effects of Dust, Black Carbon, and Other Aerosols. Lausanne:
1456 Frontiers Media SA. ISSN 1664-8714, ISBN 978-2-88963-504-7, doi: 10.3389/978-2-88963-504-7, e-book, 2020.

1457 Dagsson-Waldhauserová, P., O. Arnalds, H. Ólafsson, L. Skrabalova, G. Sigurðardóttir, M. Branis, J. Hladil, R. Skala, T.
1458 Navratil, L. Chadimova, S. Löwis, T. Thorsteinsson, H. Carlsen, I. Jónsdóttir, Physical properties of suspended dust during
1459 moist and low wind conditions in Iceland. Icelandic Agricultural Sciences 27, 25-39, 2014.

1460 Dagsson-Waldhauserová, P., O. Arnalds, H. Olafsson, J. Hladil, R. Skala, T. Navratil, L. Chadimova, O. Meinander: Snow–
1461 Dust Storm: Unique case study from Iceland, March 6–7, 2013. Aeolian Res 16, 69-74, 2015.

1462 Dagsson-Waldhauserová P, Magnusdottir AÖ, Olafsson H, Arnalds O: The spatial variation of dust particulate matter
1463 concentrations during two Icelandic dust storms in 2015. Atmosphere, 7, 77, 2016.

1464 Dagsson-Waldhauserová, P., Renard, J.-B., Olafsson, H., Vignelles, D., Berthet, G., Verdier, N., Duverger, V.: Vertical
1465 distribution of aerosols in dust storms during the Arctic winter. Scientific Reports 6, 1-11, 2019.

1466 Dang, C., Warren, S. G., Fu, Q., Doherty, S. J., Sturm, M., and Su, J.: Measurements of light-absorbing particles in snow
1467 across the Arctic, North America, and China: Effects on surface albedo, J. Geophys. Res. Atmos., 122, 10,149– 10,168,
1468 doi:10.1002/2017JD027070, 2017.

1469 Diaz, M.A., Welch, S.A., Sheets, J.M., Welch, K.A., Khan, A.L., Adams, B.J., McKnight, D.M., Cary, S.C, W.B, Lyons:
1470 Geochemistry of aeolian material from the McMurdo Dry Valleys, Antarctica: Insights into Southern Hemisphere dust sources.
1471 Earth and Planetary Science Letters, 547, doi:10.1016/j.epsl.2020.116460, 2020.

1472 Dijkmans, J. W. A., and Törnqvist, T.E.: Modern periglacial eolian deposits and landforms in the Søndre Strømfjord area,
1473 West Greenland and their palaeoenvironmental implications. Meddelelser Om Grønland Geoscience, 25, 3–39, 1991.

1474 Doody, J.P., Ferreira, M., Lombardo, S., Lucius, I., Misdorp, R., Niesing, H., Salman, A., and Smallegange, M. (eds): Living
1475 with coastal erosion in Europe – sediment and space for sustainability. Results from the EUROSION study, European
1476 Commission, Office for Official Publications of the European Communities. Available at:
1477 http://www.eurosion.org/project/eurosion_en.pdf (last accessed 19 November 2021), 2004.

1478 Đorđević Dragana, Tošić Ivana, Sakan Sanja, Petrović Srđan, Đuričić-Milanković Jelena, Finger David C., Dagsson-
1479 Waldhauserová P.: Can Volcanic Dust Suspended From Surface Soil and Deserts of Iceland Be Transferred to Central Balkan
1480 Similarly to African Dust (Sahara)? Frontiers in Earth Science, 7, doi:10.3389/feart.2019.00142, 2019.

1481 Dragosics, M., Meinander, O., Jonsdottir, T. et al. Insulation effects of Icelandic dust and volcanic ash on snow and ice,
1482 Arabian Journal of Geosciences Volume: 9 Issue: 2, Dust special issue, DOI: 10.1007/s12517-015-2224-6, 2016.

1483 Dörnbrack, A., Stachlewska, I. S., Ritter, C., and Neuber, R.: Aerosol distribution around Svalbard during intense easterly
1484 winds, Atmos. Chem. Phys., 10, 1473–1490, https://doi.org/10.5194/acp-10-1473-2010, 2010.

1485 Evangeliou, N., Shevchenko, V. P., Yttri, K. E., Eckhardt, S., Sollum, E., Pokrovsky, O. S., Kobelev, V. O., Korobov, V. B.,
1486 Lobanov, A. A., Starodymova, D. P., Vorobiev, S. N., Thompson, R. L., and Stohl, A.: Origin of elemental carbon in snow

1487   from western Siberia and northwestern European Russia during winter–spring 2014, 2015 and 2016, Atmos. Chem. Phys., 18,
1488   963–977, https://doi.org/10.5194/acp-18-963-2018, 2018.

1489   Finlayson-Pitts, B.J. and Pitts, J.N. Jr., Chemistry of the upper and lower atmosphere: theory, experiments, and applications,
1490   Elsevier, 969 p., 1999.

1491   Flanner, M. G., Zender, C. S., Randerson, J. T., and Rasch, P. T.: Present day climate forcing and response from black carbon
1492   in snow. J. Geophys. Res. 112:D11202. doi: 10.1029/2006JD008003, 2007.

1493   Foroutan, H., et al. Development and evaluation of a physics-based windblown dust emission scheme implemented in the
1494   CMAQ modeling system, J Adv Model Earth Syst.,9, 1, 585–608, 2017.

1495   Forsström, S., Isaksson, E., Skeie, R. B., Ström, J., Pedersen, C. A., Hudson, S. R., Berntsen, T. K., Lihavainen, H.,
1496   Godtliebsen, F. and Gerland, S.: Elemental carbon measurements in European Arctic snow packs, J. Geophys. Res. Atmos.,
1497   118, 13,614–13,627, 2013.

1498   Fountain, A.G., Levy, J.S., Gooseff, M.N., Van Horn, D: The McMurdo Dry Valleys: A landscape on the threshold of change
1499   (2014). *Geomorphology* 225, 15, P, 25-35, doi:/10.1016/j.geomorph.2014.03.044, 2014.

1500   Fox, T. A., Barchyn, T. E. and Hugenholtz, C. H.: Successes of soil conservation in the Canadian Prairies highlighted by a
1501   historical decline in blowing dust, Environ. Res. Lett., 7, 1, doi:10.1088/1748-9326/7/1/014008, 2012.

1502   Frey, W. R., and J. E. Kay: The influence of extratropical cloud phase and amount feedbacks on climate sensitivity, Climate
1503   Dynamics, 50, 7, 3097-3116, doi:10.1007/s00382-017-3796-5, 2018.

1504   Gaiero, D. M., Probst, J.-L., Depetris, P. J., Bidart, S. M., and Leleyter, L.: Iron and other transition metals in Patagonian
1505   riverborne and windborne materials: geochemical control and transport to the southern South Atlantic Ocean. Geochimica et
1506   Cosmochimica Acta, 67, 19, 3603–3623, doi:10.1016/S0016-7037(03)00211-4, 2003.

1507   Gaitán, J. J., López, C. R., and Bran, D.: Efectos del pastoreo sobre el suelo y la vegetación en la estepa patagónica. Ci. Suelo
1508   (Argentina), 27, 2, 261–270, 2009.

1509   Gallet, J.-C., Björkman, M. P., Larose, C., Luks, B., Martma, T., and Zdanowicz, C.: Protocols and recommendations for the
1510   measurement of snow physical properties, and sampling of snow for black carbon, water isotopes, major ions and
1511   microorganisms, Norsk Polarinstitutt, 27 p., 2018.

1512 Gardner, A. S. and Sharp, M. J.: A review of snow and ice albedo and the development of a new physically based broadband
1513 albedo parameterization, J. Geophys. Res., 115, F01009, doi: 10.1029/2009JF001444, 2010.

1514 Gassó, S., twitter.com/SanGassó, 2 Gassó, Santiago (@SanGassó). "Sunrise in Alaska and more #highlatitudedust is visible
1515 in Larsen Bay, just downwind from the Ten Thousand Smokes Valley in @KatmaiNPS, visible in webcams and early GOES17
1516 image." Nov 2, 2020 , Tweet, https://twitter.com/SanGassó/status/1323716227793997824?, 2020a.

1517 Gassó, Santiago (@SanGassó)."More #highlatitudedust today in #Alaska , 3 active sources identified in #NOAA20. Surface
1518 webcams confirm dust presence." Nov 2, 2020 , Twitter. https://twitter.com/SanGassó/status/1323384615344640000, 2020b.

1519 Gassó, Santiago (@SanGassó). "#highlatitudedust in SE Alaska yesterday several plumes are visible in the spots where there
1520 is little snow " Jan, 27, 2021. Twitter. https://twitter.com/SanGassó/status/1354548215186644993021, 2021a.

1521 Gassó, S., twitter.com/SanGassó, 2 Gassó, Santiago (@SanGassó), "A very nice example of #highlatitudedust activity in
1522 western #Greenland", Oct 19, 2021, https://twitter.com/SanGassó/status/1450468551379329029, 2021b.

1523 Gassó, S., and Stein, A. F.: Does dust from Patagonia reach the sub-Antarctic Atlantic Ocean? Geophysical Research Letters,
1524 34, 1, L01801. https://doi.org/10.1029/2006GL027693, 2007.

1525 Gassó, S., and Torres, O.: Temporal Characterization of Dust Activity in the Central Patagonia Desert (Years 1964–2017).
1526 Journal of Geophysical Research: Atmospheres, 124, 6, 3417–3434, doi:10.1029/2018JD030209, 2019.

1527 Gassó, S., Stein, A., Marino, F., Castellano, E., Udisti, R., and Ceratto, J.: A combined observational and modeling approach
1528 to study modern dust transport from the Patagonia desert to East Antarctica. Atmospheric Chemistry and Physics, 10, 17,
1529 8287–8303, doi:10.5194/acp-10-8287-2010, 2010.

1530 George, C., Ammann, M., D'Anna, B., Donaldson, D. J., Nizkorodov, S A.: Heterogeneous Photochemistry in the Atmosphere.
1531 Chem. Rev. 115, 4218-4258, doi: 10.1021/cr500648z, 2015.

1532 Gili, S., Vanderstraeten, A., Chaput, A., King, J., Gaiero, D., Delmonte, B., Vallelonga, P., Formenti, P., Di Biagio, C.,
1533 Cazanau, M. and Pangui, E.: Southern Africa: The Missing Piece To The Dust Provenance Puzzle of East Antarctica?
1534 Communications Earth & Environment, doi: 10.21203/rs.3.rs-923449/v1, 2021.

1535 Gillies, J. A., W. G. Nickling, and M. Tilson: Frequency, magnitude and characteristics of aeolian sediment transport:
1536 McMurdo Dry Valleys, Antarctica, J. Geophys. Res. Earth Surf., 118, 461–479, doi:10.1002/jgrf.20007.2013.

1537 Ginoux, P., J. M. Prospero, T. E. Gill, N. C. Hsu, M. Zhao: Global-scale attribution of anthropogenic and natural dust
1538 sources and their emission rates based on MODIS Deep Blue aerosol products. Rev. Geophys. 50, RG3005, 2012.

1539 Groot Zwaaftink, C. D., Grythe, H., Skov, H., and Stohl, A.: Substantial contribution of northern high-latitude sources to
1540 mineral dust in the Arctic, Journal of Geophysical Research-Atmospheres, 121, 13678-13697, doi: 10.1002/2016jd025482,
1541 2016.

1542 Groot Zwaaftink, C. D., Arnalds, O., Dagsson-Waldhauserová, P., Eckhardt, S., Prospero, J. M., and Stohl, A.: Temporal and
1543 spatial variability of Icelandic dust emission and atmospheric transport, Atmos. Chem. Phys., 17, 10865-10878, 2017.

1544 Gunnarsson, A., Gardarsson, S. M., Pálsson, F., Jóhannesson, T., and Sveinsson, Ó. G. B.: Annual and interannual variability
1545 and trends of albedo for Icelandic glaciers. The Cryosphere 15, 547–570, 2020.

1546 Hadley, D., G. L. Hufford, and J. J. Simpson: Resuspension of relic volcanic ash and dust from Katmai: Still an aviation
1547 hazard, Weather Forecast., 19, 5, 829–840, doi:10.1175/1520-0434(2004)019<0829:RORVAA>2.0.CO;2, 2004.

1548 Hadley, O., and Kirchstetter, T.: Black-Carbon reduction of snow albedo. Nat. Clim. Change 2, 437–440. doi:
1549 10.1038/nclimate1433, 2012.

1550 Hardy M. and Cornu S. Location of natural trace elements in silty soils using particle-size fractionation. Geoderma, 133, 295-
1551 308, doi:10.1016/j.geoderma.2005.07.015, 2006.

1552 Harrison, A. D., K. Lever, A. Sanchez-Marroquin, M. A. Holden, T. F. Whale, M. D. Tarn, J. B. McQuaid, and B. J. Murray:
1553 The ice-nucleating ability of quartz immersed in water and its atmospheric importance compared to K-feldspar, Atmos. Chem.
1554 Phys., 19, 17, 11343-11361, doi:10.5194/acp-19-11343-2019, 2019.

1555 Hedding DW, Werner Nel, Ryan L. Anderson, Aeolian processes and landforms in the sub-Antarctic: preliminary observations
1556 from Marion Island, Polar Research, 34, 1, 26365, doi:10.3402/polar.v34.26365, 2015.

1557 Heindel RC, Lauren E Culler, Ross A Virginia, Rates and processes of aeolian soil erosion in West Greenland, The Holocene,
1558 27,9, 1281-1290, doi:10.1177/0959683616687381, 2017.

1559 Hernández, M. A., González, N., and Hernández, L.: Late Cenozoic Geohydrology of Extra-Andean Patagonia, Argentina. In
1560 J. Rabassa (Ed.), The Late Cenozoic of Patagonia and Tierra del Fuego, Vol. 11, 497–509, Elsevier, doi:10.1016/S1571-
1561 0866(07)10024-5, 2008.

1562 Hobbs, W. H.: Wind: The dominant transportation agent within extramarginal zones to continental glaciers. The Journal of
1563 Geology, 50, 5, 556–59, doi:10.1086/625072, 1942.

1564 Hojan, M., Rurek, M., Więcław, M., and Krupa, A.: Effects of Extreme Dust Storm in Agricultural Areas (Poland, the Greater
1565 Lowland). Geosciences, 9, 106, doi:10.3390/geosciences9030106, 2019.

1566 Hugenholtz, C. H. and Wolfe, S. A.: Rates and environmental controls of aeolian dust accumulation, Athabasca River
1567 Valley, Canadian Rocky Mountains, Geomorphology, 121, 3, 274–282, doi:10.1016/j.geomorph.2010.04.024, 2010.

1568 IPCC, 2013: Climate Change 2013: The Physical Science Basis. Contribution of Working Group I to the Fifth Assessment
1569 Report of the Intergovernmental Panel on Climate Change [Stocker, T.F., D. Qin, G.-K. Plattner, M. Tignor, S.K. Allen, J.
1570 Boschung, A. Nauels, Y. Xia, V. Bex and P.M. Midgley (eds.)]. Cambridge University Press, Cambridge, United Kingdom
1571 and New York, NY, USA, 1535 p., 2013.

1572 IPCC, 2019: IPCC Special Report on the Ocean and Cryosphere in a Changing Climate [H.-O. Pörtner, D.C. Roberts, V.
1573 Masson-Delmotte, P. Zhai, M. Tignor, E. Poloczanska, K. Mintenbeck, A. Alegría, M. Nicolai, A. Okem, J. Petzold, B. Rama,
1574 N.M. Weyer (eds.)]. In press. (last accessed 19 November 2021), 2019.

1575 IPCC, 2021: Climate Change 2021: The Physical Science Basis. Contribution of Working Group I to the Sixth Assessment
1576 Report of the Intergovernmental Panel on Climate Change [Masson-Delmotte, V., P. Zhai, A. Pirani, S.L. Connors, C. Péan,
1577 S. Berger, N. Caud, Y. Chen, L. Goldfarb, M.I. Gomis, M. Huang, K. Leitzell, E. Lonnoy, J.B.R. Matthews, T.K. Maycock,
1578 T. Waterfield, O. Yelekçi, R. Yu, and B. Zhou (eds.)]. Cambridge University Press. In Press, (last accessed 19 November
1579 2021), 2021.

1580 Irish, V. E., et al.: Ice nucleating particles in the marine boundary layer in the Canadian Arctic during summer 2014, Atmos.
1581 Chem. Phys., 19, 2, 1027-1039, doi:10.5194/acp-19-1027-2019, 2019.

1582 Ito, A., and Kok, J. F.: Do dust emissions from sparsely vegetated regions dominate atmospheric iron supply to the Southern
1583 Ocean?, Journal of Geophysical Research-Atmospheres, 122, 3987-4002, doi: 10.1002/2016jd025939, 2017.

1584 IUSS Working Group WRB: World Reference Base for Soil Resources 2014, update 2015 International soil classification
1585 system for naming soils and creating legends for soil maps. World Soil Resources Reports No. 106. FAO, Rome, 2015.

1586 Jacobi, H.-W., Obleitner, F., Da Costa, S., Ginot, P., Eleftheriadis, K., Aas, W., and Zanatta, M.: Deposition of ionic species
1587 and black carbon to the Arctic snowpack: combining snow pit observations with modeling, Atmos. Chem. Phys., 19, 10361–
1588 10377, https://doi.org/10.5194/acp-19-10361-2019, 2019.

Janjic Z. I., J. P. Gerrity, Jr. and S. Nickovic: An Alternative Approach to Nonhydrostatic Modeling, Mon. Wea. Rev., 129, 1164-1178, 2001.

Jickells, T., and Moore, C. M.: The importance of Atmospheric Deposition for Ocean Productivity, Annu. Rev. Ecol. Evol. Syst., 46, 481-501, doi: 10.1146/annurev-ecolsys-112414-054118, 2015.

Jickells, T. D., An, Z. S., Andersen, K. K., Baker, A. R., Bergametti, G., Brooks, N., Cao, J. J., Boyd, P. W., Duce, R. A., Hunter, K. A., Kawahata, H., Kubilay, N., laRoche, J., Liss, P. S., Mahowald, N., Prospero, J. M., Ridgwell, A. J., Tegen, I., and Torres, R.: Global iron connections between desert dust, ocean biogeochemistry, and climate, Science, 308, 67-71, doi: 10.1126/science.1105959, 2005.

Johnson, M. S., Meskhidze, N., Kiliyanpilakkil, V. P., and Gassó, S.: Understanding the transport of Patagonian dust and its influence on marine biological activity in the South Atlantic Ocean. Atmospheric Chemistry and Physics, 11, 6, 2487–2502, 2011.

Kanakidou, M., Myriokefalitakis, S., and Tsigaridis, K.: Aerosols in atmospheric chemistry and biogeochemical cycles of nutrients, Environmental Research Letters, 13, doi: 10.1088/1748-9326/aabcdb, 2018.

Kandler, K.; Schneiders, K.; Heuser, J.; Waza, A.; Aryasree, S.; Althausen, D.; Hofer, J.; Abdullaev, S.F.; Makhmudov, A.N. Differences and Similarities of Central Asian, African, and Arctic Dust Composition from a Single Particle Perspective. Atmosphere 2020, 11, 269. doi:10.3390/atmos11030269, 2020.

Kasimov, N. S., Vlasov, D. V., and Kosheleva, N. E.: Enrichment of road dust particles and adjacent environments with metals and metalloids in eastern Moscow, Urban Clim., 32, 100638, doi:10.1016/j.uclim.2020.100638, 2020.

Kavan, J., Ondruch J, Nývlt D, Hrbáček F, Carrivick JL, Láska K.: Seasonal hydrological and suspended sediment transport dynamics in proglacial streams, James Ross Island, Antarctica. Geografiska Annaler: Series A, Physical Geography 99, 38-55, doi: 10.1080/04353676.2016.1257914, 2017.

Kavan, J., Dagsson-Waldhauserová P, Renard JB, Láska K, Ambrožová, K.: Aerosol concentrations in relationship to local atmospheric conditions on James Ross Island, Antarctica. Frontiers in Earth Science 6: DOI: 10.3389/feart.2018.00207, 2018.

Kavan, J., Kamil Láska K, Adam Nawrot A, and Tomasz Wawrzyniak T.: High Latitude Dust Transport Altitude Pattern Revealed from Deposition on Snow, Svalbard. Atmosphere 2020, 11, 1318; doi:10.3390/atmos11121318., 2020a.

1614 Kavan, J, Nývlt D, Láska K, Engel Z, Kňažková M.: High latitude dust deposition in snow on glaciers of James Ross Island,
1615 Antarctica. Earth Surface Processes and Landforms. DOI: 10.1002/esp.4831, 2020b.

1616 Khan, A. L., Dierssen, H., Schwarz, J. P., Schmitt, C., Chlus, A., Hermanson, M., Painter, T. H., and McKnight, D. M.: Impacts
1617 of coal dust from an active mine on the spectral reflectance of Arctic surface snow in Svalbard, Norway, J. Geophys. Res.,
1618 122, 1767–1778, doi:10.1002/2016jd025757, 2017.

1619 Kňažková, M., Hrbáček, F., Kavan, J., Nývlt, D. Effect of hyaloclastite breccia boulders on meso-scale periglacial-aeolian
1620 landsystem in semi-arid Antarctic environment, James Ross Island, Antarctic Peninsula. Cuadernos de Investigación
1621 Geográfica. doi: 10.18172/cig.3800, 2020.

1622 Koroleva, T. V., Krechetov, P. P., Semenkov, I. N., Sharapova, A. V. and Kondrat'ev, A. D.: Transformation of chemical
1623 composition of snow in the impact areas of the first stage of the expandable launch system Proton in Central Kazakhstan, Russ.
1624 Meteorol. Hydrol., 41(8), 585–591, doi:10.3103/S1068373916080094, 2016.

1625 Koroleva, T. V., Sharapova, A. V. and Krechetov, P. P.: A chemical composition of snow on areas exposed to space-rocket
1626 activities pollution (Altai republic), Gig. i Sanit., doi:10.1882/0016-9900-2017-96-5-432-437, 2017.

1627 Kuhlman, H.: Den potentielle jordfygning på danske marker. Teoretiske beregninger vedrørende jordmaterialets
1628 vindbevægelighed. Geografisk Tidsskrift - Danish Journal of Geography, 59. Retrieved from
1629 https://tidsskrift.dk/geografisktidsskrift/article/view/46533, 1960.

1630 Kuhns, H., Gillies, J., Etyemezian, V., Nikolich, G., King, J., Zhu, D., Uppapalli, S., Engelbrecht, J., and Kohl, S.: Effect of
1631 Soil Type and Momentum on Unpaved Road Particulate Matter Emissions from Wheeled and Tracked Vehicles. Aerosol
1632 Science and Technology - AEROSOL SCI TECH., 44, 187-196, doi:10.1080/02786820903516844, 2010.

1633 Kupiainen K.: Road dust from pavement wear and traction sanding. Monographs of the Boreal Environment Research,
1634 No. 26, Mono_26.indd (helsinki.fi), 2007.

1635 Kupiainen, K., Ritola, R., Stojiljkovic, A., Pirjola, L., Malinen, A., and Niemi, J. Contribution of mineral dust sources to street
1636 side ambient and suspension PM10 samples. Atmospheric Environment, 147, 178-189. doi:10.1016/j.atmosenv.2016.09.059,
1637 2016.

1638 Kylling A., Groot Zwaaftink, C. D., and Stohl, A.: Mineral dust instantaneous radiative forcing in the Arctic. Geophysical
1639 Research Letters, 45, 4290–4298. doi:10.1029/2018GL077346, 2018.

1640 Lamy, F., Gersonde, R.,Winckler, G., Esper, O., Jaeschke, A., Kuhn, G.; Ullermann, J., Martinez-Garcia, A., Lambert, F.,
1641 Kilian, R.: Increased dust deposition in the Pacific Southern Ocean during glacial periods. Science, 343, 403–407, 2014.

1642 Lancaster, N., Nickling, W.G. and Gillies, J.A.: Sand transport by wind on complex surfaces: field studies in the McMurdo
1643 Dry Valleys, Antarctica. J. Geophys. Res., 115, F03027, 2010.

1644 Lappalainen, H. K., Petäjä, T., Vihma, T., Räisänen, J., Baklanov, A., Chalov, S., Esau, I., Ezhova, E., Leppäranta, M.,
1645 Pozdnyakov, D., Pumpanen, J., Andreae, M. O., Arshinov, M., Asmi, E., Bai, J., Bashmachnikov, I., Belan, B., Bianchi, F.,
1646 Biskaborn, B., Boy, M., Bäck, J., Cheng, B., Chubarova, N., Duplissy, J., Dyukarev, E., Eleftheriadis, K., Forsius, M.,
1647 Heimann, M., Juhola, S., Konovalov, V., Konovalov, I., Konstantinov, P., Köster, K., Lapshina, E., Lintunen, A., Mahura, A.,
1648 Makkonen, R., Malkhazova, S., Mammarella, I., Mammola, S., Buenrostro Mazon, S., Meinander, O., Mikhailov, E., Miles,
1649 V., Myslenkov, S., Orlov, D., Paris, J.-D., Pirazzini, R., Popovicheva, O., Pulliainen, J., Rautiainen, K., Sachs, T., Shevchenko,
1650 V., Skorokhod, A., Stohl, A., Suhonen, E., Thomson, E. S., Tsidilina, M., Tynkkynen, V.-P., Uotila, P., Virkkula, A., Voropay,
1651 N., Wolf, T., Yasunaka, S., Zhang, J., Qiu, Y., Ding, A., Guo, H., Bondur, V., Kasimov, N., Zilitinkevich, S., Kerminen, V.-
1652 M., and Kulmala, M.: Overview: Recent advances in the understanding of the northern Eurasian environments and of the urban
1653 air quality in China – a Pan-Eurasian Experiment (PEEX) programme perspective, Atmos. Chem. Phys., 22, 4413–4469,
1654 doi:10.5194/acp-22-4413-2022, 2022.

1655 Lewandowski, M., Kusiak, M.A., Werner, T., Nawrot, A., Barzycka, B., Laska, M., Luks, B.: Seeking the Sources of Dust:
1656 Geochemical and Magnetic Studies on "Cryodust" in Glacial Cores from Southern Spitsbergen (Svalbard, Norway).
1657 Atmosphere 2020, 11, 1325, doi:10.3390/atmos11121325, 2020.

1658 Llanos, M. E., Behr, S. J., Gonzalez, J. H., Colombani, E. N., Buono, G. G., and Escobar, J. M.: Informe de las Variaciones
1659 del Lago Colhue Huapi mediante sensores remotos y su relación con las precipitaciones. Retrieved January 5, 2018, from
1660 https://inta.gob.ar/documentos/informe-de-las-variaciones-del-lago-colhue-huapi-mediante-sensores-remotos-y-su-relacion-
1661 con-las-precipitaciones, 2016.

1662 Lutz, S., Anesio, A., Raiswell, R. et al.: The biogeography of red snow microbiomes and their role in melting Arctic glaciers,
1663 Nat. Commun. 7, 11968, 2016.

1664 Mahowald, N.: Aerosol Indirect Effect on Biogeochemical Cycles and Climate, Science, 334, 794-796, doi:
1665 10.1126/science.1207374, 2011.

1666 Mahowald, N. M., Baker, A. R., Bergametti, G., Brooks, N., Duce, R. A., Jickells, T. D., Kubilay, N., Prospero, J. M., and
1667 Tegen, I.: Atmospheric global dust cycle and iron inputs to the ocean, Global Biogeochem. Cy., 19, doi:
1668 10.1029/2004gb002402, 2005.

1669 Mahowald, N. M., Kloster, S., Engelstaedter, S., Moore, J. K., Mukhopadhyay, S., McConnell, J. R., Albani, S., Doney, S. C.,
1670 Bhattacharya, A., Curran, M. A. J., Flanner, M. G., Hoffman, F. M., Lawrence, D. M., Lindsay, K., Mayewski, P. A., Neff, J.,
1671 Rothenberg, D., Thomas, E., Thornton, P. E., and Zender, C. S.: Observed 20th century desert dust variability: impact on
1672 climate and biogeochemistry, Atmos. Chem. Phys., 10, 10875-10893, doi: 10.5194/acp-10-10875-2010, 2010.

1673 Manninen, T., Anttila, K., Jääskeläinen, E., Riihelä, A., Peltoniemi, J., Räisänen, P., Lahtinen, P., Siljamo, N., Thölix, L.,
1674 Meinander, O., Kontu, A., Suokanerva, H., Pirazzini, R., Suomalainen, J., Hakala, T., Kaasalainen, S., Kaartinen, H., Kukko,
1675 A., Hautecoeur, O., and Roujean, J.-L.: Effect of small-scale snow surface roughness on snow albedo and reflectance, The
1676 Cryosphere, 15, 793–820, doi:10.5194/tc-15-793-2021, 2021.

1677 Markuse, Pierre: High latitude dust storm (silt), Nuussuaq Peninsula, Greenland - October 1st, 2020,
1678 https://www.flickr.com/photos/pierre_markuse/50447335522/ , contains modified Copernicus Sentinel data [2020], processed
1679 by Pierre Markuse, originally posted to Flickr by Pierre Markuse at https://flickr.com/photos/24998770@N07/50447335522.,
1680 reviewed on 25 October 2020 by FlickreviewR 2, licensed under the terms of the cc-by-2.0.2020, 2020.

1681 Martin, J. H., and Fitzwater, S. E.: Iron deficiency limits phytoplankton growth in the north-east Pacific sub Arctic, Nature,
1682 331, 341-343, 1988.

1683 Martínez-García, A., Sigman, D. M., Ren, H., Anderson, R. F., Straub, M., Hodell, D. A., Jaccard, S. L., Eglinton, T. I., and
1684 Haug, G. H.: Iron fertilization of the Sub-Antarctic Ocean during the last ice age, Science, 343, 1347-1350, 2014.

1685 Mazzonia, E., and Vazquez, M.: Desertification in Patagonia. In E. M. Latrubesse (Ed.), Natural Hazards and Human-
1686 Exacerbated Disasters in Latin America, Vol. 13, 351–377, Elsevier, doi:10.1016/S0928-2025(08)10017-7, 2009.

1687 McCutcheon, J., Lutz, S., Williamson, C. et al.: Mineral phosphorus drives glacier algal blooms on the Greenland Ice Sheet.
1688 Nat. Commun. 12, 570, doi:10.1038/s41467-020-20627-w, 2021.

1689 Meinander, O., Kazadzis, S., Arola, A., Riihelä, A., Räisänen, P., Kivi, R., Kontu, A., Kouznetsov, R., Sofiev, M., Svensson,
1690 J., Suokanerva, H., Aaltonen, V., Manninen, T., Roujean, J.-L., and Hautecoeur, O.: Spectral albedo of seasonal snow during
1691 intensive melt period at Sodankylä, beyond the Arctic Circle, Atmos. Chem. Phys., 13, 3793–3810, doi:10.5194/acp-13-3793-
1692 2013, 2013.

1693 Meinander, O.; Kontu, A.; Virkkula, A.; et al., Brief communication: Light-absorbing impurities can reduce the density of
1694 melting snow, Cryosphere, Volume: 8 Issue: 3 Pages: 991-995, doi: 10.5194/tc-8-991-2014, 2014.

1695   Meinander, O., Dagsson-Waldhauserová, P., and Arnalds, O.: Icelandic volcanic dust can have a significant influence on the
1696   cryosphere in Greenland and elsewhere, Polar Research Volume: 35, doi: 10.3402/polar.v35.31313, 2016.

1697   Meinander O., Backman, L., Saranko,O., Asmi, E., Rodriguez, E. and Sanchez, R.: Effects of high latitude dust on snow UV
1698   albedo and solar UV irradiance measured at Marambio during 2013-2017 with comparison to simulated UV irradiances,
1699   Geophysical Research Abstracts Vol. 20, EGU2018-2007, 2018 EGU General Assembly 2018, available at
1700   https://meetingorganizer.copernicus.org/EGU2018/EGU2018-2007.pdf, 2018.

1701   Meinander, O., S. Chalov, H. Lappalainen, J. Ekman, K. Eleftheriadis, D. Frolov, A. Hyvärinen, V. Ivanov, N. Karvosenoja,
1702   K. Kupiainen, O. Popovicheva, I. Semenkov, L. Sogacheva, and The MSU Workshop Participants: About Black Carbon in the
1703   Arctic and Significance Compared to Hight-Latitude Dust Sources (Finnish-Russian Workshop at the Lomonosov Moscow
1704   State University, 17-18 September 2019, in Co-operation with MSU, INAR, PEEX, MFA/IBA and FMI), In: Tiia Laurila,
1705   Anna Lintunen, Markku Kulmala (eds.), Proceedings of The Center of Excellence in Atmospheric Science (CoE ATM) Annual
1706   Seminar 2019, Report series in aerosol science, available at: http://www.faar.fi/wp-
1707   content/uploads/2019/11/CoE_proceedings_2019-compressed.pdf, p. 457-465, 2019a.

1708   Meinander O., Dagsson-Waldhauserová P., Björnsson H., Petersen G.N., Moore K., Larsen J.N. and Heininen L.: Report of
1709   the IASC Workshop on Effects and Extremes of High Latitude Dust, 13-14 FEB 2019, in co-operation with the IceDust Aerosol
1710   Association, IBA-FIN-BCDUST-project of MFA of Finland and EU COST InDust Action. Available at
1711   https://iasc.info/news/iasc-news/472-workshop-report-iasc-workshop-on-effects-and-extremes-of-high-latitude-dust, last
1712   accessed 3 June 2021, 2019b.

1713   Meinander, O.; Heikkinen, E.; Aurela, M.; Hyvärinen, A.: Sampling, Filtering, and Analysis Protocols to Detect Black Carbon,
1714   Organic Carbon, and Total Carbon in Seasonal Surface Snow in an Urban Background and Arctic Finland (>60°N).
1715   Atmosphere, 11, 923, doi:10.3390/atmos11090923, 2020a.

1716   Meinander O., Kontu A., Kouznetsov R., Sofiev M.: Snow Samples Combined With Long-Range Transport Modeling to
1717   Reveal the Origin and Temporal Variability of Black Carbon in Seasonal Snow in Sodankylä (67°N). Front. Earth Sci. 12 June
1718   2020, doi:10.3389/feart.2020.00153, 2020b.

1719   Meinander, O., Piedehierro, A., Welti, A., Kouznetsov, R., Heinonen, A., Viisanen, Y. and Laaksonen, A.: Saharan dust
1720   transported and deposited in Finland on February 23rd, 2021. EAC 2021 August 30-Septembre 3 2021, Abstract AAS 19-2
1721   Paper ID 399, abstract available at:
1722   https://www.conftool.com/eac2021/index.php?page=browseSessions&form_session=206#paperID399; talk available at:
1723   https://www.youtube.com/watch?v=ssJ6k8sT0so. Book of abstracts for the 2021 European Aerosol Conference, A live virtual
1724   event, hosted by The Aerosol Society, https://eac2021.co.uk/book-of-abstracts, 2021, 2021.

1725 Meskhidze, N., Volker, C., Al-Abadleh, H. A., Barbeau, K., Bressac, M., Buck, C., Bundy, R. M., Croot, P., Feng, Y., Ito, A.,
1726 Johansen, A. M., Landing, W. M., Mao, J. Q., Myriokefalitakis, S., Ohnemus, D., Pasquier, B., and Ye, Y.: Perspective on
1727 identifying and characterizing the processes controlling iron speciation and residence time at the atmosphere-ocean interface,
1728 Mar. Chem., 217, 103704, doi: 10.1016/j.marchem.2019.103704, 2019.

1729 Meteosat 2019: Two dust clouds, one from northern Africa and one from Central Europe, travelled north towards Iceland and
1730 Greenland in late April 2019. Dust over Europe 22 April 2019 12:00 UTC, 23 April 06:00–12:30 UTC, 24 April 06:00 UTC,
1731 by Jochen Kerkmann and Vesa Nietosvaara (EUMETSAT), Ivan Smiljanicv (SCISYS), Izabela Zablocka (IMGW), Mike
1732 Fromm (US Naval Research Laboratory, Published on 22 April 2019, available at: https://www.eumetsat.int/dust-over-europe,
1733 2019.

1734 Miller, M.E., Bowker, M.A., Reynolds, R.L. and Goldstein, H.L.: Post-fire land treatments and wind erosion – lessons from
1735 the Milford Flat Fire, UT, USA. Aeolian Research, 7, 29– 44, 2012.

1736 Mills, M. M., Ridame, C., Davey, M., La Roche, J., and Geider, R. J.: Iron and phosphorus co-limit nitrogen fixation in the
1737 eastern tropical North Atlantic, Nature, 429, 292-294, doi: 10.1038/nature02550, 2004.

1738 Mockford, T., Bullard, J., Thorsteinsson, T..: The dynamic effects of sediment availability on the relationship between wind
1739 speed and dust concentration. Earth Surface Processes and Landforms, 43, 11, 2484–2492, 2018.

1740 Montes, A., Rodríguez, S. S., and Domínguez, C. E.: Geomorphology context and characterization of dunefields developed by
1741 the southern westerlies at drying Colhué Huapi shallow lake, Patagonia Argentina. Aeolian Research, 28, Supplement C, 58–
1742 70, doi:10.1016/j.aeolia.2017.08.001, 2017.

1743 Moore, C. M., Mills, M. M., Arrigo, K. R., Berman-Frank, I., Bopp, L., Boyd, P. W., Galbraith, E. D., Geider, R. J., Guieu,
1744 C., Jaccard, S. L., Jickells, T. D., La Roche, J., Lenton, T. M., Mahowald, N. M., Maranon, E., Marinov, I., Moore, J. K.,
1745 Nakatsuka, T., Oschlies, A., Saito, M. A., Thingstad, T. F., Tsuda, A., and Ulloa, O.: Processes and patterns of oceanic nutrient
1746 limitation, Nat. Geosci., 6, 701-710, doi: 10.1038/ngeo1765, 2013.

1747 Mori, Tatsuhiro, Goto-Azuma, Kumiko, Kondo, Yutaka, Ogawa-Tsukagawa, Yoshimi, Miura, Kazuhiko, Hirabayashi,
1748 Motohiro, Oshima, Naga, Koike, M., Kupiainen, Kaarle, Moteki, Nobuhiro, Ohata, Sho, Sinha, P.R., Sugiura, Konosuke, Aoki,
1749 Teruo, Schneebeli, Martin, Steffen, Konrad, Sato, Atsushi, Tsushima, A., Makarov, V., Nagatsuka, N.: Black Carbon and
1750 Inorganic Aerosols in Arctic Snowpack, Journal of Geophysical Research: Atmospheres. 124, doi:10.1029/2019JD030623,
1751 2019.

1752 Moroni B., Becagli S., Bolzacchini E., Busetto M., Cappelletti D., Crocchianti S., Ferrero L., Frosini D., Lanconelli C., Lupi
1753 A., Maturilli M., Mazzola M., Perrone G., Sangiorgi G., Traversi R., Udisti R., Viola A. and Vitale V.: Vertical profiles and
1754 chemical properties of aerosol particles upon Ny-Ålesund (Svalbard Islands). Advances in Meteorology,
1755 doi:10.1155/2015/292081.2015, 2015.

1756 Moroni B., Cappelletti D., Ferrero L., Crocchianti S., Busetto M., Mazzola M., Becagli S., Traversi R. and Udisti R.: Local
1757 vs. long-range sources of aerosol particles upon Ny-Ålesund (Svalbard Islands): mineral chemistry and geochemical records.
1758 Rendiconti Lincei. Scienze Fisiche e Naturali, doi: 10.1007/s12210-016-0533-7, 2016.

1759 Moroni B, Arnalds O, Dagsson-Waldhauserová P, Crocchianti S, Vivani R and Cappelletti D. Mineralogical and Chemical
1760 Records of Icelandic Dust Sources Upon Ny-Ålesund (Svalbard Islands). Front. Earth Sci. 6:187, doi:
1761 10.3389/feart.2018.00187, 2018.

1762 Murray, B. J., D. O'Sullivan, J. D. Atkinson, and M. E. Webb: Ice nucleation by particles immersed in supercooled cloud
1763 droplets, Chem. Soc. Rev., 41, 19, 6519-6554, doi:10.1039/c2cs35200a, 2012.

1764 Murray, K.T., Miller, M.F. and Bowser, S.S.: Depositional processes beneath coastal multi-year sea ice. Sedimentology, 60,
1765 391–410, 2013.

1766 Murray, B. J., K. S. Carslaw, and P. R. Field: Opinion: Cloud-phase climate feedback and the importance of ice-nucleating
1767 particles, Atmos. Chem. Phys., 21, 2, 665-679, doi:10.5194/acp-21-665-2021, 2021.

1768 Möller, R., Möller, M., Kukla, P. A., and Schneider, C.: Impact of supraglacial deposits of tephra from Grimsvötn volcano,
1769 Iceland, on glacier ablation. J. Glaciol. 62, 933–943, doi: 10.1017/jog.2016.82, 2016.

1770 Nagatsuka, Naoko, Goto-Azuma, Kumiko, Tsushima, Akane, Fujita, Koji , Matoba, Sumito, Onuma, Yukihiko, Dallmayr,
1771 Remi, Kadota, Moe , Hirabayashi, Motohiro, Ogata, Jun, Ogawa-Tsukagawa, Yoshimi, Kitamura, Kyotaro, Minowa,
1772 Masahiro, Komuro, Yuki , Motoyama, Hideaki , Aoki, Teruo: Variations in mineralogy of dust in an ice core obtained from
1773 northwestern Greenland over the past 100 years. Climate of the Past, 17, 1341-1362, doi: 10.5194/cp-17-1341-2021, 2021.

1774 Nemuc, A., Basart, S., Tobias, A., Nickovic, S., Barnaba, F., Kazadzis, S., Mona, L.,, Amiridis, V., Vukovic, A., Christel, I.,
1775 Dagsson-Waldhauserová, P., Monteiro, A.: International Network to Encourage the Use of Monitoring and Forecasting Dust
1776 Products (InDust). European Review, 1-13, doi:10.1017/S1062798720000733, 2020.
1777
1778 Neuman, C. M.: Observations of winter aeolian transport and niveo-aeolian deposition at crater lake, pangnirtung pass,
1779 N.W.T., Canada, Permafr. Periglac. Process., 1, 3–4, 235–247, doi:10.1002/ppp.3430010304, 1990.

1780 Nickling, W.: Eolian sediment transport during dust storms: Slims River valley, Yukon Territory. Canadian Journal of Earth
1781 Science, 15, 1069-1084, 1978.

1782 Nickling, W. G., and Brazel, A. J.: Surface wind characteristics along the icefield ranges, Yukon Territory, Canada. Arctic and
1783 Alpine Research, 17, 125–134. doi:10.2307/1550842, 1985.

1784 Nickovic, S., Cvetkovic, B., Madonna, F., Rosoldi, M., Pejanovic, G., Petkovic, S., and Nikolic, J.: Cloud ice caused by
1785 atmospheric mineral dust – Part 1: Parameterization of ice nuclei concentration in the NMME-DREAM model, Atmos. Chem.
1786 Phys., 16, 11367-11378, doi:10.5194/acp-16-11367-2016, 2016.

1787 Nielsdottir, M. C., Moore, C. M., Sanders, R., Hinz, D. J., and Achterberg, E. P.: Iron limitation of the postbloom
1788 phytoplankton communities in the Iceland Basin, Global Biogeochemical Cycles, 23, doi: 10.1029/2008gb003410, 2009.

1789 Nordic Council of Ministers. Road dust and PM10 in the Nordic countries. Measures to Reduce Road Dust Emissions from
1790 Traffic. Publication number 2016:790. Publish date 27.01.17, available at: https://www.norden.org/en/publication/road-dust-
1791 and-pm10-nordic-countries (last accessed 4.11.2021), 2017.

1792 Ovadnevaite, J., Ceburnis, D., Plauskaite-Sukiene, K., Modini, R., Dupuy, R., Rimselyte, I., Ramonet, R., Kvietkus, K.,
1793 Ristovski, Z., Berresheim, H., and O'Dowd, C.D.: Volcanic sulphate and Arctic dust plumes over the North Atlantic Ocean.
1794 Atmospheric Environment 43, 4968-4974, 2009.

1795 Pejanovic, G., S. Nickovic, M. Vujadinovic, A. Vukovic, V. Djurdjevic, M. Dacic: Atmospheric deposition of minerals in dust
1796 over the open ocean and possible consequences on climate. WCRP OSC Climate Research in Service to Society, 24-28 October
1797 2011, Denver, CO, USA, 2011.

1798 Peltoniemi, J. I., Gritsevich, M., Hakala, T., Dagsson-Waldhauserová, P., Arnalds, Ó., Anttila, K., Hannula, H.-R., Kivekäs,
1799 N., Lihavainen, H., Meinander, O., Svensson, J., Virkkula, A., and de Leeuw, G.: Soot on Snow experiment: bidirectional
1800 reflectance factor measurements of contaminated snow, The Cryosphere, 9, 2323-2337, doi:10.5194/tc-9-2323-2015, 2015.

1801 Perron, M. M. G., Strzelec, M., Gault-Ringold, M., Proernse, B. C., Boyd, P. W., and Bowie, A. R.: Assessment of leaching
1802 protocols to determine the solubility of trace metals in aerosols, Talanta, 208, doi: 10.1016/j.talanta.2019.120377, 2020.

1803 Popovicheva, O., Diapouli, E., Makshtas, A., Shonija, N., Manousakas, M., Saraga, D., Uttal, T., and Eleftheriadis K.: East
1804 Siberian Arctic background and black carbon polluted aerosols at HMO Tiksi. Science of the Total Environment, 655, 924-
1805 938, doi.org/10.1016/j.scitotenv.2018.11.165, 2019.

1806 Price, H. C., et al.: Atmospheric Ice-Nucleating Particles in the Dusty Tropical Atlantic, J. Geophys. Res., 123, 4, 2175-2193,
1807 doi:10.1002/2017JD027560, 2018.

1808 Prospero, J. M., Ginoux, P., Torres, O., Nicholson, S. E., and Gill, T. E., ENVIRONMENTAL CHARACTERIZATION OF
1809 GLOBAL SOURCES OF ATMOSPHERIC SOIL DUST IDENTIFIED WITH THE NIMBUS 7 TOTAL OZONE MAPPING
1810 SPECTROMETER (TOMS) ABSORBING AEROSOL PRODUCT, Rev. Geophys., 40, 1, 1002,
1811 doi:10.1029/2000RG000095, 2002.

1812 Prospero, J.M., Bullard, J.E., Hodgkins, R.: High-latitude dust over the North Atlantic: inputs from Icelandic proglacial dust
1813 storms. Science 335, 1078–1082, 2012.

1814 Qin, Y., Abatzoglou, J.T., Siebert, S. et al.: Agricultural risks from changing snowmelt. Nat. Clim. Chang. 10, 459–465,
1815 doi:10.1038/s41558-020-0746-8, 2020.

1816 Querol, A. Tobías, N. Pérez, A. Karanasiou, F. Amato, M. Stafoggia, C.P. García-Pando, P. Ginoux, F. Forastiere, S. Gumy,
1817 P. Mudu: Monitoring the impact of desert dust outbreaks for air quality for health studies. Environ. Int., 130, p. 104867,
1818 2019.

1819 Raiswell, R., Hawkings, J. R., Benning, L. G., Baker, A. R., Death, R., Albani, S., Mahowald, N., Krom, M. D., Poulton, S.
1820 W., and Wadham, J.: Potentially bioavailable iron delivery by iceberg-hosted sediments and atmospheric dust to the polar
1821 oceans, Biogeosciences, 13, 3887-3900, 2016.

1822 Ranjbar, K., O'Neill, N.T., Ivanescu, L., King, J., Hayes, P.L.: Remote sensing of a high- Arctic, local dust event over Lake
1823 Hazen (Ellesmere Island, Nunavut, Canada), Atmospheric Environment, 118102, ISSN 1352-2310,
1824 doi:10.1016/j.atmosenv.2020.118102, 2021.

1825 Richards-Thomas, T., McKenna-Neuman, C., and Power, I.M. Power: Particle-scale characterization of volcaniclastic dust
1826 sources within Iceland. Sedimentology, 68,3, 1137-1158, doi: 10.1111/sed.12821, 2021.

1827 Romanias M.N., Y. Ren, B. Grosselin, V. Daele, A. Mellouki, P. Dagsson-Waldhauserová, F. Thevenet: Reactive uptake of
1828 NO2 on volcanic particles: A possible source of HONO in the atmosphere, Journal of Environmental Sciences, Vol 95, pp
1829 155-164, September 2020. doi: 10.1016/j.jes.2020.03.042, 2020.

1830 Ryan-Keogh, T. J., Macey, A. I., Nielsdottir, M. C., Lucas, M. I., Steigenberger, S. S., Stinchcombe, M. C., Achterberg, E. P.,
1831 Bibby, T. S., and Moore, C. M.: Spatial and temporal development of phytoplankton iron stress in relation to bloom dynamics
1832 in the high-latitude North Atlantic Ocean, Limnology and Oceanography, 58, 533-545, doi: 10.4319/lo.2013.58.2.0533, 2013.

1833 Rymer, K.: Aeolian activity in central Spitsbergen (Ebba Valley) in the years 2012–2017. In Proceedings of the XXXVII Polar
1834 Symposium "Polar Change—Global Change", Poznan, Poland, 7–10 June 2018; p. 61, 2018.

1835 Rymer, K.G., Rachlewicz, G., Buchwal, A., Temme, A.J.A.M., Reimann, T., van der Meij, W.M.: Contemporary and past
1836 aeolian deposition rates in periglacial conditions (Ebba Valley, central Spitsbergen). Catena 211, 105974, 2022.

1837 Samonova O.A. and Aseyeva E.N.: Particle size partitioning of metals in humus horizons of two small erosional landforms in
1838 the middle Protva basin – a comparative study. GEOGRAPHY, ENVIRONMENT, SUSTAINABILITY, 13, 1, 260-271,
1839 doi:10.24057/2071-9388-2019-116, 2020.

1840 Sanchez-Marroquin, A. O. Arnalds, K. J. Baustian-Dorsi, J. Browse, P. Dagsson-Waldhauserová, A. D. Harrison, E. C. Maters,
1841 K. J. Pringle, J. Vergara-Temprado, I. T. Burke, J. B. McQuaid, K. S. Carslaw, B. J. Murray: Iceland is an episodic source of
1842 atmospheric ice-nucleating particles relevant for mixed-phase clouds. Science Advances 6, 26, eaba8137,
1843 doi:10.1126/sciadv.aba8137, 2020.

1844 Šantl-Temkiv, T., R. Lange, D. Beddows, U. Rauter, S. Pilgaard, M. Dall'Osto, N. Gunde-Cimerman, A. Massling, and H.
1845 Wex: Biogenic Sources of Ice Nucleating Particles at the High Arctic Site Villum Research Station, Environ. Sci. Technol.,
1846 53, 18, 10580-10590, doi:10.1021/acs.est.9b00991, 2019.

1847 Schroth, A. W., Crusius, J., Sholkovitz, E. R. and Bostick, B. C.: Iron solubility driven by speciation in dust sources to the
1848 ocean, Nat. Geosci., 2, 5, 337–340, doi:10.1038/ngeo501, 2009.

1849 Schroth, A. W., Crusius, J., Gassó, S., Moy, C. M., Buck, N. J., Resing, J. A., and Campbell, R. W.: Atmospheric deposition
1850 of glacial iron in the Gulf of Alaska impacted by the position of the Aleutian Low, Geophysical Research Letters, 44, 5053-
1851 5061, doi: 10.1002/2017gl073565, 2017.

1852 Schuler, T. V., Kohler, J., Elagina, N., Hagen, J. O. M., Hodson, A. J., Jania, J. A., Kääb, A. M., Luks, B., Małecki, J., Moholdt,
1853 G., Pohjola, V. A., Sobota, I., and Van Pelt, W. J. J.: Reconciling Svalbard Glacier Mass Balance, Front Earth Sci., 8, 156,
1854 doi:10.3389/feart.2020.00156, 2020.

1855 Semenkov, I. N. and Koroleva, T. V.: The spatial distribution of fractions and the total content of 24 chemical elements in soil
1856 catenas within a small gully's catchment area in the Trans Urals, Russia, Appl. Geochemistry, 106, 1–6, doi:
1857 10.1016/j.apgeochem.2019.04.010, 2019.

1858 Semenkov, I. and Yakushev, A.: Dataset on heavy metal content in background soils of the three gully catchments at Western
1859 Siberia, Data Br., doi:10.1016/j.dib.2019.104496, 2019.

1860 Semenkov, I. N., Usacheva, A. A. and Miroshnikov, A. Y.: Distribution of global fallouts cesium-137 in taiga and tundra
1861 catenae at the Ob River basin, Geol. Ore Depos., 57, 2, 138–155, doi:10.1134/S1075701515010055, 2015a.

1862 Semenkov, I. N., Miroshnikov, A. Y., Asadulin, E. E., Usacheva, A. A., Velichkin, V. I. and Laverov, N. P.: The Ob river
1863 basin as a source of Kara Sea contamination with global fallout of Cesium-137, Dokl. Earth Sci., 463, 1, 704–706,
1864 doi:10.1134/S1028334X1507003X, 2015b.

1865 Semenkov, I. N., Krupskaya, V. and Klink, G.: Data on the concentration of fractions and the total content of chemical elements
1866 in catenae within a small catchment area in the Trans Urals, Russia, Data in Brief, 29, doi: 10.1016/j.dib.2019.104224, 2019.

1867 Semenkov, I. N., Sharapova, A. V., Koroleva, T. V., Klink, G. V., Krechetov, P. P. and Lednev, S. A.: Nitrogen-containing
1868 substances in the snow of the fall areas of the Proton launch vehicle stages in 2009 – 2019, Led i sneg, 61, 301-310, doi:
1869 10.31857/S2076673421020090, 2021.

1870 Sharapova, A. V., Semenkov, I. N., Koroleva, T. V., Krechetov, P. P., Lednev, S. A. and Smolenkov, A. D.: Snow pollution
1871 by nitrogen-containing substances as a consequence of rocket launches from the Baikonur Cosmodrome, Sci. Total Environ.,
1872 709, 136072, doi: 10.1016/j.scitotenv.2019.136072, 2020.

1873 Shepherd, G., Terradellas E., Baklanov A., Kang A., Sprigg W., Nickovic S., Darvishi Boloorani A., Al-Dousari A., Basart
1874 S., Benedetti A. et al.: Global assessment of sand and dust storms, UNEP, WMO, UNCCD; United Nations Environment
1875 Programme, 123 p.,URL:http://apps.unep.org/publications/pmtdocuments/Global_assessment_of_sand_and_dust_storms-
1876 2016.pdf, 2016.

1877 Shi, Z., Krom, M. D., Jickells, T. D., Bonneville, S., Carslaw, K. S., Mihalopoulos, N., Baker, A. R., and Benning, L. G.:
1878 Impacts on iron solubility in the mineral dust by processes in the source region and the atmosphere: A review, Aeolian
1879 Research, 5, 21-42, doi: 10.1016/j.aeolia.2012.03.001, 2012.

1880 Shugar, D. H., Clague, J. J., Best, J. L., Schoof, C., Willis, M. J., Copland, L., Roe, G. H.: River piracy and drainage basin
1881 reorganization led by climate-driven glacier retreat. Nature Geoscience 10, 370, 2017.

1882 Sofiev, M., Vira, J., Kouznetsov, R., Prank, M., Soares, J., Genikhovich, E.: Construction of the SILAM Eulerian atmospheric
1883 dispersion model based on the advection algorithm of Michael Galperin, Geosci. Model Developm. 8, 3497-3522, 2015.

1884 Speirs, J.C., McGowan, H.A. and Neil, D.T. Meteorological controls on sand transport and dune morphology in a polar-desert:
1885 Victoria Valley, Antarctica. Earth Surf. Proc. Land., 33, 1875–1891, 2008.

1886 Spolaor A, Moroni B, Luks B, Nawrot A, Roman M, Larose C, Stachnik Ł, Bruschi F, Kozioł K, Pawlak F, Turetta C, Barbaro
1887 E, Gallet J-C and Cappelletti D. Investigation on the Sources and Impact of Trace Elements in the Annual Snowpack and the
1888 Firn in the Hansbreen (Southwest Spitsbergen). Front. Earth Sci. 8:536036, doi: 10.3389/feart.2020.536036, 2021.

1889 Stockdale, A., Krom, M. D., Mortimer, R. J., Benning, L. G., Carslaw, K. S., Herbert, R. J., Shi, Z., Myriokefalitakis, S.,
1890 Kanakidou, M., and Nenes, A.: Understanding the nature of atmospheric acid processing of mineral dusts in supplying
1891 bioavailable phosphorus to the oceans, Proc Natl Acad Sci U S A, 113, 14639-14644, doi: 10.1073/pnas.1608136113, 2016.

1892 Stojiljkovic, A., Kauhaniemi, M., Kukkonen, J., Kupiainen, K., Karppinen, A., Denby, B. R., Kousa, A., Niemi, J. V., and
1893 Ketzel, M.: The impact of measures to reduce ambient air PM10 concentrations originating from road dust, evaluated for a
1894 street canyon in Helsinki, Atmos. Chem. Phys., 19, 11199–11212, doi: 10.5194/acp-19-11199-2019, 2019.58-9, 2019.

1895 Storelvmo, T., I. Tan, and A. V. Korolev: Cloud Phase Changes Induced by CO_2 Warming—a Powerful yet Poorly Constrained
1896 Cloud-Climate Feedback, Current Climate Change Reports, 1, 4, 288-296, doi:10.1007/s40641-015-0026-2, 2015.

1897 Sweeney M., Mason J. A., Mechanisms of dust emission from Pleistocene loess deposits, Nebraska, USA, Journal of
1898 Geophysical Research 118, 3, 1460-1471, doi:10.1002/jgrf.20101, 2013.

1899 Tagliabue, A., and Arrigo, K. R.: Iron in the Ross Sea: 1. Impact on CO_2 fluxes via variation in phytoplankton functional
1900 group and non-Redfield stoichiometry, Journal of Geophysical Research: Oceans, 110, 2005.

1901 Tan, I., and T. Storelvmo: Evidence of Strong Contributions From Mixed-Phase Clouds to Arctic Climate Change, Geophys.
1902 Res. Lett., 46, 5, 2894-2902, doi:10.1029/2018GL081871, 2019.

1903 Tang, M, Cziczo, D.J., Grassian, V. H:. Interactions of sater with mineral dust aerosol: Water adsorption, hygroscopicity, cloud
1904 condensation, and ice nucleation. Chem. Rev. 116, 4205-4259, 2016.

1905 Tarr, R. S., and L. Martin. Glacier deposits of the continental type in Alaska, Geology, 21, 289–300, doi:10.1086/622063,
1906 1913.

1907 Television Midtvest 2021, video link: Se videoen: Kraftig blæst får biler til at forsvinde i støvsky | TV MIDTVEST, 2021.

1908 Terradellas, E., Nickovic, S., and Zhang, X. Y.: Airborne dust: a hazard to human health, environment and society. WMO
1909 Bull, 64, 2, 42-46, 2015.

1910 Terradellas, E., Zhang, X. Y, Farrel, D., Nickovic, S., and Baklanov, A.: Airborne dust: Overview of atmospheric dust content
1911 in 2016. WMO Airborne Dust Bull 1, 1-3, 2017.

Field Code Changed
Field Code Changed

Tobo, Y. K. Adachi, P. J. DeMott, T. C. J. Hill, D. S. Hamilton, N. M. Mahowald, N. Nagatsuka, S. Ohata, J. Uetake, Y. Kondo, M. Koike: Glacially sourced dust as a potentially significant source of ice nucleating particles. Nat Geosci, 12, 4, 253-258, doi:10.1038/s41561-019-0314-x, 2019.

Urupina D., Lasne, J., Romanias, M., Thiery, V., Dagsson-Waldhauserová, P., Thevenet, F.: Uptake and surface chemistry of SO2 on natural volcanic dusts, Atmospheric Environment, Vol 217, pp 116942, DOI: 10.1016/j.atmosenv.2019.116942, 2019.

UNCCD / Vukovic, A.: Sand and Dust Storms Source Base-map. Visualization Tool. https://maps.unccd.int/sds/ and https://www.youtube.com/watch?v=4tsbspJvuAs, 2021.

USGCRP: Impacts, Risks, and Adaptation in the United States: The Fourth National Climate Assessment, Volume II. In: D. R. Reidmiller, C. W. Avery, D. R. Easterling, K. E. Kunkel, K. L. M. Lewis, T. K. Maycock, and B. C. Stewart (Eds.). Washington, DC, doi:10.7930/NCA4.2018, 2018.

Usher, C.R., Michel, A.E., and Grassian, V.H.: Chemical Reviews,103, 12, 4883-4940, doi: 10.1021/cr020657y, 2003.

Valle, H. F. Del, Elissalde, N. O., Gagliardini, D. A., and Milovich, J.: Status of desertification in the Patagonian region: Assessment and mapping from satellite imagery. Arid Soil Research and Rehabilitation, 12, 2, 95–121, doi:10.1080/15324989809381502, 1998.

Varga, G., Dagsson-Waldhauserová, P., Gresina, F. and Helgadottir A.: Saharan dust and giant quartz particle transport towards Iceland. Scientific Reports 11, 11891, 2021.

Vergara-Temprado, J., A. K. Miltenberger, K. Furtado, D. P. Grosvenor, B. J. Shipway, A. A. Hill, J. M. Wilkinson, P. R. Field, B. J. Murray, and K. S. Carslaw: Strong control of Southern Ocean cloud reflectivity by ice-nucleating particles, P. Natl. Acad. Sci. USA, doi:10.1073/pnas.1721627115, 2018.

von Friesen, L.W. and Riemann, L.: Nitrogen Fixation in a Changing Arctic Ocean: An Overlooked Source of Nitrogen? Frontiers in Microbiology, 11, 1664-302X, doi: 10.3389/fmicb.2020.596426, 2020.

Vukovic, A.: Report on consultancy to develop Global Sand and Dust Source Base Map, no. CCD/18/ERPA/21, UNCCD, 2019.

Vukovic Vimic, A.: Global high-resolution dust source map, InDust webinar, 21 April 2021, https://cost-indust.eu/events/indust-events, 2021.

Wang, Q., Fan, X. & Wang, M.: Evidence of high-elevation amplification versus Arctic amplification. Sci Rep, 6, 19219. https://doi.org/10.1038/srep19219, 2016.

Wahlström E., Reinikainen, T. and Hallanaro E.-L.: Ympäristön tila Suomessa, ISBN 951-662-523-1, 364 p., 1996.

Wheaton, E. E.: Prairie dust storms — A neglected hazard, Nat. Hazards, 5, 1, 53–63, doi:10.1007/BF00127139, 1992.

Wheaton, E. E. and Chakravarti, A. K.: Dust storms in the Canadian Prairies, Int. J. Climatol., 10, 8, 829–837, doi:10.1002/joc.3370100805, 1990.

Wientjes, I. G., R. S. Van De Wal, G. J. Reichart, A. Sluijs, and J. Oerlemans: Dust from the dark region in the western ablation zone of the Greenland ice sheet, The Cryosphere, 5, 589–601, doi:10.5194/tc-5-589-2011, 2011.

Winton, V. H. L., Dunbar, G. B., Bertler, N. A. N., Millet, M. A., Delmonte, B., Atkins, C. B., Chewings, J. M., and Andersson, P.: The contribution of aeolian sand and dust to iron fertilization of phytoplankton blooms in southwestern Ross Sea, Antarctica, Global Biogeochemical Cycles, 28, 423-436, doi: 10.1002/2013gb004574, 2014.

Winton, V.H.L., Dunbar, G.B., Atkins, C.B., Bertler, N.A.N., Delmonte, B., Andersson, P., Bowie, A., Edwards, R.: The origin of lithogenic sediment in the south-western Ross Sea and implications for iron fertilization. Antarctic Science, doi:10.1017/S095410201600002X, 2016a.

Winton, V. H. L., Edwards, R., Delmonte, B., Ellis, A., Andersson, P. S., Bowie, A., Bertler, N. A. N., Neff, P., and Tuohy, A.: Multiple sources of soluble atmospheric iron to Antarctic waters, Global Biogeochemical Cycles, 30, 421-437, doi: 10.1002/2015gb005265, 2016b.

Wolfe S.A.: Cold-Climate Aeolian Environments, Reference Module in Earth Systems and Environmental Sciences, 10.1016/B978-0-12-818234-5.00036-5, 2020.

Zhu, L., Ives, A., Zhang, C., Guo, Y., and Radeloff, V.: Climate change causes functionally colder winters for snow cover-dependent organisms. Nature Climate Change, 9, 1-8, doi:10.1038/s41558-019-0588-4, 2019.

Zhu, Y., Toon, O.B., Jensen, E.J. et al.: Persisting volcanic ash particles impact stratospheric SO_2 lifetime and aerosol optical properties. Nat Commun 11, 4526, doi:10.1038/s41467-020-18352-5, 2020.

Zwoliński, Z., Kostrzewski, A., and Pulina, M. (Eds.): Dawne i współczesne geoekosystemy Spitsbergenu [Ancient and modern geoecosystems of Spitsbergen], Bogucki Wydawnictwo Naukowe, Poznań, 456 p., 2013.